Engineered Remediation and Natural Attenuation of Halogenated Alkanes (Carbon Tetrachloride and 1,2,3-trichloropropane): A Study of Contaminant Reactivity and Reductant Morphology

Vaishnavi Sarathy
M.Sc. (Chemistry) Indian Institute of Technology, Bombay, 2000
M.S. (Environmental Science) University of Delaware, 2002

A dissertation presented to the faculty of the
OGI School of Science & Engineering
at Oregon Health & Science University
in partial fulfillment of the
requirements for the degree
Ph.D.
in
Environmental Science and Engineering

June 2008

The dissertation “Engineered and natural attenuation of halogenated alkanes (carbon tetrachloride and 1,2,3-trichloropropane): A study of contaminant reactivity and reductant morphology” has been examined and approved by the following examination committee:

Dr. Paul G. Tratnyek, Thesis Advisor
Professor, OHSU

Dr. Richard L. Johnson
Professor, OHSU

Dr. James E. Amonette
Senior Research Scientist, Pacific Northwest National Laboraory

---

Dr. Gwynn R. Johnson
Assistant Professor, Portland State University

Acknowledgments

My Ph.D. is a cumulative result of support from various people. I am very grateful to my advisor, Dr. Paul Tratnyek, for being extremely approachable, helpful, encouraging, and enabling me to develop a very sensible approach toward science and my career in general. My colleagues (Rachel Waldemer, Syeda Ahmed, Jim Nurmi, Elsa Chang, and others) over the years were very supportive, and made the 5.5 years seem much shorter. Lorne Isabelle and Nancy Christie were constant reliable sources of help whenever any graduate student needed it. Last but not the least, my husband and my mother were always there to back me up, and help me work extra hours to finish my thesis.

Table of Contents

List of Figures

List of Tables

Abstract

Engineered and Natural Attenuation of Halogenated Alkanes (Carbon Tetrachloride and 1,2,3-Trichloropropane): A Study of Contaminant Reactivity and Reductant Morphology

Vaishnavi Sarathy M.S., M.Sc.

Ph.D., OGI School of Science & Engineering
at Oregon Health & Science University

June 2008

Thesis Advisor: Dr. Paul Tratnyek

Carbon tetrachloride (CT), and 1,2,3-trichloropropane (TCP)—two chlorinated aliphatic compounds that have very different susceptibilities to dechlorination—were studied for their reactivity via different abiotic pathways. Batch experiments performed with CT involved reduction by Fe^0, which produced chloroform as the major product via hydrogenolysis. The yield of chloroform—Y_{CF}, which is a parameter that we want to minimize—was found to be dependent on the nature of the surface, and was low when the surface contained magnetite. Based on results from batch experiments with nano-Fe^0 with a magnetite shell (Fe^{H2}), we proposed an alternate pathway for CT dechlorination where CCl_3^- is formed by a concerted $2e^-$ reduction (with simultaneous dissociation of a C—Cl bond), without $CCl_3^{\bullet}$ being formed as an intermediate. We concluded that conditions that can force CCl_3^- to go to the carbene versus into solution, will help lower Y_{CF}. Other batch experiments studying kinetics of CT dechlorination indicated that nano-Fe^0 is not faster than larger iron on a surface-area normalized basis. We investigated the aging of Fe^{H2} in water—which is one of the most important uncertainties associated with

the use of iron nanoparticles for remediation—by various analytical techniques including XRD, TEM, CT reaction kinetics, electrochemistry, etc. Our results show evidence for rapid destruction of the original Fe(III) oxide film on Fe^{H2} during immersion (0-2 days) and the subsequent formation of a new mixed-valence Fe(II)-Fe(III) oxide shell.

Batch experiments with TCP were performed under all possible abiotic degradation pathways. TCP is more recalcitrant than CT towards remediation by oxidation-reduction processes, and exhibits little or no reaction with common reductants, such as Fe^0. It does, however, react at measurable rates with some unaged dry Fe^{H2}, palladized nano-Fe^0, and zinc. TCP can also be significantly (but slowly) degraded via hydrolysis at high pH and temperatures. Oxidation of TCP is much more feasible than reduction, especially when involving strong free-radical intermediates like hydroxyl radical (in activated hydrogen peroxide) and sulfate radical (in activated persulfate). Activated persulfate, in particular, not only quickly oxidizes, but also completely dechlorinates TCP, and may be among the most viable options for field applications.

1

Fate and Redox Chemistry of Chlorinated Aliphatics in Groundwater

Abstract

The majority of organic compounds contaminating groundwater are chlorinated aliphatics that enter the groundwater as a result of extensive use as dry cleaning agents, industrial solvents, fumigants and pesticides in agriculture, etc. Natural attenuation, defined here as biotic or abiotic degradation under environmental conditions, is often insufficient to effectively degrade these chemicals over time frames and distances necessary to meet cleanup goals. Engineered remediation technologies can be designed to be fast, but may still produce recalcitrant chlorinated byproducts. Abiotic remediation of VOCs can be either *in situ* or *ex situ*, and occurs via hydrolysis, reduction, oxidation, and/or elimination. Carbon tetrachloride (CT), and 1,2,3-trichloropropane (TCP)—two compounds that have very different susceptibility to dechlorination—are studied for their reactivity via different abiotic pathways. Their low soil-sorption (K_{oc}), and octanol-water (K_{ow}) partition coefficients mean that while they are moderately hydrophobic, they do not sorb significantly to soil organic matter, and are mobile and persistent in groundwater. CT is difficult to oxidize, so it is much more likely to react via *in situ* reductive techniques than the highly recalcitrant and persistent TCP—which is also slow to react via oxidation, and hydrolysis/elimination reactions.

INTRODUCTION

Chlorinated aliphatic VOCs (volatile organic compounds)—carbon tetrachloride, chloroform, 1,2-dichloroethane, 1,2,3-trichloropropane, trichloroethene, etc.—are xenobiotic chemicals, that have been released to the environment over the past century, and now contaminate groundwater, drinking water, and soils extensively [1]. Sources include dry-cleaning agents, solvents, fumigants used in agriculture, paints, pesticides, industrial discharge, etc. [2]. These compounds are denser than water, and very insoluble in water. This property causes concentrated pools of chlorinated solvents—called DNAPL (dense non-aqueous phase liquid)—to exist in the bottom of aquifers, where they are very difficult to treat [2]. Chlorinated DNAPLs typically entered groundwater from intentional or unintentional spills including leaking above- and under-ground storage tanks, in the mid 20th century. Most chlorinated solvents do not naturally degrade in the environment, do not sorb significantly to soil, and some can be remarkably persistent in groundwater [2]. Long residence times imply risks of contaminated flow reaching surface waters, and drinking water sources. It is, therefore, of utmost importance to have quick remediation methods.

REMEDIATION TECHNIQUES

Natural attenuation. Remediation treatments can be natural or engineered, and both biotic and abiotic. Natural attenuation, which can be abiotic processes and/or bioremediation under ambient environmental conditions, is not always fast or sufficient for remediation of most VOCs in groundwater, especially for short-term goals [3]. Abiotic natural degradation processes typically include substitution and elimination, in the absence of naturally occurring redox agents. Half-lives of chlorinated aliphatics reacting via hydrolysis at pH 7 and 25 °C—which can include nucleophilic substitution by H_2O or OH^-, and/or elimination—range from 41 years for carbon tetrachloride (CT), to 72 years for 1,2-dichloroethane (1,2-DCA) [4]. Some compounds like 2,2-dichloropropane have uncommonly short half-lives (36 hours) for hydrolysis, but this is

not the norm [4]. Sulfide is another common nucleophile, also present in groundwaters, and can degrade CT and 1,2-DCA in 7 and 6 years respectively [5, 6].

Naturally occurring microbial populations in the subsurface—which are often predominantly anaerobic—can degrade most chlorinated aliphatics, although usually not as fast as microbes in aerobic conditions [7]. Biotransformation of haloaliphatics also occurs via pathways similar to abiotic degradation, i.e., either nucleophilic substitution, oxidation, or reductive dehalogenation [8]. Hurdles occurring in these processes include: (*i*) products of biodegradation are usually chlorinated and more recalcitrant to reduction by anaerobes, (*ii*) high concentration of chlorinated aliphatics associated with DNAPLs can be toxic to indigenous microbes, and (*iii*) very low concentrations of contaminants may not be enough to sustain microbial communities [9].

In situ abiotic engineered remediation. The alternative to natural attenuation is engineered abiotic/microbial remediation—whether *in situ* or *ex situ*. *Ex situ* techniques, also called "pump and treat"—whether chemical such as the use of redox agents, or physical such as air-sparging—usually require less initial investment, but are energy intensive over the long-term, and ineffective at treating source-zone contamination [10]. All abiotic chemical treatment methods involve hydrolysis, elimination, reduction and/or oxidation. Examples of abiotic *in situ* remediation include: (*i*) addition of nucleophiles such as inorganic sulfide, or increasing pH and/or temperature to facilitate substitution/elimination [11], (*ii*) addition of *in situ* chemical oxidants, such as persulfate, permanganate, etc. with or without facilitators such as increased temperature, (*iii*) permeable reactive barriers (PRBs) made of granular iron that are placed in the flow path of groundwater, and (*iv*) injection of nanoparticles of iron/other reductants via injection wells [12].

Effect of redox potential on remediation. The use of the above mentioned *in situ* abiotic remediation techniques are dependent on the compound or mixture of compounds that needs to be remediated. Polychlorinated organics, such as CT, or trichloroethylene (TCE), are most amenable to reduction, due to the high electrophilicity of the carbon in the C—Cl bond, but are relatively poor candidates for oxidation [13]. Lesser-chlorinated VOCs such as chloromethane or dichloromethane are not very amenable to reduction for the same reason, and are more likely to degrade via oxidative techniques [14, 15] (Figure

1.1). Compounds such as TCP, or 1,2-DCA, though polychlorinated, are recalcitrant to both oxidation and reduction—in great part, due to the very weak electrophilicity of the carbon atom caused by electronegative chlorines being equally dispersed throughout the molecule—and react significantly only with strong redox agents [16, 17]. Thermodynamic reactivity with reductants (or affinity for electrons), and kinetics of reaction, both correlate with one-electron reduction potentials, and E_{LUMO} (energy of the lowest occupied molecular orbital for the contaminant) [18, 19]. Figure 1.2 shows E_{LUMO} values for commonly occurring groundwater contaminants. Lower E_{LUMO} values correlate with increased chlorination (or greater chlorines per carbon), and higher reduction potentials.

PROBE VOCS–CT AND TCP

In this study, we have selected two chlorinated alkanes on different ends of the redox and reactivity spectrum—CT and TCP—for analysis of reactivity via different redox pathways. CT and TCP are both "reasonably anticipated to be human carcinogens" [20, 21]. Primary routes of exposure include inhalation, ingestion, and dermal contact. CT levels in the environment are regulated by various regulations, including the clean air act (CAA), the clean water act (CWA), the comprehensive environmental response, compensation, and liability act (CERCLA), the safe drinking water act, the emergency planning and community right to know act (EPCRA), and the resource conservation and recovery act (RCRA). TCP, however, is an emerging contaminant, and is only regulated by the CAA, EPCRA, and RCRA [22, 23].

***Physical Properties*.** A summary of the physical properties of TCP (along with CT and TCE for comparison) is given in Table 1.1. The three constants listed: Henry's constant (H), the octanol-water partition coefficient (K_{ow}), and the soil-sorption coefficient, (K_{oc}) are a measure of partitioning between air/water, organic matter/water (or hydrophobicity), and soil/solution-phase respectively. The numbers in Table 1.1 indicate that hydrophobicities of both CT and TCP are similar to other organics. Neither compound partitions strongly to soil from solution. When exposed to air, CT is much more likely to volatilize than TCP—which is less volatile than water.

The physical characteristics mentioned above indicate that CT can partition easily to the atmosphere, and is thus more viable than TCP to “pump and treat” air-sparging technologies. However, its high atmospheric stability makes the process less meaningful than *in situ* reduction. TCP is a much more problematic and persistent contaminant in groundwater, however, atmospheric TCP can breakdown in sunlight due to photo-oxidative processes [20, 24].

Abiotic Reactivity. Both chemicals vary significantly in their abiotic reactivity. Hydrogenolysis is the predominant pathway via which CT reacts with most reducing agents. In PRBs, and other reducing media, CT tends to form chloroform (CF) as a major product, which can then further dechlorinate to dichloromethane (DCM), and chloromethane (CM). All three products are carcinogens, and progressively more recalcitrant towards reduction (Figure 1.1). Through an alternate pathway (via dichlorocarbene, which is formed by a 2 electron reduction of CT), CT can also form $HCOO^-$, CH_4, and CO [25] (Figure 1.3). Kinetic pathways of CT have been described in several earlier studies [14, 26]. An equally important current problem is to maximize benign byproducts—i.e., minimize yield of CF (Y_{CF})—while maintaining fast kinetics [27, 28].

TCP reacts significantly with oxidants and very strong reducing agents—where reduction takes place via elimination or hydrogenolysis depending on conditions. Reaction byproducts via reduction are usually mono- or di-chlorinated propanes or propenes [17, 29]. Strong reductants can potentially reduce TCP all the way to propene or propane. Hydrolysis or elimination is only significant in conditions with very high pHs (>11), and/or high temperatures [11, 30].

Bioremediation. Engineered bioremediation can be an efficient and sometimes, cost effective alternative to abiotic treatment. CT and TCP are predominantly degraded by anaerobic cultures. The highly oxidizing nature of the carbon in CT means that it can potentially function as an electron acceptor by a wide range of bacteria—sulfate reducers, methanogens, iron reducers, denitrifiers, acetogens, etc.—depending on the strength and availability of other acceptors such as nitrate, sulfate, Fe(III), etc [31]. In contrast, TCP can function as a weak electron donor/acceptor, but probably is neither in ambient environment, due to the presence of much stronger donors/acceptors. TCP is usually

degraded by cometabolic processes, though recently a genetically engineered bacterial culture has shown the capacity to use TCP as the primary energy source [32]. Generally, biodegradation of TCP is known to produce recalcitrant chlorinated byproducts, whereas biodegradation of CT has often produced low yields of CF [33, 34].

SUMMARY

Engineered remediation of TCP and CT can involve completely different pathways, and therefore, offer insights into treatment of mixed plumes. This is instructive because mixed plumes may sometimes require multiple sequential modes of remediation (with different redox conditions) to treat the contaminant and its chlorinated byproducts. Challenges to engineered remediation technologies (as mentioned earlier), can be logistical, kinetic, or related to production of recalcitrant and harmful byproducts. Logistic challenges include requirement/creation of artificial conditions such as pH, temperature, ionic strength, redox potential, etc. in groundwater. PRBs, which involve reduction by walls of granular iron placed in the flow path of groundwater [35], are among the most common technology used to dechlorinate DNAPLs. The limitations of this pathway—both kinetic and related to the formation of recalcitrant byproducts—have led to the evolution of a new technology with involves the injection of nanoparticles into groundwater via wells [12]. There are many uncertainties involved in this method [12], one of which (aging) is addressed in Chapter 3. Other uncertainties include transport and fate of nanoparticles once injected. Though it is likely that reactivity of nano-Fe^0 is much higher on a per particle basis, most of this is due to higher specific surface area. Reactivity of nanoparticles may be affected by their transport in groundwater (which is not expected to be more than a few meters), and formation of larger particles due to aggregation and cementation [12].

Therefore, even in the most well designed technologies for contaminant remediation, there are a number of hurdles that block a complete understanding of kinetics and pathways of VOC degradation. Other than those mentioned above, limitations that are particularly relevant to our research include: *(i)* prediction of product branching pathways, especially with CT, *(ii)* perception of faster kinetics with nano-sized

reductants, and *(iii)* synergistic behavior between reductant and reductate. Most of these uncertainties have been described with respect to reductants, because reductants typically constitute heterogeneous systems with greater potential to affect such processes. Besides other objectives, this study aims at getting a better understanding of (*i*), (*ii*), and (*iii*): Chapter 2 analyzes the effect of various parameters on product branching, Chapter 3 studies kinetics of reduction by iron nanoparticles, and Chapter 4 examines the changes in chemistry of iron and CT, and their synergistic effects.

IMPLICATIONS OF THIS STUDY

One of our objectives in this work was to develop a better understanding of the kinetics and pathways of dechlorination of CT. Chapter 2 describes the dependence of the yield of chloroform (Y_{CF}—a parameter that we want to minimize) on various experimental parameters. Y_{CF} was found to depend on the nature and composition of the oxide layer covering iron particles. Specifically, low values of Y_{CF} correlated with the presence of magnetite on iron surface, due to preferential stabilization of the dichlorocarbene, which can go on to form non-halogenated benign byproducts such as CH_4, $HCOO^-$, and CO. Kinetics of CT dechlorination were observed to be mass-transfer independent in chapter 3. The surface area normalized rate constant k_{SA} was shown to be the optimum parameter to compare kinetics between different iron-CT systems in a semi-*qualitative* fashion. A comparison of different iron types revealed that nano-sized iron particles were not intrinsically faster than micron-sized particles. However purer iron particles were faster than impure iron types. Still, injection of nanoparticles may be a viable technology due to the low loads of iron needed, and the low Y_{CF} values generated by some irons. In this context, it is important to overcome uncertainties associated with this technology. Chapter 4 addressed the aging of iron nanoparticles in solution. An initial depassivation of the oxide layer on the nanoparticles (maghemite in this specific case with unaged Fe^{H2}) was observed over two days of aging in solution, followed by re-oxidation to give a magnetite-rich oxide shell over long-term aging. This behavior had an effect on various parameters including k_{obs}, Y_{CF}, E_{corr}, H_2 production rate, etc, most of which exhibited a peaked profile (peaking at 2 days), when plotted against time.

Our other objective included studying pathways of dechlorination of TCP—a compound quite different in reactivity and redox potential than CT. TCP is an emerging contaminant beginning to be observed in drinking water wells in California, and has not been studied extensively earlier. In Chapter 5, we studied feasibilities and kinetics of dechlorination of TCP via all possible natural and engineered pathways, e.g., reduction, oxidation, hydrolysis, and elimination. TCP was quite recalcitrant towards all processes except oxidation. However strong reducing conditions—such as Zn, or Fe/Pd—caused reduction of TCP over the order of 2 weeks or so. Strong oxidants like persulfate, showed fast and efficient degradation of TCP with minimal chlorinated byproducts over the order of 1-2 days. However, natural attenuation was not viable for TCP degradation, except where pH and/or temperature were very elevated.

REFERENCES

1. Riley, R. G.; Zachara, J. M.; Wobber, F. J. *Chemical Contaminants on DOE Lands and Selected Mixtures for Subsurface Science Research*; DOE/ER-0547T Richland, WA, 1992; p 77.

2. Pankow, J. F.; Cherry, J. A., *Dense Chlorinated Solvents and Other DNAPLs in Groundwater: History, Behavior, and Remediation*. Waterloo Press: Portland, OR, 1996; p 522.

3. Innovative Treatment Remediation Demonstration Program *Literature Review: Natural Attenuation Mechanisms and Rates for Chloromethane Subsurface Contaminants at Hanford;* Albuquerque, NM, 2000; p 33.

4. Jeffers, P. M.; Ward, L. M.; Woytowitch, L. M.; Wolfe, N. L., Homogeneous hydrolysis rate constants for selected chlorinated methanes, ethanes, ethenes, and propanes. *Environ. Sci. Technol.* **1989,** *23* (8), 965-969.

5. Kriegman-King, M. R.; Reinhard, M., Transformation of carbon tetrachloride in the presence of sulfide, biotite, and vermiculite. *Environ. Sci. Technol.* **1992,** *26* (11), 2198-2206.

6. Barbash, J. E.; Reinhard, M., Abiotic dehalogenation of 1,2-dichloroethane and 1,2-dibromoethane in aqueous solution containing hydrogen sulfide. *Environ. Sci. Technol.* **1989,** *23* (11), 1349-1357.

7. Ventullo, R. M.; Larson, R. J., Metabolic diversity and activity of heterotrophic bacteria in ground water. *Environ. Toxicol. Chem.* **1985,** *4* (6), 759-771.

8. Leisinger, T., Microorganisms and xenobiotic compounds. *Experientia* **1983,** *39* (11), 1183.

9. Alexander, M., Biodegradation of organic chemicals. *Environ. Sci. Technol.* **1985,** *18* (2), 106-111.

10. Mackay, D. M.; Cherry, J. A., Groundwater contamination: Pump-and-treat remediation. *Environ. Sci. Technol.* **1989,** *23* (6), 630-636.

11. Pagan, M.; Cooper, W. J.; Joens, J. A., Kinetic studies of the homogeneous abiotic reactions of several chlorinated aliphatic compounds in aqueous solution. *App. Geochem.* **1998,** *13* (6), 779-785.

12. Tratnyek, P. G.; Johnson, R. L., Nanotechnologies for environmental cleanup. *NanoToday* **2006,** *1* (2), 44-48.

13. March, J., *Advanced Organic Chemistry: Reactions, Mechanisms, and Structure.* McGraw-Hill: New York, 1977; p 1328.

14. Matheson, L. J.; Tratnyek, P. G., Reductive dehalogenation of chlorinated methanes by iron metal. *Environ. Sci. Technol.* **1994,** *28* (12), 2045-2053.

15. Kieblinga, D.; Schneidera, R.; Kraak, P.; Haftendornb, M.; Wendta, G., Perovskite-type oxides – catalysts for the total oxidation of chlorinated hydrocarbons. *App. Cat. B-Environ.* **1998,** *19* (2), 143-151.

16. Hunter, F., Fenton's treatment of 1,2,3-trichloropropane: chemical reaction byproducts, pathways, and kinetics. In *Proceedings of the International Symposium on Chemical Oxidation: Technology for the Nineties*, Technomic: 1997; Vol. 6, p 50-71.

17. Klausen, J.; Vikesland, P. J.; Kohn, T.; Burris, D. R.; Ball, W. P.; Roberts, A. L., Longevity of granular iron in groundwater treatment processes: solution composition effects on reduction of organohalides and nitroaromatic compounds. *Environ. Sci. Technol.* **2003,** *37* (6), 1208-1218.

18. Scherer, M. M.; Balko, B. A.; Gallagher, D. A.; Tratnyek, P. G., Correlation analysis of rate constants for dechlorination by zero-valent iron. *Environ. Sci. Technol.* **1998,** *32* (19), 3026-3033.

19. Totten, L. A.; Roberts, A. L., Calculated one- and two-electron reduction potentials and related molecular descriptors for reduction of alkyl and vinyl halides in water. *Crit. Rev. Environ. Sci. Technol.* **2001,** *31* (2), 175-221.

20. Agency for Toxic Substances and Disease Registry, US Public Health Service Commissioned Corps, *Toxicological profile for 1,2,3-Trichloropropane*; 1992; p 119.

21. Agency for Toxic Substances and Disease Registry, U.S. Public Health Service Commissioned Corps, *Toxicological Profile for Carbon Tetrachloride,* 1989; p 145.

22. 11th Report on Carcinogens, National Toxicology Program, *1,2,3-trichloropropane*; NIH: 2005.

23. 11th Report on Carcinogens, National Toxicology Program, *Carbon Tetrachloride*; NIH: 2005.

24. Mu, Y. J.; Mellouki, A., Rate constants for the reactions of OH with chlorinated propanes. *Phys. Chem. Chem. Phys.* **2001,** *3* (13), 2614-2617.

25. Criddle, C. S.; McCarty, P. L., Electrolytic model system for reductive dehalogenation in aqueous environments. *Environ. Sci. Technol.* **1991,** *25* (5), 973-978.

26. Johnson, T. L.; Scherer, M. M.; Tratnyek, P. G., Kinetics of halogenated organic compound degradation by iron metal. *Environ. Sci. Technol.* **1996,** *30* (8), 2634-2640.

27. Támara, M.; Butler, E. C., Effects of iron purity and groundwater characteristics on rates and products in the degradation of carbon tetrachloride by iron metal. *Environ. Sci. Technol.* **2004,** *38* (6), 1866-1876.

28. Nurmi, J. T.; Tratnyek, P. G.; Sarathy, V.; Baer, D. R.; Amonette, J. E.; Pecher, K.; Wang, C.; Linehan, J. C.; Matson, D. W.; Penn, R. L.; Driessen, M. D., Characterization and properties of metallic iron nanoparticles: Spectroscopy, electrochemistry, and kinetics. *Environ. Sci. Technol.* **2005,** *39* (5), 1221-1230.

29. Focht, R. M.; Gillham, R. W., Dechlorination of 1,2,3-Trichloropropane by zero-valent iron, Preprint Extended Abstracts. In *209th ACS National Meeting*, American Chemical Society, Division of Environmental Chemistry: Anaheim, CA, 1995; Vol. 35, No. 1, p 741-744.

30. Ellington, J. J. *Hydrolysis rate constants for enhancing property-reactivity relationships*; Office of Research and Development,Environmental Research Lab, Athens, GA, USA: 1989; p 59.

31. Boopathy, R., Anaerobic biotransformation of carbon tetrachloride under various electron acceptor conditions. *Biores. Technol.* **2002,** *84*, 69-73.

32. Bosma, T.; Janssen, D. B., Conversion of chlorinated propanes by Methylosinus trichosporium OB3b expressing soluble methane monooxygenase. *App. Microbiol. Biotechnol.* **1998,** *50* (1), 105-112.

33. Van Eekert, M. H. A.; Schroder, T. J., Degradation and fate of carbon tetrachloride in unadapted methanogenic granular sludge. *App. Environ. Microbiol.* **1998,** *64* (7), 2350-2356.

34. Egli, C.; Tschan, T.; Scholtz, R.; Cook, A. M.; Leisinger, T., Transformation of tetrachloromethane to dichloromethane and carbon dioxide by Acetobacterium woodii. *App. Environ. Microbiol.* **1988,** *54* (11), 2819-2824.

35. Tratnyek, P. G.; Scherer, M. M.; Johnson, T. J.; Matheson, L. J., Permeable reactive barriers of iron and other zero-valent metals. In *Chemical Degradation Methods for Wastes and Pollutants: Environmental and Industrial Applications*, Tarr, M. A., Ed. Marcel Dekker: New York, 2003; p 371-421.

36. Vogel, T. M.; Criddle, C. S.; McCarty, P. L., Transformations of halogenated aliphatic compounds. *Environ. Sci. Technol.* **1987,** *21* (8), 722-736.

Table 1.1. Physical properties of 1,2,3-trichloropropane, as compared to carbon tetrachloride, and trichloroethylene.

Property	1,2,3-TCP	CT	TCE	Notes
Vapor Pressure	3.1	99.3	131.5	Torr (mm Hg) @ 25º C
Henry's Constant	2.94	286	93.7	x 10^{-4} atm m^3 $mole^{-1}$ @ 25º C
Solubility	1.75	0.8	1.1	g/L @ 20º C
log K_{oc}	1.99	2.04	126	
log K_{ow}	1.98 – 2.54	2.64	2.42	

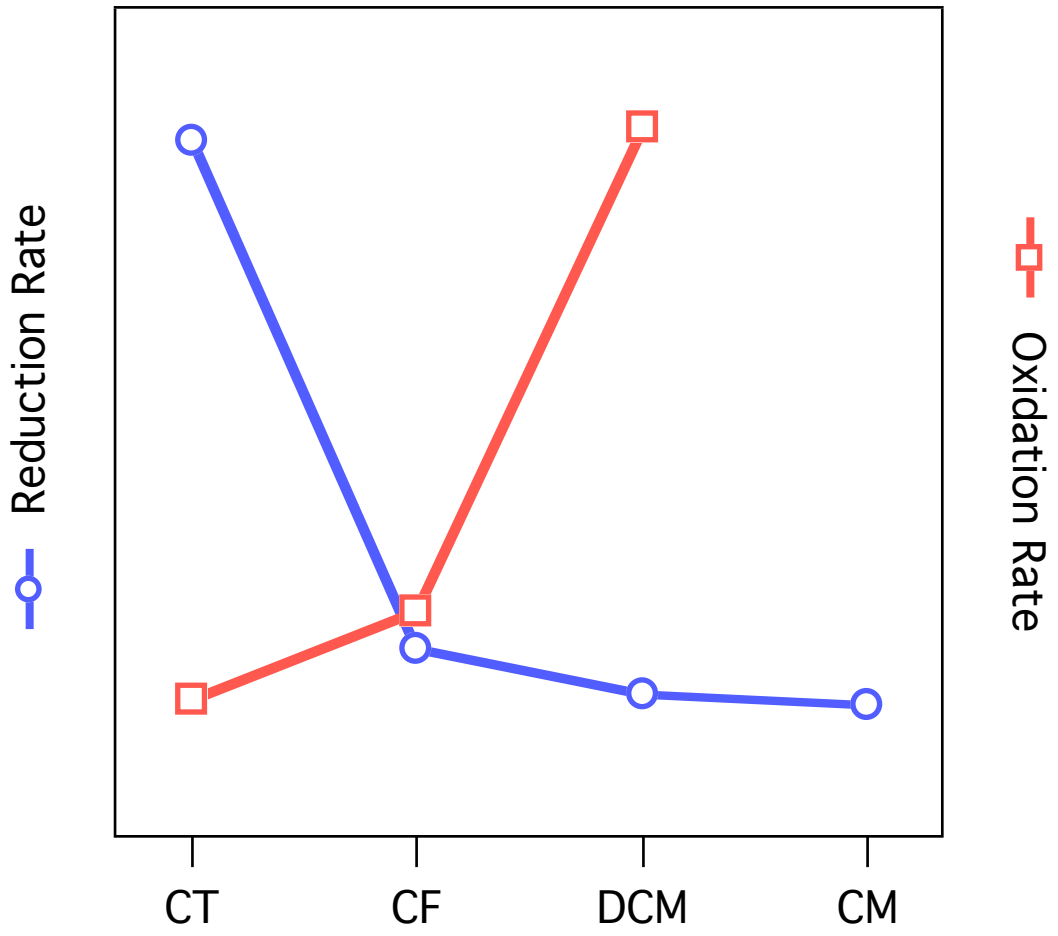

Figure 1.1. Variation of reduction and oxidation rates with extent of chlorination of methanes. CT, CF, DCM, and CM stand for carbon tetrachloride, chloroform, dichloromethane, and chloromethane, respectively. Adapted from [36].

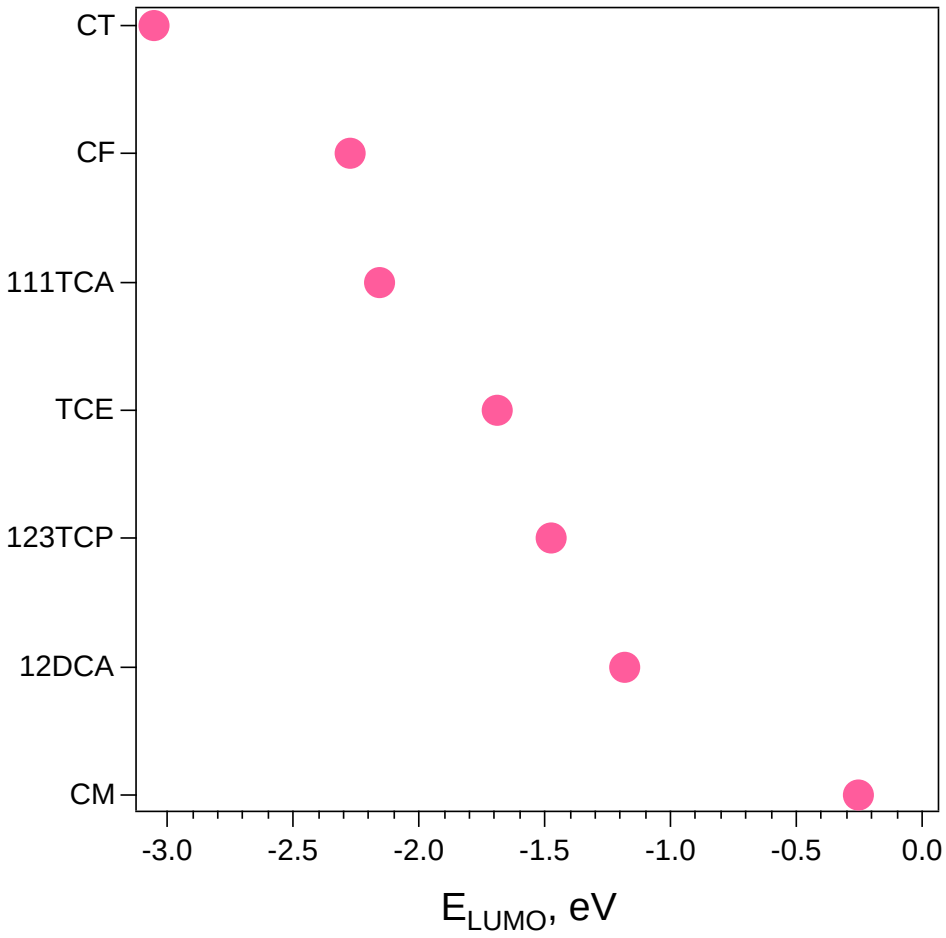

Figure 1.2. LUMO (lowest occupied molecular orbital) energies plotted for different chlorinated aliphatics [18].

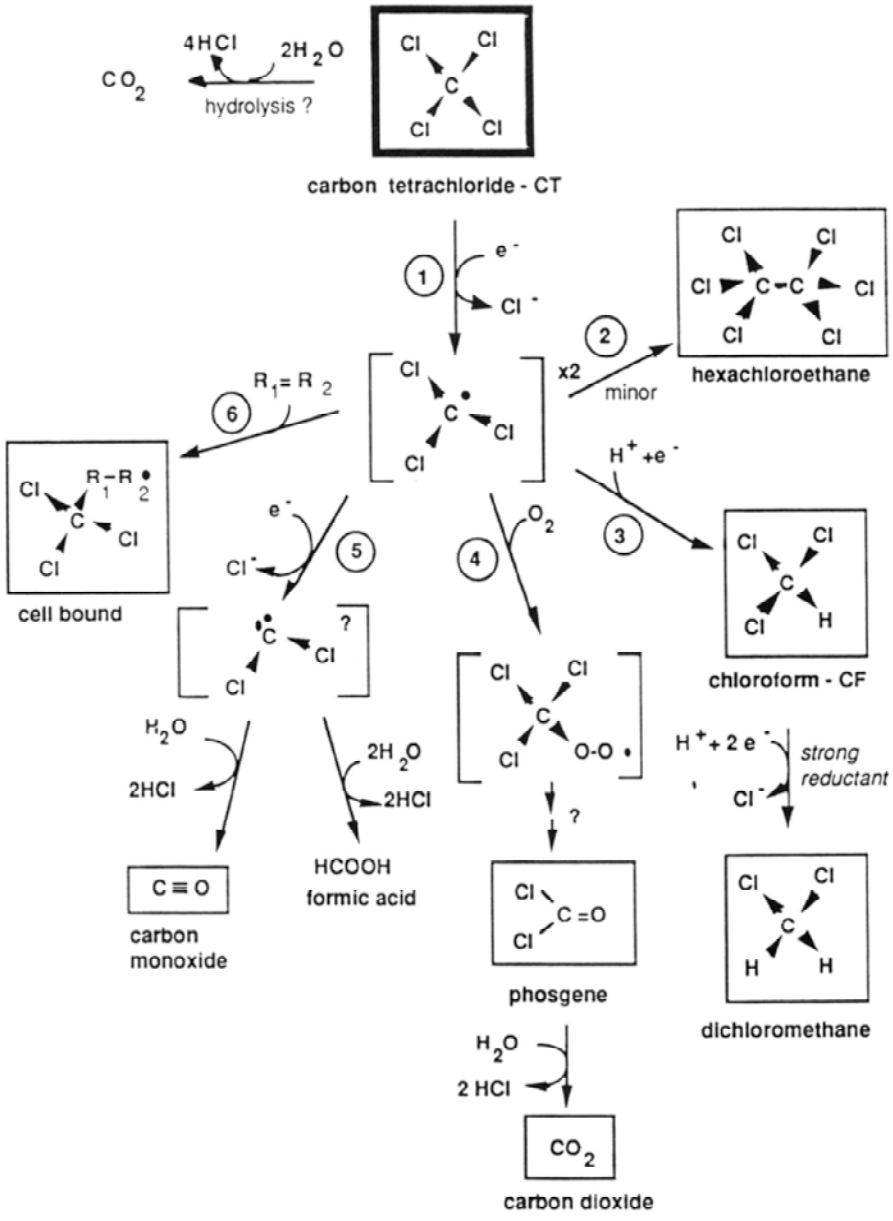

Figure 1.3. Pathways of reductive dechlorination of carbon tetrachloride Reprinted with permission from Criddle et al. 1991, ES&T [25]. Copyright (1991) American Chemical Society).

2

Pathways of Degradation of Carbon Tetrachloride: influence of reductant and other variables

Abstract

The degradation of carbon tetrachloride (CT) is known to proceed via two pathways, one forming the more toxic and recalcitrant chloroform (CF), and the other forming relatively benign products such as CO, CH_4, and formate ($HCOO^-$). The objective of this study was to improve our current knowledge of the interface between surface chemistry of the iron (oxidation state, oxide composition, etc.), reductive capacity of iron, and pathways of degradation of CT, in order to be able to minimize the yield of CF (Y_{CF}). Fe^{H2}, a nano-sized iron with a core of Fe^0 and a shell of magnetite was our probe iron type for most experiments. Experiments conducted with Fe^{H2} of different ages indicated that the presence of magnetite on the surface is likely responsible for lowering Y_{CF}. The use of radical traps (d8-isopropanol, which is a $D^\bullet$ donor), and experiments conducted in D_2O (a D^+ donor) indicated that $CCl_3^\bullet$ is not a controlling intermediate in the formation of CF. We also proposed an alternate pathway for CT dechlorination where CCl_3^- is formed by a concerted $2e^-$ reduction (with simultaneous dissociation of a C—Cl bond), without $CCl_3^\bullet$ being formed as an intermediate. From experiments that varied pH to test effects on Y_{CF}, we deduced that in this system CCl_3^- is found only in solution phase. Therefore, the major factor influencing Y_{CF} formation is the surface stabilization of the carbene.

Surfaces or conditions that can force the CCl_3^- to go to the carbene versus into solution, such as a magnetite-rich surface, will help lower Y_{CF}.

INTRODUCTION

Zero-valent iron (Fe^0) is among the strongest abiotic reducing agents that react with carbon tetrachloride (CT), and are applicable in groundwater remediation strategies. Fe^0 degrades CT a few orders of magnitude faster than other reducing iron systems such as magnetite, pyrite, and Fe^{2+} sorbed on goethite [1-7]. CT reduction by iron typically follows pseudo-first order kinetics in the presence of excess iron, and is believed to proceed via two parallel competing pathways (Figure 2.1): one forms the toxic and more recalcitrant chloroform (CF) and dichloromethane (DCM) as the major and minor products respectively, and the other leads to relatively benign, and hence, more environmentally desirable products like formate ($HCOO^-$), carbon monoxide (CO), and in some cases, methane (CH_4) [1, 5, 6].

One of the primary concerns with CT reduction by most reductants, is the high yield of CF that is often obtained [2-6, 8]. Batch experiments using Fisher Electrolytic Iron (Fe^{EL}, 100 mesh)—a reagent-grade, micron-sized Fe^0—have typically produced 50-80% CF, as reported in numerous earlier studies [2-4], and confirmed in results presented here. Research groups working with iron oxides in batch systems have found similar yields of CF with predominantly Fe^{3+} systems like Fe^{2+} adsorbed on goethite, but lower yields with magnetite [1, 5, 8].

The yield of CF (Y_{CF})—operationally defined here as the fraction of CT reacted that appears as CF—is likely to be affected by a wide range of system variables including pH, buffer, solution chemistry, surface chemistry (and oxidation state) of the iron, iron loading, history and handling of Fe^0 used, etc. [2, 4, 9]. Figure 2.2, which is a fundamental and interpretive conceptual model of the processes shown in Figure 2.1, also shows reactive intermediates involved in product branching. It can be seen that Y_{CF} will primarily depend on the relative stabilities and reactivities of the intermediates $CCl_3^{\bullet}$, CCl_2:, and CCl_3^-, which can in turn be affected by the nature of the surface or solution chemistry. The nature of the surface (and hence the iron type) may affect the product

distribution in at least two ways: (*i*) by contributing sorbed protons or hydrogen atoms to the above mentioned intermediates which can then form CF, and/or (*ii*) by (de)stabilizing $CCl_3^{\bullet}$, CCl_2:, or CCl_3^-. Similarly, it is likely that the availability or lack of $H^{\bullet}$ or H^+, either sorbed on the surface or in solution, can favor CF pathway or the carbene pathway, respectively.

However, the current understanding of factors controlling the mechanism of CT degradation is not rigorous enough that we can predict the Y_{CF} under any particular conditions. One major focus of our work, therefore, is to develop a more complete understanding and control of experimental factors that affect Y_{CF}, with emphasis on microscopic effects of macroscopic variables on surface chemistry. In particular, the objective of this chapter was to understand the mechanism of CT degradation on iron surfaces in order to be able to minimize Y_{CF}.

In order to study the dynamics and relative stabilities of different radical species as they influence the yield of chloroform, we analyzed the effects on Y_{CF} of varying *(i)* $[CT]_0$ with respect to iron loading, *(ii)* chloride concentrations, *(iii)* isotopic composition of the solvent, and *(iv)* pH. To look at the role the surface properties of the iron/oxides played in CT degradation, we compared different iron types. The effect of aging of iron nanoparticles on Y_{CF} has been analyzed in Chapter 4.

Irons from different sources (of different sizes and compositions) were used to study reactivity with CT. Fe^{H2} (a nano-sized iron) was, however, used predominantly as a probe in this study because (*i*) it is relatively easy to study surface (oxide) changes as a function of time, in nano-sized iron particles, (*ii*) the increasing use of iron nanoparticles in the remediation industry increases their relevance as potential dechlorinating agents of chlorinated aliphatics, and (*iii*) Fe^{H2} in particular had a consistently lower Y_{CF} compared to other iron types [2].

MATERIALS AND METHODS

Reagents. All chemicals were obtained in the highest purity commercially available and used as received. These include carbon tetrachloride and chloroform (Sigma Aldrich, HPLC grade); deuterated chloroform, deuterated water, per-deuterated (d8) isopropanol,

and sodium chloride (Fisher Chemicals); nitrogen gas (Airgas Inc.). All stocks and reaction solutions were prepared with N_2 degassed deionized water.

Iron Samples. The nano-particulate iron types used in this study were obtained from 4 sources. The material from Toda Americas Inc. (Schaumberg, IL) is produced by reduction of goethite and hematite by H_2 at high temperatures (200 – 600 °C). Two other samples of nano-sized iron we used were both prepared by reductive precipitation of $FeCl_3$ with $NaBH_4$. Throughout, we refer to these materials as Fe^{H2} and Fe^{BH} respectively, as we did in a previous publication [2]. We used two Fe^{BH} samples from (*i*) W.-X. Zhang (Lehigh University) [10] (also called aged Fe^{BH} in this paper due to its being much older than the other sample), and (*ii*) J. Linehan (PNNL, Richland, WA). Ball milled nano iron (Fe^{AR}) was supplied from Arcadis Inc. (Colorado). The other micron-sized and granular iron types we used were 100 mesh electrolytic iron (Fe^{EL}) from Fisher (Pittsburgh, PA, 99%), and construction grade iron (Fe^{PL}) from Peerless powders and abrasives (Detroit, MI, "PMP traditional" size 8/50, > 90%).

The nano-sized iron samples were stored in an anoxic glove box (95% N_2, 5% H_2); Fe^{EL} and Fe^{PL} were stored in a vacuum desiccator. All nano iron samples except the Fe^{BH} from J. Linehan (which was received dry), were obtained from the supplier in a slurry form and were "flash dried"[1] with acetone [2]. The surface areas measured by BET gas adsorption were 5.2 ± 1.95, 5.0, 28.6, 1.94, 0.12, 1.54 m^2/g respectively for Fe^{H2}, Fe^{BH}, aged Fe^{BH}, Fe^{AR}, Fe^{EL}, and Fe^{PL}.

Experimental Procedure. Batch reactions were performed to test the rate of reduction and product yield during CT degradation using different types of iron. In an anoxic chamber, a pre-determined mass of iron was put in 120 mL serum vials such that the total surface area of the iron ranged from 0.3 to 1.5 m^2/L. The vials were then filled with de-ionized de-oxygenated water (N_2 sparged), then capped with Hycar rubber septa, leaving no headspace, crimp-sealed and covered with aluminum foil to exclude light effects. The time taken to inject CT through the septum after adding water to the iron in the vial is referred to as the "pre-exposure time", typically 24 hours. The 24 hour pre-exposure

[1] Flash-drying is a procedure by which we vacuum dried iron slurry in an anoxic atmosphere by rinsing with acetone [2].

period allowed pH to stabilize to a relatively stable pH of ~10 which is important because all the experiments in this study were unbuffered. CT (usually 0.1 mL) was introduced as a saturated aqueous stock solution which gave an initial concentration ($[CT]_0$) of 4.01 x 10^{-6} M. A number of experimental parameters were varied within this batch reaction system including [CT_0], isotopic composition of solvent, chloride concentration, pH and iron type. Replicates and controls without iron were done for most experiments. In experiments where pH was varied, only 1M HCl and NaOH were used to control pH, in order to avoid secondary buffer effects. These were typically added 1 hour prior to spiking with CT.

The vials were mixed on a rotary shaker at 24 rpm at room temperature during reaction, and samples (usually 0.1 mL) were taken out at regular time intervals, and diluted to 10 mL in 20 mL headspace autosampler vials. The headspace of these vials was analyzed by gas chromatography (GC; DB 624 column from Agilent Inc.) with electron capture detection (ECD), to measure for CT and CF. Experiments, which involved analysis of deuterated products, were performed in vials with 30 mL water, and 30 mL headspace. After CT injection, these vials were shaken, headspace samples were withdrawn at regular intervals and directly injected in an Autosystem XL GC with a TurboMass Gold mass spectrometer (MS). It was assumed that equilibration between headspace and solution was instantaneous relative to the rate of reaction.

Kinetics and Y_{CF} determination. We arrived at equations (1) and (2) to model the pseudo-first order disappearance and appearance of CT and CF respectively. $[CT]_0$ and $[CT]_t$ are the concentrations of CT initially and at time *t* respectively; Y_{CF} is mathematically defined in equation 3. Equations 1 and 2 were then fit globally to obtain values for k_{CT} and Y_{CF}.

$$[CT]_t = [CT]_0 e^{-k_{CT}t} \quad (1)$$

$$[CF]_t = [CT]_0 Y_{CF}(1 - e^{-k_{CT}t}) \quad (2)$$

$$Y_{CF} = \frac{[CF]_\infty}{[CT]_0} \quad (3)$$

In the deuterated experiments where headspace was directly analyzed with the GC/MS, k_{CT} was calculated according to the method described in [7], and Y_{CF} was calculated as a ratio of CF remaining to CT consumed at the end of the experiment, and not from equations 1 and 2.

Fitting. A number of fitting procedures were tried to obtain most consistent results. Fitting of equation 2.1, 2.2, and 2.3 was generally carried out either by floating or fixing $[CT]_0$. It was observed that fixing $[CT]_0$ to the nominal value gave us most consistent results. Variation of fitting techniques did not affect k_{CT} significantly but caused small variations in $[CT]_0$, which in turn caused large fluctuations in Y_{CF} since $Y_{CF}=\frac{[CF]_\infty}{[CT]_0}$.

Y_{CF} can be determined in one of four ways: *(i)* by letting CT float while fitting data through equations 2.1-2.3 together, *(ii)* by fixing CT, while fitting data through equations 2.1-2.3 together, *(iii)* fixing CT and globally fitting equations 2.1-2.3 for a large data set, and *(iv)* assigning $Y_{CF} = \frac{[CF]_t}{[CT]_{reacted,t}}$, using end-point data at time *t*. Figure 2.3 shows a typical concentration versus time plot for disappearance of CT, and different Y_{CF} values obtained from fits *(i)* and *(ii)*. After experimenting with the various fitting methods, we concluded that the most consistent set of Y_{CF} values came from methods *(ii)* and *(iii)*.

RESULTS AND DISCUSSION

Comparison of different irons. We showed previously that Y_{CF} followed the trend $Fe^{H2} < Fe^{BH} < Fe^{EL}$ [2]. Here, we verify this key finding by repeating experiments with Fe^{H2}, aged Fe^{BH}, and Fe^{EL}, and also testing Fe^{AR}, Fe^{BH}, and Fe^{PL} for the first time. Among the different types of iron, Fe^{H2} and Fe^{AR} consistently gave the lowest Y_{CF} (Figure 2.4A). Microscopic and spectroscopic analyses like transmission electron microscopy (TEM), X-ray photoelectron spectroscopy (XPS), and X-ray diffraction (XRD) on Fe^{H2} and Fe^{BH} have earlier revealed an Fe^0 core in both cases, and a shell composed predominantly of magnetite and boron-rich oxides, in each case respectively [2]. Other irons like Fe^{EL} are expected to have significant exposure of Fe^0 to solution. We have hypothesized that the

low Y_{CF} shown by Fe^{H2} may be in part due to its magnetite shell, and Fe^0-solution contact may result in higher Y_{CF} [2].

In experiments where we measured Y_{CF} as a function of pre-exposure of Fe^{H2} to water (Chapter 4), Y_{CF} was found to decrease with increasing levels of magnetite, and increase with Fe^0-solution contact. These results, and the fact that other researchers have observed low Y_{CF} values with pure magnetite [1, 11], may indicate that the presence of a significant quantity of magnetite on the surface is a factor in favoring the dichlorocarbene pathway. Other systems that have yielded low levels of chloroform are those with palladized iron as the reductant [12], where low Y_{CF} values are due to more complete reduction of CT, CF, and DCM via hydrogenolysis, rather than a change in the relative distribution of the product forming pathways.

Relative iron loading. The effect of the relative CT dose ([CT] relative to [Fe]) on Y_{CF} was analyzed by keeping [Fe^0] constant, while varying $[CT]_0$ from 0.4 mM to 0.1 mM using three types of iron—Fe^{H2}, Fe^{BH}, and Fe^{EL}. Since earlier studies have shown that rate increases proportionally with mass of Fe^0 [3], and may also be dependent on $[CT]_0$ [13], this variation was expected to affect rate rather than Y_{CF}. The lack of any trend in Y_{CF} (Figure 2.4B) indicates that the availability of reactive surface sites is not limiting, even at high $[CT]_0$, to stabilize CCl_3^- and/or CCl_2: (given than relative stabilities of these species may influence Y_{CF}).

Concentration of chloride. Previous studies have suggested that chloride could affect the rate of CT degradation by Fe^0, possibly via pitting on the iron-oxide surface [13, 14]. However, evidence for this hypothesis is still weak. In this study, we varied chloride concentrations to test an alternate hypothesis—that it would influence Y_{CF} via one or more potentially reversible steps involving Cl^- (Figure 2.2), such that increasing chloride concentrations would cause decreased production of the dichlorocarbene and therefore increase Y_{CF} (Le Chatelier's principle). Chloride concentrations were varied from 0 to 40 mM. In the same set of experiments, age of the iron (in solution) was also simultaneously varied up to 20 days. Trends in aging were the same as with no chloride in the system (data not shown). Neither k_{CT} nor Y_{CF} showed any trend with increasing chloride concentration. We hypothesize that this may be because: (*i*) chloride by itself does not

cause sufficient change in oxide surface chemistry to affect either k_{CT} or Y_{CF}, and (*ii*) the reaction $CCl_3^- \rightarrow CCl_2{:} + Cl^-$ is not reversible in our system.

Isotope effects. In trying to elucidate pathways of dechlorination, we wanted to determine the relative roles of $CCl_3^{\bullet}$ and CCl_3^- in the formation of CF (Figure 2.2) by adding $D^{\bullet}$ and D^+ donors that should give diagnostic products that we could analyze via GC/MS. To compare the effect of proton and hydrogen atom donors on Y_{CF}, we conducted experiments in H_2O, D_2O, and H_2O with 3.9 mM d8-isopropanol, with Fe^{H2} as the reductant, and 0, 1, and 3 day pre-exposures in each set-up. The different pre-exposures were carried out to account for possible slow kinetics of H^+/D^+ exchange between surface hydroxyls and the solvent.

The products obtained under each experimental condition are summarized in Table 2.1. Starting with the assumption that (in the heavy water system) D_2O only provides D^+ and not $D^{\bullet}$, the fact that the only product observed in the reactions conducted in D_2O was $CDCl_3$ indicates that $CCl_3^-{:} + D^+ \rightarrow CDCl_3$ is the pathway by which products are formed, and $CCl_3^{\bullet}$ does not lead directly to products. In contrast, in Fe^{2+}/goethite systems with CCl_2Br_2 in D_2O, $CHCl_2Br$ rather than $CDCl_2Br$ has been observed as the major product [8]. These data are not sufficient to draw a conclusion about the role of surface hydroxyls in the formation of $CHCl_3$ (Table 2.1).

The Y_{CF} values for both H_2O systems (with and without d8-isopropanol) showed similar values and trends. They were ~0.5 for the 0-day pre-exposure system, and ~0.3 for the 1- and 3-day pre-exposure systems. This decrease in Y_{CF} with pre-exposure time is most likely related to the aging of the iron, and has been attributed to an increase in oxide (magnetite) upon increased pre-exposure (Chapter 4). The D_2O system showed lower Y_{CF} values than the H_2O systems at 0- and 1-day pre-exposures, perhaps due to probable lower solubility of CCl_3^- in D_2O versus H_2O [15], and/or lower rates of reaction due to a kinetic isotope effect.

d8-isopropanol, was injected in roughly equimolar concentrations to CT in the 0- and 1-day pre-exposure systems, and in concentrations 1000 times in excess in the 3-day pre-exposure system, and therefore should have been equal to or in excess of any $CCl_3^{\bullet}$ produced in the systems. It is a $D^{\bullet}$ donor and was therefore expected to act as a trap for,

and hence test for the presence of, $CCl_3^{\bullet}$ radicals. However, since no $CDCl_3$ was produced, we must conclude that the $CCl_3^{\bullet}$ radical is not active in producing CF either because: (*i*) the radical itself is not formed (the trichloromethyl anion being formed in a concerted 2 e^- transfer with cleavage of one chloride, from CT), or (*ii*) it is very short lived and therefore does not react even with a radical-trap like $D^{\bullet}$.

At least one other study on the reduction of CT by magnetite coated iron cathodes has shown production of near-stoichiometric CH_4 (a product of the carbene pathway) without any intermediate CF (implying that $CCl_3^{\bullet}$ may have been skipped) [16]. In contrast, in both Fe^{2+}/goethite systems, and biogenic magnetite systems, the presence of $CCl_3^{\bullet}$ was confirmed by d8-isopropanol experiments, and radical trapping experiments using dimethylbutene (DMB) respectively [1, 5]. We hypothesize that the contradiction arises because of the higher reducing capacity of Fe^{H2} nanoparticles, which have an Fe^0 core, and may therefore favor a concerted 2 e^- reduction to CCl_3^-. In fact, a 2 e^- transfer (with simultaneous cleavage of 2 C–Cl bonds) is thermodynamically favored over 1 e^- reduction to form $CCl_3^{\bullet}$ [17]. However studies on goethite/Fe^{2+} systems have shown that this does not occur [5], and we do not consider cleavage of 2 C–Cl bonds to be likely. These interpretations suggest a scheme for the reduction of CT in Figure 2.5, which is a modified version of Figure 2.2 and takes into account both the passive nature of the $CCl_3^{\bullet}$ radicals and the 2 e^- transfer with cleavage of 1 C-Cl bond.

Effect of pH and surface charge on mechanism. The existence of CCl_3^- as a surface stabilized species is likely to depend on the pH of the system [7]. The pH at which we worked (~9, which is higher than point of zero charge—pzc—of magnetite [18]) would cause the magnetite surface to be negatively charged, and destabilize the trichloromethyl anion. The CCl_3^- formed on the surface can then go to solution phase to form CF. We therefore expect Y_{CF} to increase with increasing pH as shown in [7].

We varied the pH of the batch system by adding 1M NaOH and/or 1M HCl in order to not introduce potential passivating agents (inorganic buffers like borate, phosphate, etc.), or hydrogen atom donors (all organic buffers). k_{CT} was observed to increase with increasing pH (Figure 2.6A). This trend is opposite of that reported in [3] (where Fe^{EL} was the reductant), but follows the trend in [7] (where magnetite was the

reductant), indicating that the CT reduction by Fe^{H2} is mediated by the magnetite surface. This trend may be reflective of more negatively charged surfaces favoring higher rates due to higher electron density [7].

On the basis of the predominant trend, we interpreted Figure 2.6B to mean that Y_{CF} shows no trend with pH. If the reaction $CCl_3^- + H^+ \rightarrow CHCl_3$ occurs on the surface, or if CCl_3^- were a surface species, Y_{CF} would have been expected to increase with decreasing pH (due to increased stability of CCl_3^- on the positively charged surface). Since this does not occur, it is very likely that this reaction occurs only in the solution phase, and therefore CCl_3^- likely exists only in solution phase. In this case, increasing pH will decrease solution phase $[H^+]$. We can explain Y_{CF} being independent of solution phase $[H^+]$, because Y_{CF} is limited by $[CCl_3^-]$ which is much lower in concentration than $[H^+]$ at any instant. It follows that product branching must be dependent on the dynamics of surface stabilized CCl_3^- going into solution phase, or to the carbene.

Other effects. CO, CH_4, and $HCOO^-$ are expected to be among the products produced in the dichlorocarbene pathway [1, 5, 19]. We analyzed for CO and CH_4 at the end of some batch reactions, but did not measure either compound. While it is possible that we do not have CH_4 in our system, we wanted to interpret the lack of CO observed by studying the adsorption of CO on irons used in this study. From Figure 2.7, we see that CO does not sorb significantly to Fe^{H2}. However, when Fe^{EL} is added to a solution saturated in CO, greater than 50% of the CO sorbs on to Fe^{EL} in 2 hours (which is the timeframe of our batch experiments). This can have at least two important implications: first, [CO] measured at the end of the experiment will be impacted, and second, sorption of CO on Fe^0 may have secondary effects on the dichlorocarbene pathway—either by reducing active surface sites where radical intermediates may be stabilized, or by decreasing the activation energy for production of CO. However, the majority of our experiments were with Fe^{H2} to which CO does not sorb much. Therefore, this is not expected to impact our results significantly.

CONCLUSIONS AND IMPLICATIONS FOR REMEDIATION

Our interpretation of the modified reaction pathways in Fe^{H2}/CT systems (Figure 4) suggests a correlation between reductive capacity, oxidation state of iron, composition of the surface (i.e., oxide layer), and the pathways of degradation of CT. We had hypothesized that changing the surface charge on the surface—by varying the pH around the pzc—would affect the stability of CCl_3^- and hence change Y_{CF}. This is unlikely if the CCl_3^- is in solution phase. Our earlier hypothesis that the reaction $CCl_3^- \rightarrow CCl_2: + Cl^-$ is irreversible in this system, is in fact consistent with our observation that CCl_3^- reacts to form CF only in solution phase (or goes to CCl_2:).

Magnetite on the surface of iron appears to help lower Y_{CF}, most likely by stabilization of a radical intermediate. In this system, this intermediate has to be the dichlorocarbene. To reiterate our understanding of Figure 4 in the context of the Fe^{H2}-water-CT system, (*i*) $CCl_3^{\bullet}$ is not significant in this system, (*ii*) CCl_3^- formed on the surface dissociates to surface stabilized carbene, or partitions into solution phase where it can react with protons to form CF, and (*iii*) CCl_2: exists only as a surface-stabilized intermediate, due to which extent of product branching depends on stability of CCl_2:, and hence on the oxide surface.

The presence of an Fe^0 core and magnetite shell in Fe^{H2} may: (*i*) offer an increased reductive capacity over pure magnetite, and (*ii*) help in lowering Y_{CF} to values less than 25% due to the magnetite shell. Given that most studies of iron oxides (other than magnetite) and Fe^0 report Y_{CF} of 50% or higher, our findings are particularly significant for *in situ* remediation of CT, since magnetite coated Fe^0 particles may offer an optimum alternative to conventional Fe^0 in PRBs such that Y_{CF} is reduced without compromising the kinetics of reaction.

REFERENCES

1. McCormick, M. L.; Adriaens, P., Carbon tetrachloride transformation on the surface of nanoscale biogenic magnetite particles. *Environ. Sci. Technol.* **2004,** *38* (4), 1045-1053.

2. Nurmi, J. T.; Tratnyek, P. G.; Sarathy, V.; Baer, D. R.; Amonette, J. E.; Pecher, K.; Wang, C.; Linehan, J. C.; Matson, D. W.; Penn, R. L.; Driessen, M. D., Characterization and properties of metallic iron nanoparticles: Spectroscopy, electrochemistry, and kinetics. *Environ. Sci. Technol.* **2005,** *39* (5), 1221-1230.

3. Matheson, L. J.; Tratnyek, P. G., Reductive dehalogenation of chlorinated methanes by iron metal. *Environ. Sci. Technol.* **1994,** *28* (12), 2045-2053.

4. Támara, M.; Butler, E. C., Effects of iron purity and groundwater characteristics on rates and products in the degradation of carbon tetrachloride by iron metal. *Environ. Sci. Technol.* **2004,** *38* (6), 1866-1876.

5. Elsner, M.; Haderlein, S. B.; Kellerhals, T.; Luzi, S.; Zwank, L.; Angst, W.; Schwarzenbach, R. P., Mechanisms and products of surface-mediated reductive dehalogenation of carbon tetrachloride by Fe(II) on goethite. *Environ. Sci. Technol.* **2004,** *38* (7), 2058-2066.

6. Kriegman-King, M. R.; Reinhard, M., Transformation of carbon tetrachloride by pyrite in aqueous solution. *Environ. Sci. Technol.* **1994,** *28* (4), 692-700.

7. Danielsen, K. M.; Hayes, K. F., pH dependence of carbon tetrachloride reductive dechlorination by magnetite. *Environ. Sci. Technol.* **2004,** *38* (18), 4745 -4752.

8. Pecher, K.; Haderlein, S. B.; Schwarzenbach, R. P., Reduction of polyhalogenated methanes by surface-bound Fe(II) in aqueous suspensions of iron oxides. *Environ. Sci. Technol.* **2002,** *36* (8), 1734-1741.

9. Kriegman-King, M. R.; Reinhard, M., Transformation of carbon tetrachloride by pyrite in aqueous solution. *Environ. Sci. Technol.* **1994,** *28* (4), 692-700.

10. Zhang, W.-X., Nanoscale iron particles for environmental remediation. *J. Nanopart. Res.* **2003,** *5*, 323-332.

11. Danielsen, K. M.; Gland, J. L.; Hayes, K. F., Influence of amine buffers on carbon tetrachloride reductive dechlorination by the iron oxide magnetite. *Environ. Sci. Technol.* **2005,** *39* (3), 756-763.

12. Lien, H.-L.; Zhang, W.-X., Transformation of chlorinated methanes by nanoscale iron particles. *J. Environ. Eng.* **1999,** *125* (11), 1042-1047.

13. Johnson, T. L.; Scherer, M. M.; Tratnyek, P. G., Kinetics of halogenated organic compound degradation by iron metal. *Environ. Sci. Technol.* **1996,** *30* (8), 2634-2640.

14. Gaspar, D. J.; Lea, A. S.; Engelhard, M. H.; Baer, D. R.; Miehr, R.; Tratnyek, P. G., Evidence for localization of reaction upon reduction of CCl_4 by granular iron. *Langmuir* **2002,** *18* (20), 7688-7693.

15. Glasoe, P. K.; Schultz, S. D., Solubility of H_2O and D_2O in carbon tetrachloride, toluene, and cyclohexane at various temperatures. *J. Chem. Eng. Data* **1972,** *17*, 66-88.

16. Li, T.; Farrell, J., Reductive dechlorination of trichloroethene and carbon tetrachloride using iron and palladized-iron cathodes. *Environ. Sci. Technol.* **2000,** *34* (1), 173-179.

17. Balko, B. A.; Tratnyek, P. G., Photoeffects on the reduction of carbon tetrachloride by zero-valent iron. *J. Phys. Chem., B* **1998,** *102* (8), 1459-1465.

18. Cornell, R. M.; Schwertmann, U., *The Iron Oxides: Structure, Properties, Reactions, Occurrence and Uses*. VCH: Weinheim, Federal Republic of Germany, 1996; p 573.

19. Criddle, C. S.; McCarty, P. L., Electrolytic model system for reductive dehalogenation in aqueous environments. *Environ. Sci. Technol.* **1991,** *25* (5), 973-978.

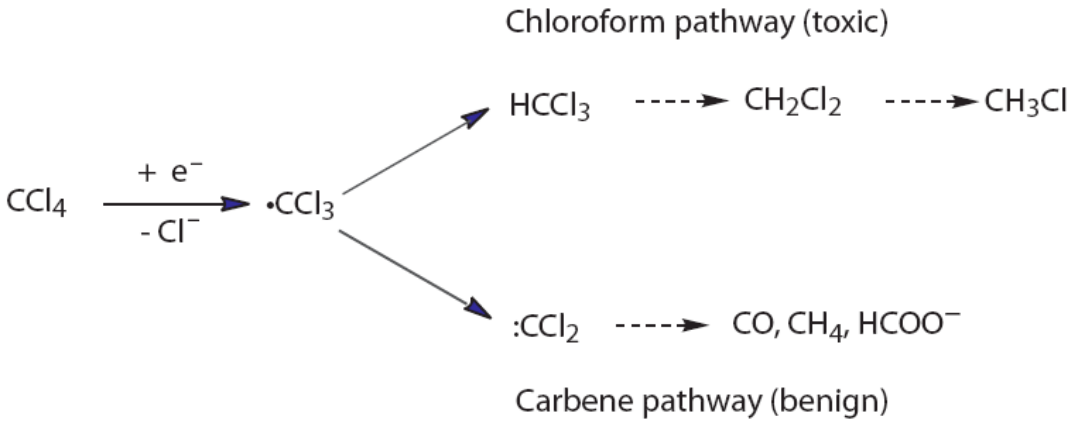

Figure 2.1. Simple conceptual model for branching among the two major product formation pathways in the reduction of CT. Dashed arrows indicate multiple steps that are not elaborated here.

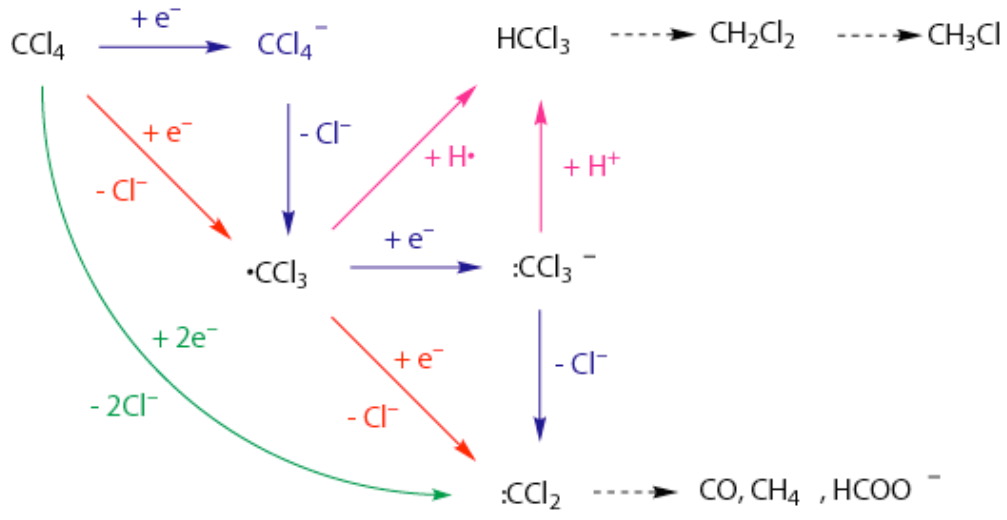

Figure 2.2. Detailed conceptual model showing feasible steps in the dechlorination of CT. In general, horizontal, vertical, and diagonal arrows represent electron transfers, atom transfers, and concerted electron and atom transfers, respectively. Dashed arrows indicate multiple steps that are not elaborated here.

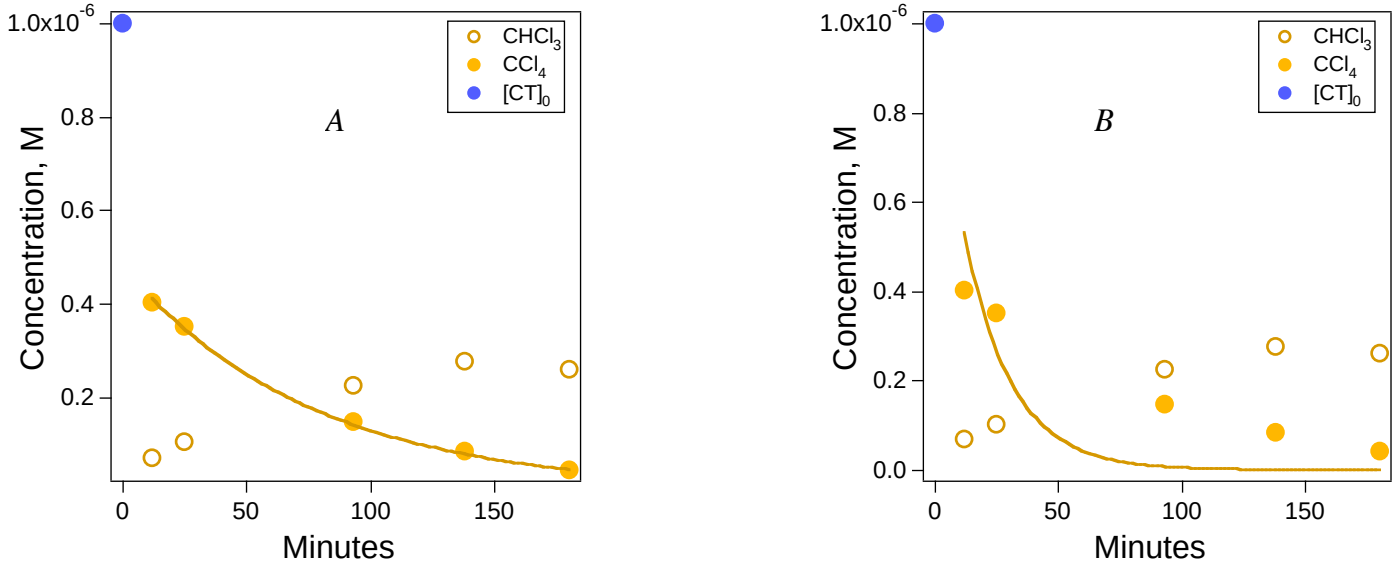

Figure 2.3. Sample concentration versus time plots for degradation of CT by nano Fe^0 (Fe^{H2}) showing fit achieved by (*A*) floating $[CT]_0$, and (*B*) fixing $[CT]_0$. The respective yields of chloroform, and first-order rate constant are (*A*) Y_{CF} = 0.65 ; k_{CT} = 0.013 min^{-1}, and (*B*) Y_{CF} = 0.23 ; k_{CT} = 0.053 min^{-1}. In this experiment, nominal $[CT]_0$ = 1x10^{-6} M, represented by the blue circle.

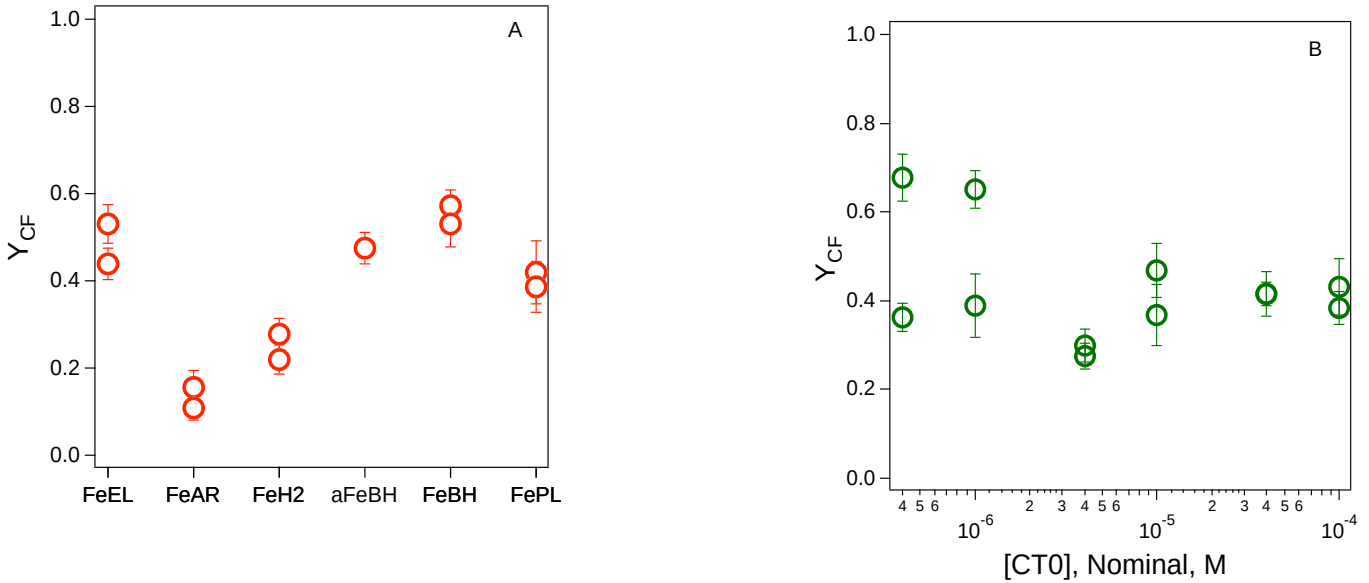

Figure 2.4. The CF yield plotted versus (*A*) different iron types; Fe^{H2}, Fe^{BH}, and Fe^{AR} are nano-sized iron particles produced by different methods; "aFe^{BH}" represents aged Fe^{BH}; $[CT]_0$ = 4.01 μM, (*B*) varying $[CT]_0$ for the Fe^{H2}/CT system. Pre-exposure was 24 hours in both (*A*) and (*B*). In both figures, error bars represent one standard deviation from fitting. Replicates were performed for each iron type, and $[CT]_0$.

Table 2.1. Products formed under different $H^+/D^+/D^-$ donor conditions and pre-exposure times. Y_{CF} numbers are in italics. The concentration of d8-isopropanol was 3.9 μM for 0- and 1-day pre-exposures, and 3.9 mM for 3-day pre-exposure.

Solvent system / Pre-exposure	H_2O	H_2O with d8-isopropanol	D_2O
0-day	$CHCl_3$; *0.50*	$CHCl_3$; *0.48*	$CDCl_3$; *0.22*
1-day	$CHCl_3$; *0.36*	$CHCl_3$; *0.35*	$CDCl_3$; *0.24*
3-day	$CHCl_3$; *0.39*	$CHCl_3$; *0.40*	$CDCl_3$; *0.32*

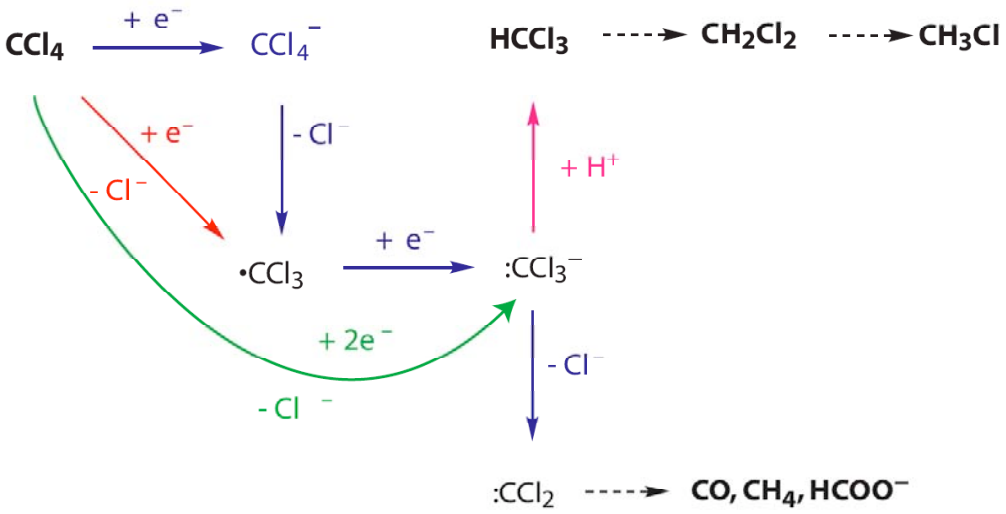

Figure 2.5. Modified conceptual model showing only pathways that have not been excluded by our results with the unbuffered Fe^{H2}/CT system. The new hypothesized 2 e^- reduction pathway is in green.

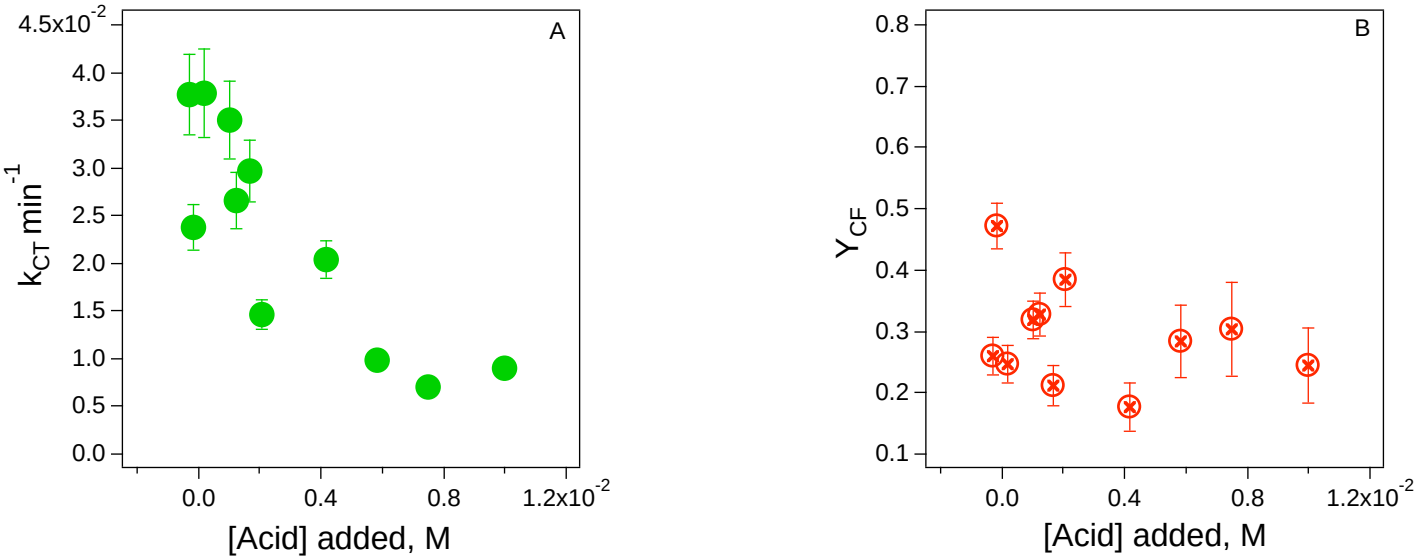

Figure 2.6. k_{CT} (*A*) and Y_{CF} (*B*) plotted against the concentration of 1 M HCl added to the batch reactors containing Fe^{H} Since measuring pH involved some amount of uncertainty due to the buffering action of the iron, both k_{CT} and Y_{CF} are plotted against the more reproducible variable.

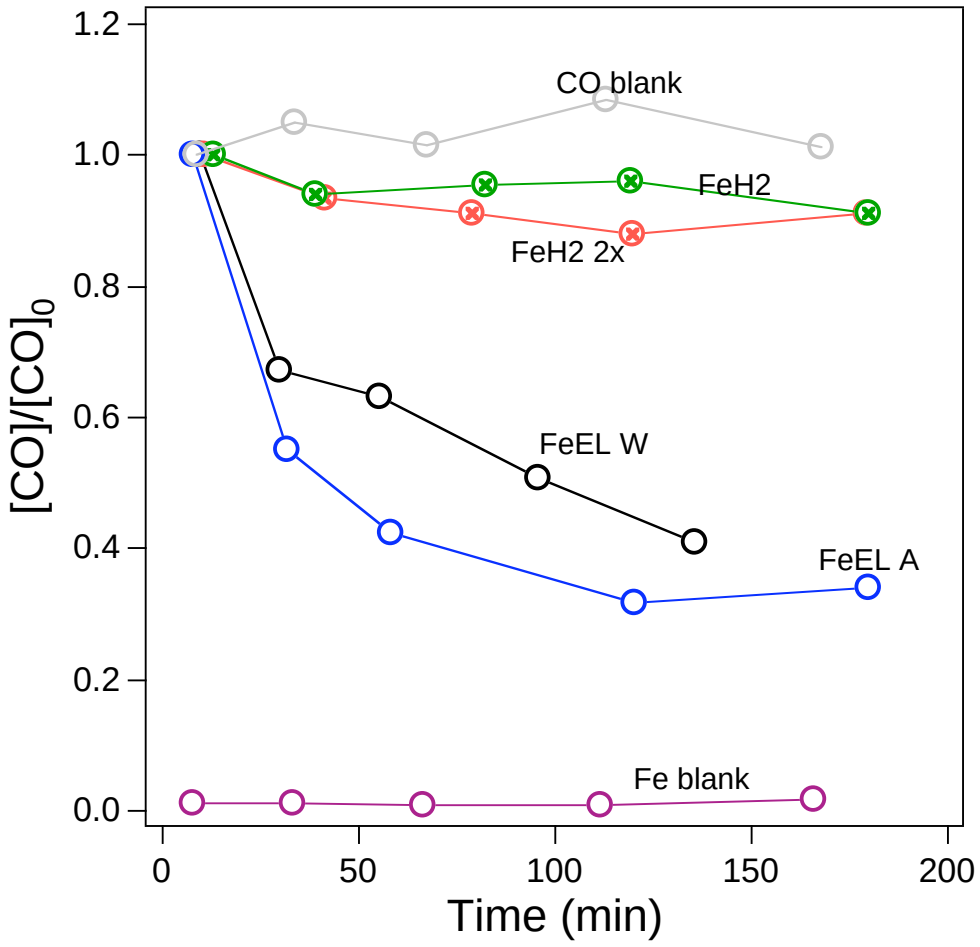

Figure 2.7. Sorption of carbon monoxide onto iron as a function of time. Batch experiments consisted of aqueous solutions saturated with CO with added iron (Fe^{EL} or Fe^{H2}). $[CO]_0 = 9 \times 10^{-4}$ M. *A*, and *W* stand for acid washed and water washed, respectively. In the curve labeled '2x', twice the amount of Fe^{H2} normally used in batch experiments (2 x 0.15 g per 120 mL) was used.

3

Kinetics of Carbon Tetrachloride Degradation

Abstract

Rates of carbon tetrachloride (CT) reduction by the various forms of Fe^0 and Fe^{II} vary widely. In order to compare the kinetics of CT degradation among different systems, the parameter used is typically the surface-area normalized pseudo first-order rate constant (k_{SA}). k_{SA} within a system is a constant only when k_{obs} (the pseudo first-order rate constant) and iron load, ($\rho_a = \rho_m a_s$, where ρ_m is the mass of iron per unit volume, and a_s is the surface area of iron per unit mass) share a linear relationship with each other, and CT reduction rates in the system are not mass-transfer limited. In batch systems with CT and nano-sized zero-valent iron (Fe^{H2}), we found that the kinetics are indeed not mass-transfer limited, and are completely controlled by reaction on the iron surface. We also studied the variation of k_{obs} with ρ_a over a wide range of relative iron loads, and found that k_{obs} depends on *relative* iron load $\left(\frac{\rho_a}{[CT]_0}\right)$ as opposed to ρ_a. Strict linearity was observed only over a short range—not more than an order of magnitude variation in m^2/mol. Generally, the ranges between 10^4-10^8 and 10^8-10^9 m^2/mol were best fit (independently) by the relation $k_{obs} = c \times \left(\frac{\rho_a}{[CT]_0}\right)^a$, a saturation-type correlation of the

form $k_{obs}=\frac{l\times\frac{\rho_a}{[CT]_0}}{m+\frac{\rho_a}{[CT]_0}}$, respectively (where l, m, c, and a are constants). Despite this complication, k_{SA} is still a useful parameter, both (*i*) when the variation in the range of relative iron loads is within an order of magnitude, and (*ii*) for the purposes of qualitative comparisons. Log k_{SA} versus log k_M (mass-normalized rate constant) plots were used to represent rate constants for different systems. Inspection of these plots shows that nanoparticles of iron do not react with CT faster on a surface-area basis than micron-sized particles. However, all pure Fe^0 was faster on both a surface-area, and mass normalized basis than impure millimeter sized granular iron. It was also observed that in most systems, kinetics did not strongly correlate with the yield of chloroform.

INTRODUCTION

Carbon tetrachloride (CT) can be reduced by a number of environmentally relevant reductants, among which zero-valent iron (Fe^0) is one of the most effective. Typically, Fe^0 is used for groundwater remediation in permeable reactive barriers (PRBs), but recent studies have sought to further optimize the kinetics of CT reduction by using nano-scale Fe^0, via injection wells [1-3]. While there are a number of uncertainties associated with nanoparticles as remediating agents, one of our concerns in this study is the widespread perception of greater intrinsic reactivity of Fe^0 nanoparticles [4]. In the same context, it is important to understand how rates of CT reduction by iron of different sizes compare on a surface area normalized basis, since all reactions in a heterogeneous system with Fe^0 take place on the surface [5, 6].

To compare rates among different types of irons, we continue to use CT as the probe contaminant, in part because we have studied its properties and reaction pathways extensively in earlier work [5-7] and this work (chapter 2). Reduction of CT is believed to be kinetically limited by dissociative electron transfer [8]:

$$CCl_4 + 1e^- \rightarrow CCl_3^- + Cl^- \qquad (3.1)$$

The availability of electrons, is naturally proportional to the concentration of electron donor, which is Fe^0 in this case, which is represented by $\rho_m a_s$, where ρ_m refers to the mass load of iron, in g/L, and a_s is the surface area, in m^2/g [6].

Therefore, in equation 3.2, the concentration of electrons is represented by $A \times \rho_m a_s$, where A is the fraction of reactive surface sites.

$$Rate = k \times [CCl_4] \times A \times \rho_m \times a_s \tag{3.2}$$

When Fe is in excess, kinetics can be assumed to be pseudo-first order, so

$$k_{obs} = k \times A \times \rho_m a_s \tag{3.3}$$

where k_{obs} is the pseudo-first order disappearance coefficient of CT (this is often referred to as k_{CT} in this work).

Equation 3.3 implies that k_{obs} will be controlled by the availability of electrons (or in other words, number of reactive surface sites, and amount of iron). Factors such as pH, iron size, and oxide composition may indirectly affect rate if they influence *A*. For example, nano-Fe^0 may produce an intrinsically (i.e., surface area-independent) faster reaction if the redox potential of equation 3.1 changes, or if the activation energy of the reaction is reduced as a result of smaller particle size.

To compare kinetics of CT degradation over different systems as a result of different experimental variables—including particle size—we need to have a size- and composition-independent parameter, which we can contrast across different systems. In the past, we have used k_{SA} (the surface area- normalized rate constant) for this purpose [6]. In later work, we have also defined another parameter k_M (the mass-normalized rate constant) [5]. They are defined as:

$$k_{SA} = \frac{k_{obs}}{\rho_m a_s} = \frac{k_{obs}}{\rho_a} \tag{3.4}$$

$$k_M = \frac{k_{obs}}{\rho_m} \tag{3.5}$$

where $\rho_a = \rho_m a_s$. Therefore, the relation between k_{SA} and k_M is simply

$$k_{SA} = \frac{k_M}{a_s} \tag{3.6}$$

While k_{SA} may be good approximation to compare different systems in most cases, it is useful to understand the exact variation of k_{obs} with ρ_a. Assumption of linearity

between these parameters is the standard model and the validity of this assumption is supoorted by many studies [6, 7, 9] over relatively narrow ranges of ρ_a. However, some work [10-13] with various types of irons, wider ranges of ρ_a, and contaminants other than CT, has indicated that the net relationship between these two variables over a broad range of iron loads is not always linear. summarizes prior work containing data that can be used to understand the relation between k_{obs} and ρ_a for different contaminants and iron types [10-13]. Upon analyzing plots of data from [10-13] (not shown here), three types of relationships are evident: *(i)* linearity over a narrow range of Fe loads, *(ii)* exponential behavior at low Fe loads: $k_{obs}=\left(\frac{\rho_a}{[CT]_0}\right)^a$, and *(iii)* saturation type behavior ($y=\frac{l\times\frac{\rho_a}{[CT]_0}}{m+\frac{\rho_a}{[CT]_0}}$) at high Fe loads. This, however, is not sufficient for a global description of variation of k_{obs} with ρ_a from Table 3.1, because the range of Fe loads for *(i)*, *(ii)*, and *(iii)* appear to vary with the study, iron type used, and even the contaminant. Also, not all behaviors were seen in each study. For example, in studies with 1,1,1-trichloroethane (111TCA), *(i)* and *(ii)* were observed, but only *(ii)* was fully documented [14]. Other researchers [10-13] have fit saturation-type equations to their data—indicative of *(i)* and *(iii)*. The inconsistencies among these treatments and observations have not been fully explained yet.

A better understanding of the above dependencies will help us clarify what processes actually dominate CT degradation kinetics, and how variations in k_{SA} should be interpreted. For example, the rate of a surface reation in a heterogeneous system can be influenced by one or more of the following steps: *(a)* bulk diffusion, *(b)* diffusion of reactants (CT) through boundary layer surrounding the surface, *(c)* adsorption of CT onto the surface, *(d)* reaction on surface, *(e)* regeneration of surface sites, *(f)* desorption of products (chloroform), and/or other intermediates from surface, *(g)* diffusion of products through the boundary layer, and in some cases *(h)* bulk diffusion of products into solution phase [15]. Some processes like *(b)*, *(c),* and *(f)* depend on contaminant type and iron particle size, while others like *(a)* are driven by physical parameters like mixing. In this

chapter, we also examine many of these steps to converge on what we believe are rate-determining processes in our system.

In the above context, the specific objectives in this study are to: *(i)* determine if k_{SA} is a constant in our systems, i.e., whether k_{obs} varies linearly with $\frac{\rho_m a_s}{[CT]_0}$, *(ii)* develop a framework to compare k_{SA} values of various reductants, and *(iii)* understand the effects of different environmental and reaction variables such as iron type, and iron particle size on the kinetics of CT degradation.

MATERIALS AND METHODS

Data from literature. Previously reported data for variation of k_{obs} with ρ_m or ρ_a for systems with some form of iron as reductant and different contaminants/reductates were gathered from all citable sources available as of October 2007. Sources, data, and experimental conditions from these studies are all summarized in Table 3.1. We designed our experiments to include the full range of iron loads (in m^2/L and m^2/mol) covered by these studies.

Reagents and methods. New data for CT degradation by different amounts of iron were obtained from batch reactions, where all reagents and batch experiment protocols are identical to the method description in chapter 2. $Fe^{H2(W)}$ (slurry-dried nano iron from Toda Americas) was the probe iron used in this study. Additional details about this material can be found in Chapter 4. Iron loads and $[CT]_0$ were varied in experiments in order to determine their effects on kinetics.

Fitting. Equations used for fitting were described in Chapter 2 (equations 2.1, 2.2, and 2.3). Concentration versus time data were fit to these equations to obtain k_{CT} and Y_{CF} (yield of chloroform—defined in Chapter 2), according to the fitting procedures described in Chapter 2.

RESULTS

Characteristics of k_{SA}. From the results summarized in Table 3.1, we noted that there are ranges of observed linearity and non-linearity between k_{obs} and ρ_a. Even between studies

that used the same iron type, the range of Fe (in g/L) that exhibited linear behavior versus k_{obs} was different. However, the corresponding range in m^2/L was more similar between studies that used the same iron type, but still varied enough to indicate that the response of k_{obs} might be influenced by a ratio of Fe load to contaminant concentration (m^2/mol, or mol/m^2) rather than just Fe load (m^2/L or g/L). The data in Table 3.1 are not sufficient to determine if the nature of contaminant is also important. For clarity, we have ignored data from Wust et al. [11]—whose results were relatively complicated to interpret—and Choe [12]—who used a very different reactant, nitrate.

To supplement the literature data, we designed experiments with Fe^{H2} and CT in order to cover a wide range of iron loads including all values of m^2/L (and m^2/mol) listed in Table 3.1. We achieved a range of 10^2-10^9 m^2/mol, or 1-100 m^2/L. It was not feasible to get lower and higher values due to limitations imposed by accurately dispensing nano Fe^0, and solubility of CT, but this is still a wider range than has been achieved in any previous study, with batch reactors.

Data from batch experiments done by us are plotted in Figure 3.1(a, b), which shows variation of k_{CT} obtained with m^2/L—which has been the more traditional mode of representation in most publications [7, 9]—and $[CT]_0$, respectively. If k_{CT} varies only as a function of ρ_a (m^2/L), it follows that (*i*) data points with the same ρ_a, but different $[CT]_0$ values should fall on top of each other in Figure 3.1a, and, similarly, if k_{CT} varies as a function of $[CT]_0$ alone, (*ii*) data points with the same $[CT]_0$ but different ρ_a should show no variation in Figure 3.1b. However, this is not observed (points colored blue and green in Figure 3.1(a, b) correspond to situations (*i*) and (*ii*) respectively). It seems to stand therefore, that k_{CT} is neither completely described by Fe load (ρ_a), nor by $[CT]_0$. Therefore, we hypothesized that k_{CT} would vary as a ratio of both these parameters, $\frac{\rho_a}{[CT]_0}$. Figure 3.2(a-f) shows variation of k_{CT} with both m^2/mol and mol/m^2, in linear and log-log forms each. The wide range of Fe loads measured show various behaviors in different regimes, which are more easily visible in the log-log versions of the plot.

Figure 3.2(e,f) shows log-log plots with at least 3 distinct regions (which have been approximately marked in Figure 3.2 f), where the middle region is clearly linear. Linear regions in a log-log plot imply a relationship of the type:

$$\log(k_{CT}) = a \times \log\left(\frac{\rho_a}{[CT]_0}\right) + c', \tag{3.7}$$

where a, and c' are constants, and c' can be written as $\log(c)$, c being another constant. Equation 3.7 implies the following relationships:

$$\log(k_{CT}) = \log\left(\frac{\rho_a}{[CT]_0}\right)^a + \log(c) \tag{3.8}$$

$$k_{CT} = c \times \left(\frac{\rho_a}{[CT]_0}\right)^a, \tag{3.9}$$

$$k_{CT} = \frac{c}{[CT]_0^a} \times (\rho_a)^a \tag{3.10}$$

Equation 3.9 is identical to the relation proposed by Cwiertny [7, 9] for constant $[111TCA]_0$. When linearity is assumed, $a = 1$, and equation 3.10 becomes:

$$\frac{k_{CT}}{\rho_a} = \frac{c}{[CT]_0} = k_{SA} \tag{3.11}$$

k_{SA} is a constant, only at constant $[CT]_0$ as per our model. However, when a is other than 1, equation 3.11 becomes

$$k_{SA} = c \times \frac{(\rho_a)^{a-1}}{([CT]_0)^a}, \tag{3.12}$$

Here k_{SA} is not a constant parameter anymore, as it is a function of ρ_a. We fit equation 3.9 to all of the data points with $10^8 < \frac{\rho_a}{[CT]_0} < 10^8$ m^2/mol. We obtained the following parameters from the fit: $c = 1.06 \times 10^{-3}$, and $a = 0.16$ (Figure 3.3a). For experiments with micron-sized Fe^0 and 111-TCA, Cwiertny and Roberts [14] obtained $a = 0.49$, by fitting a version of equation 3.9 to his data. The fitting equation, however, did not include a term for $[111TCA]_0$, and covered a narrower range of iron loads.

Other researchers working at higher iron loads [12], have found a saturation-type behavior, where k_{obs} varies linearly with ρ_a, and then gradually stabilizes to be independent of ρ_a at very high loads. In our system, this behavior can be represented by an equation of the form:

$$k_{obs} = \frac{l \times \frac{\rho_a}{[CT]_0}}{m + \frac{\rho_a}{[CT]_0}} \tag{3.13}$$

Here, l and m are constants. Fitting our data with very high $\frac{\rho_a}{[CT]_0}$ (greater than 10^8 m^2/mol) to equation 3.13 gave an adequate fit with $l = 0.6$, and $m = 8 \times 10^8$ (Figure 3.3b).

It is clear from Figure 3.2 that non-linearity is observed over a wide range of iron loads. One physical explanation for this non-linearity that has been proposed [14] is the increase of local high pH spots, causing an increase in precipitated $Fe(OH)_2$, which in turn reduces the rate of reaction by passivation of the surface. In this case, increasing iron mass may be consistent with seeing an increased number of such spots with high local pH. However, we have observed that k_{obs} is dependent on a ratio of iron load and $[CT]_0$. This implies that the factor causing the non-linearity must be dependent on both parameters, and is unlikely to be increased local pH alone. From equation 3.3, k_{obs} is linearly dependent on A—the concentration of reactive surface sites capable of donating electrons. We think that it is likely that the cause of the non-linearity also includes aggregation, and cementation processes, which are observed at high loads of Fe^0, and can cause A to not increase proportionally with $[Fe^0]$.

Based on Figure 3.2, other references [7, 9], and the above hypothesis, it appears that linearity can be assumed within small variations of $\frac{\rho_a}{[CT]_0}$, which are less than one order of magnitude in m^2/mol. Also, even for larger ranges of $\frac{\rho_a}{[CT]_0}$, depending on the exponent a, the value of k_{SA} may change negligibly (refer equations 3.9 and 3.12). The standard model (assumption of linearity between k_{obs} and ρ_a) is, and will continue to be adequate and preferred for most cases, especially at constant $[CT]_0$. However, the general model, as proposed in equations 3.9 and 3.13, is necessary to capture the full range of effects that are sometimes seen.

Equally of significance is the fact that, linearity is a function of what processes dominate kinetics. For example, in systems where kinetics are limited by mass-transfer, k_{CT} always varies linearly with surface area, and therefore before a broad comparison of

kinetics, factors to be considered are: *(i)* if the systems are mass-transfer, or surface-reaction limited, and *(ii)* if the range of 'm^2/mol' values lie within a range small enough, so as to assume k_{SA} is a constant. As mentioned earlier, the importance of *(ii)* is often minor, and can be neglected for qualitative comparisons.

Are kinetics mass-transfer limited? The effect of mass-transfer in a CT-Fe^0 system has been studied by Scherer et al [16], with a rotating disk electrode (RDE). An RDE was used to control the thickness of the diffusion layer surrounding the electrode. At depassivating potentials where oxide formation was unfavorable, it was observed that kinetics were not mass-transfer limited. Our system, however, is different because of both iron particle size, and the possibility of a thicker diffusion layer.

The rate constant of mass transfer (k_L) is related to the net pseudo first-order rate constant of contaminant degradation observed in a heterogeneous batch system, k_{obs} (k_{CT} in our system) as:

$$\frac{1}{k_{obs}} = \frac{1}{\rho_a} \times \left(\frac{1}{k_L} + \frac{1}{k_{rxn}} \right) \tag{3.14}$$

where k_L and k_{rxn} are the pseudo-first order rate constants of mass transfer and surface-mediated reaction respectively (assuming other processes such as sorption, etc. are not rate-limiting) [17]. We calculated k_L for our system from empirical equations derived from a number of other publications, as listed in Arnold et al. [17]. From [17], k_L is a function of particle size (d_p), viscosity of water (ν), terminal settling velocity (u_t), particle density (ρ_d), fluid density (ρ), and the binary diffusion coefficient of CT in water (D_{12}). The values of these parameters for our system are listed in Table 3.2, along with sources for data and correlations between these parameters.

Both k_L and k_{CT} are plotted at different surface areas and particle sizes in Figure 3.4. For our system, k_L (red line in Figure 3.4) is several orders of magnitude greater than k_{CT} (grey line in Figure 3.4), which means that the reaction is surface-reaction limited for all the ranges of surface areas considered. Additionally, from equation 3.14, the relationship between k_{obs} and ρ_a is always linear in mass-transfer limited systems. The non-linear relationship observed in Figure 3.2 (c, d) was, therefore, also an indication that our system is surface-reaction limited.

Framework for comparing kinetic parameters. One of our objectives was to design a framework for comparing rate constants of degradation of VOCs between systems with different reductant loads and surface areas. In earlier work, and in earlier sections in this chapter, we have concluded that k_{SA} has been the preferred basis of comparison between systems. However, the parameter k_M is an alternative with advantages, since there exist situations where surface area data is not available or applicable (e.g., in some *in situ* engineering applications).

Plotting k_{SA} versus k_M on a log-log plot gives us a framework to compare systems with different iron types and loads. To obtain such a plot, we have compiled all pseudo-first order disappearance rate constants (k_{CT}) for CT reduction via different irons and iron oxides, from many sources including work done in this study. Kinetic data, when plotted on such a plot (Figure 3.5-3.8), fall on lines of constant slope = 1, and constant intercept = a_s (surface area in m^2/g)—from equation 3.6. An easy way to interpret this figure is to project data on to the x- and y- axes. Points that fall to the right in the figure have higher k values on a mass-normalized basis, and points to the top of the graph have higher k values on a surface-area normalized basis. Such plots are, therefore, a flexible means of summarizing kinetic data and can be used to address issues such as: *(i)* how do other parameters affect this curve, *(ii)* are nano particles more reactive than larger iron particles, *(iii)* is the apparent upper limit of k_{SA} in Figure 3.5-3.8 real, and *(iv)* and if so, what controls rate of reaction.

Data in Figure 3.5 have been color coded with respect to iron purity and size. Nano-sized iron (in red) and micron-sized iron (in green) have a range of k_{SA} values, which are generally higher than construction grade iron (in blue). This can be attributed to the purity of such irons, since nano- and micron-sized irons typically have very few impurities. Also, granular impure iron includes more oxide and carbon that presumably contributes to surface area but not to k_{CT}. Another conclusion that can be shown from Figure 3.6 is that nano-iron is no more reactive on a surface area basis than micro-iron. In addition, Figure 3.6—which includes Fe oxides as well—indicates other phenomena that are either intuitive, or known such as: *(a)* k_{SA}s of all oxides are lower than those of ZVI, and *(b)* bimetallics show k_{SA} similar to nano-iron. Figure 3.7 is color coded with respect to Y_{CF} (yield of CF, refer chapter 2). While there does not seem to be a strong

direct correlation between k_{SA} and Y_{CF} , there is a weak correlation within the nano-iron dataset, probably indicating that strongly reducing conditions can favor both higher rates and the dichlorocarbene pathway leading to low Y_{CF}.

Another factor that is evident in Figures 3.6 – 3.8 is an apparent upper-limit to the data at k_{SA} = 2 – 4 L m^{-2} hr^{-1}. This limit, if real, could be imposed by any of the processes contributing to overall reaction kinetics: bulk diffusion of CT, diffusion of CT through static layer, adsorption of CT onto surface, reaction, and/or desorption of CT from surface [15]. Bulk diffusion is controlled by mixing rate, which is easy to vary experimentally. We have conducted experiments that varied mixing rate of the batch system, and measured the corresponding k_{CT} (Figure 3.8). The data shows that, at the speed at which we operate our rotary shaker (~24 rpm), we are at an optimum, where increasing shaker speed will not affect k_{CT}. Addition of glass beads increased k_{CT}, however, it is not clear if this is due to abrasion of aggregates of particles, or due to increased mixing. We know from the earlier section that mass-transfer rates—which include all the above processes except surface-reaction and desorption should not be limiting. Therefore, the upper-limit to the k_{SA} values observed is likely because operating conditions dictate a limiting condition. A maximum k_{CT}, must however be reached, upon increasing the surface area (per unite volume) of iron (from equation 3.13), upon reaching genuine pseudo first-order conditions.

CONCLUSIONS

k_{CT} is non-linearly dependent on the iron load (ρ_a) in m^2/L for most of the range of loads examined. However, the dependence is better explained as a function of *relative* iron load, i.e., $\frac{\rho_a}{[CT]_0}$. At $10^4 < \rho_a < 10^8$ m^2/L, our data fits an equation of the form $k_{CT} = c \times \left(\frac{\rho_a}{[CT]_0}\right)^a$, which means that the marginal increase in k_{CT} decreases with ρ_a. This may be partly explained by the increased aggregation of iron at higher iron loads, and therefore lesser availability of reactive surface sites per unit iron mass added. However, when a short range of relative iron loads is considered, linearity is a reasonable

assumption, and in most ranges, k_{SA} is a good approximation. It has also been verified that kinetics in the Fe^{H2}/CT system are not mass-transfer limited.

Plots of log k_{SA} versus log k_M log-log plot show that (*i*) there is no upper limit for k_{SA} (other than that dictated by excess of iron), (*ii*) nano-sized irons are not intrinsically faster (per unit surface area) than micron-sized irons, *(iii)* both nano- and micron- sized irons are faster than bulk granular irons, and *(iv)* there is no obvious wide-range correlation between Y_{CF} and k_{SA}. It is important to note that there are uncertainties to be kept in mind while comparing data on k_{SA}-k_M plots that are associated with the significance of k_{SA} values: (*a*) the linearity of k_{obs} versus $\frac{\rho_a}{[CT]_0}$, and (*b*) the reactive surface area of the iron particles. It is not always possible to accurately estimate reactive surface area, especially in the case of granular iron—where a large portion of the surface can be covered by unreactive oxides—and also in the case of bimetallics—where the 5% or less of the surface that contains the catalyst such as Pd/Pt is much more reactive than the rest of the surface.

REFERENCES

1. Elliott, D. W.; Zhang, W.-X., Field assessment of nanoscale bimetallic particles for groundwater treatment. *Environ. Sci. Technol.* **2002,** *35* (24), 4922-4926.

2. Geiger, C. L.; Clausen, C. A.; Brooks, K.; Coon, C.; Huntley, C.; Filipek, L.; DeVor, R.; Krug, T.; O'Hara, S.; Majors, D.; Quinn, J., Remediation of DNAPLs using emulsified zero-valent iron: Laboratory and field results. *Preprints of Extended Abstracts presented at the ACS National Meeting, American Chemical Society, Division of Environmental Chemistry* **2003,** *43* (1), 939-944.

3. Hyun, S. P.; Hayes, K. F., Site-specific abiotic reductive dechlorination of TCE using nano-scale FeS, *Preprints of Extended Abstracts presented at the ACS National Meeting, American Chemical Society, Division of Environmental Chemistry* **2005**, 45, 823-827.

4. Tratnyek, P. G.; Johnson, R. L., Nanotechnologies for environmental cleanup. *NanoToday* **2006,** *1* (2), 44-48.

5. Nurmi, J. T.; Tratnyek, P. G.; Sarathy, V.; Baer, D. R.; Amonette, J. E.; Pecher, K.; Wang, C.; Linehan, J. C.; Matson, D. W.; Penn, R. L.; Driessen, M. D.,

Characterization and properties of metallic iron nanoparticles: Spectroscopy, electrochemistry, and kinetics. *Environ. Sci. Technol.* **2005,** *39* (5), 1221-1230.

6. Johnson, T. L.; Scherer, M. M.; Tratnyek, P. G., Kinetics of halogenated organic compound degradation by iron metal. *Environ. Sci. Technol.* **1996,** *30* (8), 2634-2640.

7. Matheson, L. J.; Tratnyek, P. G., Reductive dehalogenation of chlorinated methanes by iron metal. *Environ. Sci. Technol.* **1994,** *28* (12), 2045-2053.

8. Bylaska, E. J.; Felmy, A. R.; Dixon, D. A.; Tratnyek, P. G., The free energies of the hydrogenolysis, dehydrohalogenation, and hydrolysis of 1,2,3-trichloropropane from ab initio electronic structure theory. **2008** in prep.

9. Song, H.; Carraway, E. R., Reduction of chlorinated methanes by nano-sized zero-valent iron. Kinetics, pathways, and effect of reaction conditions. *Environ. Eng. Sci.* **2006,** *23* (2), 272-284.

10. Gotpagar, J.; Grulke, E.; Tsang, T.; Bhattacharyya, D., Reductive dehalogenation of trichloroethylene using zero-valent iron. *Environ. Prog.* **1997,** *16* (2), 137-143.

11. Wüst, W. F.; Köber, R.; Schlicker, O.; Dahmke, A., Combined zero- and first-order kinetic model of the degradation of TCE and cis-DCE with commercial iron. *Environ. Sci. Technol.* **1999,** *33* (23), 4304-4309.

12. Choe, S. H.; Ljestrand, H. M.; Khim, J., Nitrate reduction by zero-valent iron under different pH regimes. *App. Geochem.* **2004,** *19* (3), 335-342.

13. Doong, R. A.; Chen, K. T.; Tsai, H. C., Reductive dechlorination of carbon tetrachloride and tetrachloroethylene by zerovalent silicon-iron reductants. *Environ. Sci. Technol.* **2003,** *37* (110), 2575-2581.

14. Cwiertny, D. M.; Roberts, A. L., On the nonlinear relationship between k_{obs} and reductant mass loading in iron batch systems. *Environ. Sci. Technol.* **2005,** *39* (22), 8948-8957.

15. Laidler, K. J., *Chemical Kinetics*. McGraw-Hill: New York, 1990; p 531.

16. Scherer, M. M.; Westall, J. C.; Ziomek-Moroz, M.; Tratnyek, P. G., Kinetics of carbon tetrachloride reduction at an oxide-free iron electrode. *Environ. Sci. Technol.* **1997,** *31* (8), 2385-2391.

17. Arnold, W. A.; Roberts, A. L., Pathways of chlorinated ethylene and chlorinated acetylene reaction with Zn(0). *Environ. Sci. Technol.* **1998,** *32* (19), 3017-3025.

18. Arnold, W. A.; Ball, W. P.; Roberts, A. L., Polychlorinated ethane reaction with zero-valent zinc: Pathways and rate control. *J. Contam. Hydrol.* **1999,** *40* (2), 183-200.

19. Denn, M. M., *Process Fluid Mechanics*. Prentice-Hall: Englwood Cliffs, NJ, 1980.

20. Wilke, C. R.; Chang, P., Correlation of diffusion coefficients in dilute solutions. *AIChE Journal* **1955,** *1* (2), 264-270.

21. Ranz, W. E.; Marshall, W. R., Evaporation from drops. *Chem. Eng. Prog.* **1952,** *48* (3), 141-146.

22. Harriott, P., Mass transfer to particles: Part I. suspended in agitated tanks. *A.I.Ch.E. Journal* **1962,** *8* (1), 93-101.

23. Scherer, M. M.; Balko, B. A.; Gallagher, D. A.; Tratnyek, P. G., Correlation analysis of rate constants for dechlorination by zero-valent iron. *Environ. Sci. Technol.* **1998,** *32* (19), 3026-3033.

24. Danielsen, K. M.; Hayes, K. F., pH dependence of carbon tetrachloride reductive dechlorination by magnetite. *Environ. Sci. Technol.* **2004,** *38* (18), 4745 -4752.

25. Lin, C. J.; Lo, S.-L.; Liou, Y. H., Degradation of aqueous carbon tetrachloride by nanoscale zerovalent copper on a cation resin. *Chemosphere* **2005,** *59* (9), 1299-1307.

26. Lien, H. L.; Zhang, W. X., Transformation of chlorinated methanes by nanoscale iron particles. *J. Environ. Eng.* **1999,** *125* (11), 1042-1047.

27. Balko, B. A.; Tratnyek, P. G., Photoeffects on the reduction of carbon tetrachloride by zero-valent iron. *J. Phys. Chem. B* **1998,** *102* (8), 1459-1465.

28. Nurmi, J. T.; Tratnyek, P. G.; Sarathy, V.; Baer, D. R.; Amonette, J. E.; Pecher, K.; Wang, C.; Linehan, J. C.; Matson, D. W.; Penn, R. L.; Driessen, M. D., Characterization and properties of metallic iron nanoparticles: spectroscopy, electrochemistry, and kinetics. *Environ. Sci. Technol.* **2005,** *39* (5), 1221-1230.

29. Elsner, M.; Haderlein, S. B.; Kellerhals, T.; Luzi, S.; Zwank, L.; Angst, W.; Schwarzenbach, R. P., Mechanisms and products of surface-mediated reductive dehalogenation of carbon tetrachloride by Fe(II) on goethite. *Environ. Sci. Technol.* **2004,** *38* (7), 2058-2066.

30. Támara, M.; Butler, E. C., Effects of iron purity and groundwater characteristics on rates and products in the degradation of carbon tetrachloride by iron metal. *Environ. Sci. Technol.* **2004,** *38* (6), 1866-1876.

31. McCormick, M. L.; Adriaens, P., Carbon tetrachloride transformation on the surface of nanoscale biogenic magnetite particles. *Environ. Sci. Technol.* **2004,** *38* (4), 1045-1053.

32. Miehr, R.; Tratnyek, P. G.; Bandstra, J. Z.; Scherer, M. M.; Alowitz, M.; Bylaska, E. J., The diversity of contaminant reduction reactions by zero-valent iron: role of the reductate. *Environ. Sci. Technol.* **2004,** *38* (1), 139-147.

33. Butler, E. C.; Hayes, K. F., Kinetics of the transformation of halogenated aliphatic compounds by iron sulfide. *Environ. Sci. Technol.* **2000,** *34* (3), 422-429.

34. Amonette, J. E.; Workman, D. J.; Kennedy, D. W.; Fruchter, J. S.; Gorby, Y. A., Dechlorination of carbon tetrachloride by Fe(II) associated with goethite. *Environ. Sci. Technol.* **2000,** *34* (21), 4606-4613.

35. Tratnyek, P. G.; Scherer, M. M.; Deng, B.; Hu, S., Effects of natural organic matter, anthropogenic surfactants, and model quinones on the reduction of contaminants by zero-valent iron. *Water Res.* **2001,** *35* (18), 4435-4443.

36. Lien, H. L.; Zhang, W., Enhanced dehalogenation of halogenated methanes by bimetallic Cu/Al. *Chemosphere* **2002,** *49*, 371-378.

37. Doong, R. A.; Chen, K. T.; Tsai, H. C., Reductive dechlorination of carbon tetrachloride and tetrachloroethylene by zerovalent silicon-iron reductants. *Environ. Sci. Technol.* **2003,** *37* (110), 2575-2581.

38. Feng, J.; Lim, T.-T., Pathways and kinetics of carbon tetrachloride and chloroform reductions by nano-scale Fe and Fe/Ni particles: comparison with commercial micro-scale Fe and Zn. *Chemosphere* **2005,** *59* (9), 1267-1277.

39. Danielsen, K. M.; Gland, J. L.; Hayes, K. F., Influence of amine buffers on carbon tetrachloride reductive dechlorination by the iron oxide magnetite. *Environ. Sci. Technol.* **2005,** *39* (3), 756-763.

40. Pecher, K.; Haderlein, S. B.; Schwarzenbach, R. P., Reduction of polyhalogenated methanes by surface-bound Fe(II) in aqueous suspensions of iron oxides. *Environ. Sci. Technol.* **2002,** *36* (8), 1734-1741.

Table 3.1. Summary of variation of k_{obs} with [Fe^0] (in g/L, m^2/L , and m^2/mol) from data in references listed in the first column. Data in red have not been included for analysis.

Source	Reductant	Reactant	[Reactant] (M)	Fe load where linearity (k_{obs} versus g/L Fe) is observed			Surface Area m^2/g	Fe load where non-linearity (k_{obs} versus g/L Fe) is observed		
				g/L	m^2/L	m^2/mol (x 10^3)		g/L	m^2/L	m^2/mol (x 10^3)
Wust et al 1999 [11]	Cast iron blasting	TCE				0-10^3	0.12			>10^3
Gotpagar et al., 1997 [10]	Fe^{EL}	TCE	3.9 x 10^{-4}		0.1-1.5	0.3-3.8			>1.5	>3.7
Johnson et al., 1996 [6]	Fe^{EL}	CT	varied				0.061			<13
Matheson and Tratnyek, 1994 [7]	Fe^{EL}	CT	1-2 x 10^{-4}	10.0-50.0	5.0-30.0	25-150	0.7	<10	<5	<25
Cwiertny and Roberts, 2007 [14]	Fe^{EL}	111TCA	1.0 x 10^{-4}	5.0-30	4.0-12.0	2-12	0.4		<4	<20
Song and Carraway, 2005 [9]	Fe^{BH}	111TCA	2.0 x 10^{-4}	0.08-0.3	2.0-9.0	10-45			>9	>45
Choe, 2000 [12]	Fe^{BH}	Nitrate	3.2 x 10^{-3}	0-50.0	0-1570	0-490	31.4			>490

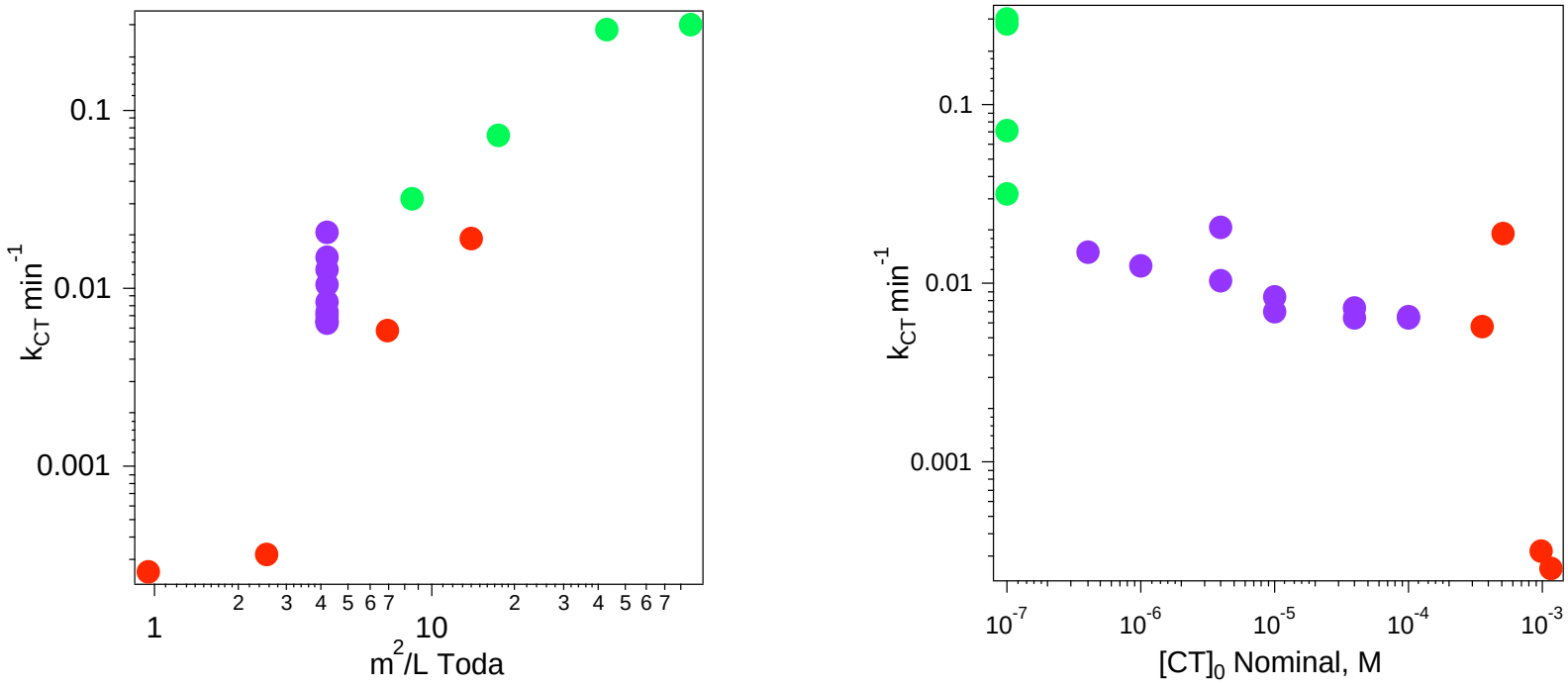

Figure 3.1. Log-log plots of k_{CT} versus (*a*) m^2/L, and (*b*) $[CT]_0$. Data points in blue represent experiments done at constant $[Fe^0]$ but varying $[CT]_0$, and those in green represent experiments done at constant $[CT]_0$ but varying $[Fe^0]$. Both $[Fe^0]$ and $[CT]_0$ vary for red data points.

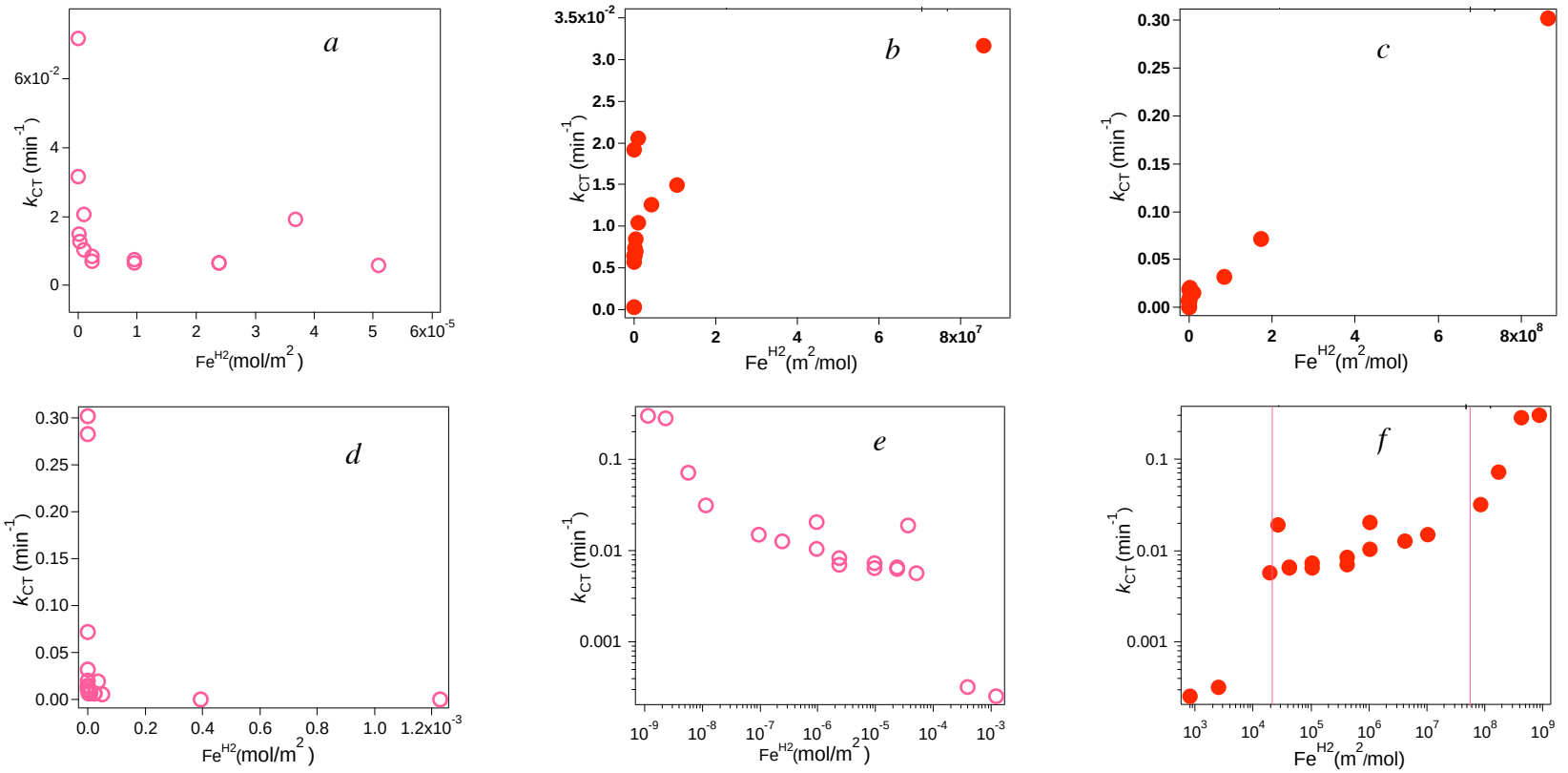

Figure 3.2. Different views of k_{CT} (or k_{obs}) versus [Fe] generated in this study. (*a*) and (*b*) show enlarged views of the whole data set, in order to show variation within small ranges of mol/m^2 (or m^2/mol respectively). (*c*), and (*d*) show the whole data set plotted against m^2/mol and mol/m^2, respectively. (*e*), and (*f*) show log-log plots of the linear versions in (*c*), and (*d*). Figure 2(*f*) divides the log-log plot into three "linear" regions.

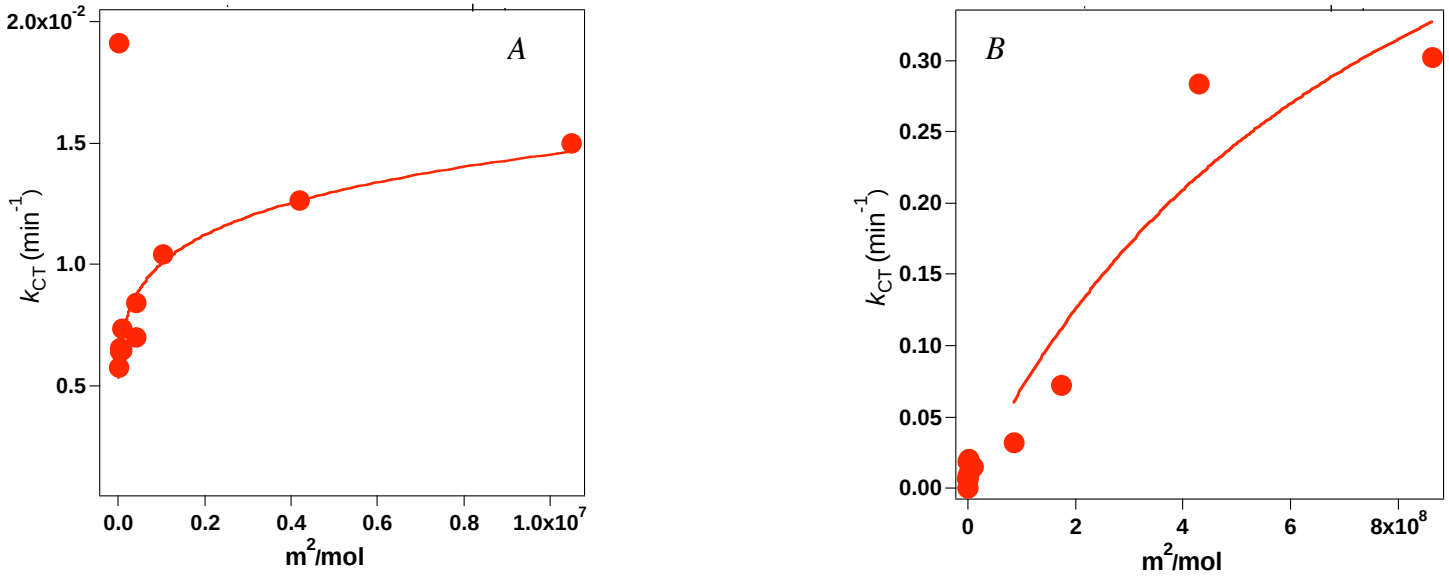

Figure 3.3. (*A*) Equation 3.9 used to fit data with $10^4 < \rho_m a_s < 10^8$, and (*B*) equation 3.13 used to fit data with $\rho_m a_s > 10^8$. The x-axis shows the relative concentration of iron (Fe^{H2})—with respect to CT—in m^2/mol.

Table 3.2. Parameters obtained for calculating mass-transfer rate constant, k_L from [18]. Sources for calculation of various parameters are given where relevant.

Parameter	Value	Source
Terminal velocity, u_t	5.31×10^{-6} m/s	Denn, 1980 [19]
Binary diffusion coefficient, D_{12}	3.52×10^{-9}	Wilke and Chang, 1955 [20]
Kinematic viscosity of fluid (water), ν	1.0×10^{-6} m^2/s	CRC Handbook
Particle size (of iron), d_p	50 nm	Toda Americas
Particle density, ρ_p	7.86 g/cc	CRC Handbook
Fluid density, ρ	1 g/cc	CRC Handbook
Mass-transfer rate constant, k_L	1.27×10^4 L m^{-2} hr^{-1}	Ranz and Marshall, 1952 [21]; Harriott, 1962 [22]

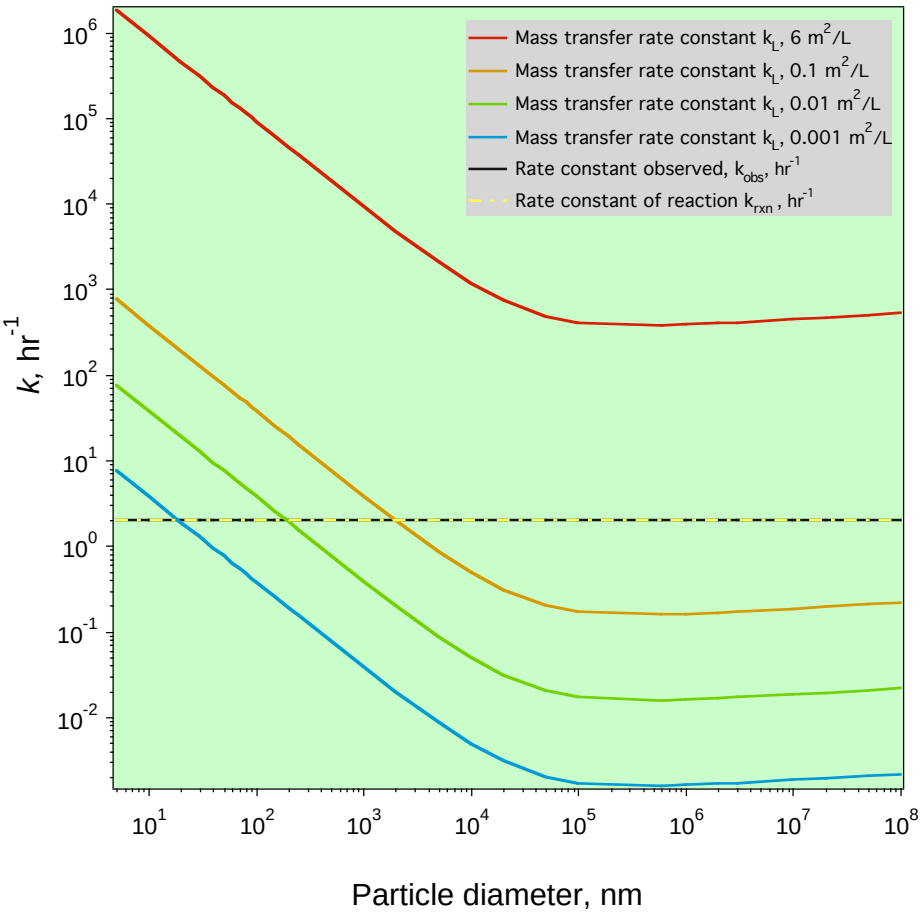

Figure 3.4. Variation of mass-transfer rate of reaction with particle diameter and surface area of iron. The curve in red was calculated for the surface area of iron in our experiments. The average observed rate constant of reaction k_{obs} (or k_{CT}) is an average of our data and is represented by the grey horizontal line. The rate constant of surface reaction, k_{rxn} in our systems has been back calculated from equation 3.14 and is represented by the yellow dashed line (but lies almost on top of the k_{obs} line).

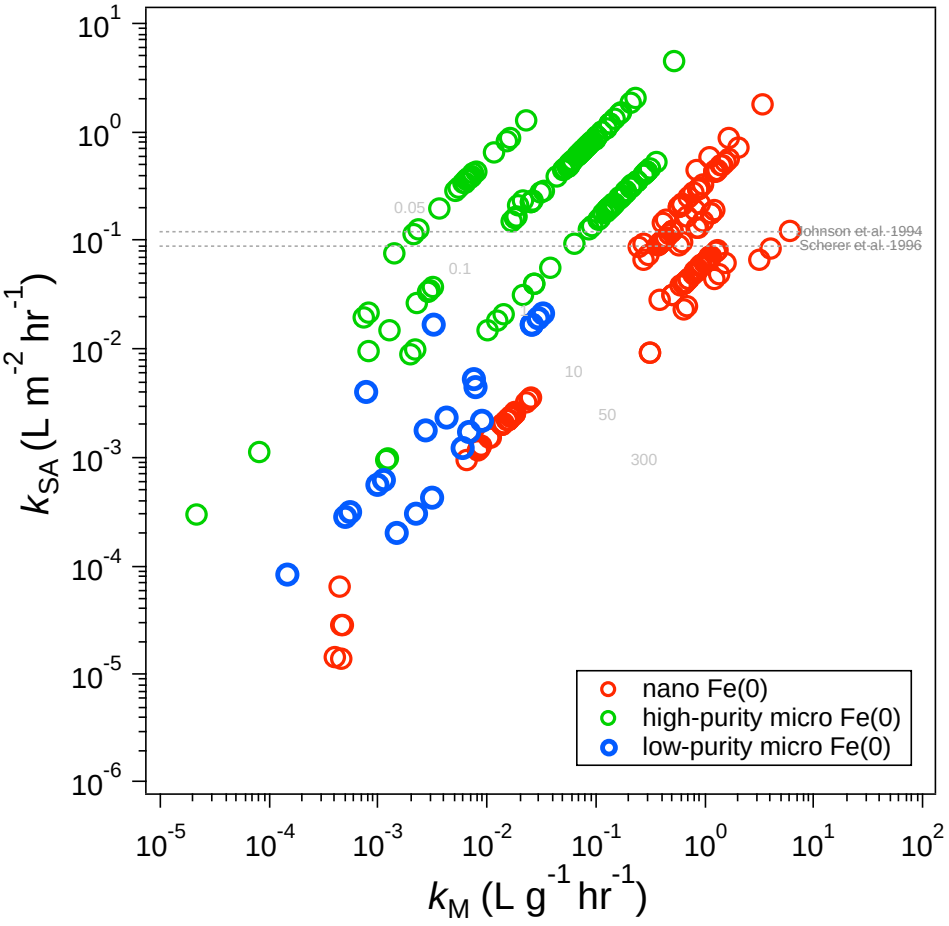

Figure 3.5. Log-log plot of k_{SA} versus k_M. Points include data for CT degradation by Fe^0 from several sources including our work. Slopes of diagonal dashed lines on which data fall are always equal to one, and intercepts are equal to log a_s, (a_s = surface area in m^2/g). This figure is color-coded according the purity/size of the iron. Diagonal dashed lines are represent constant a_s. Horizontal dashed lines represent k_{SA} values observed in earlier work by our group including experimental data from [6], and QSAR predictions from [23].

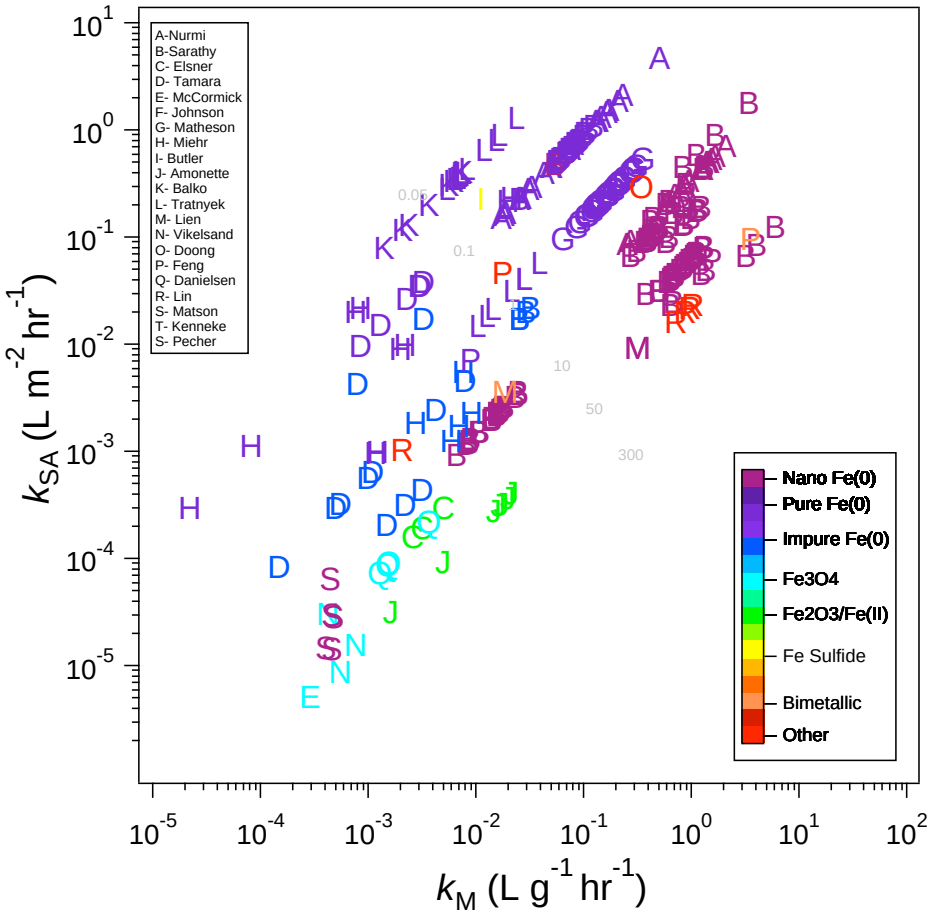

Figure 3.6. k_{SA}-k_M plots that expand on the type of reductant used in the data. Most of the data are for various types of Fe^0 but iron oxides and sulfides, and a few others are included. The legend shows the source of the data, listed by names of first authors of the respective publications [6, 24-40].

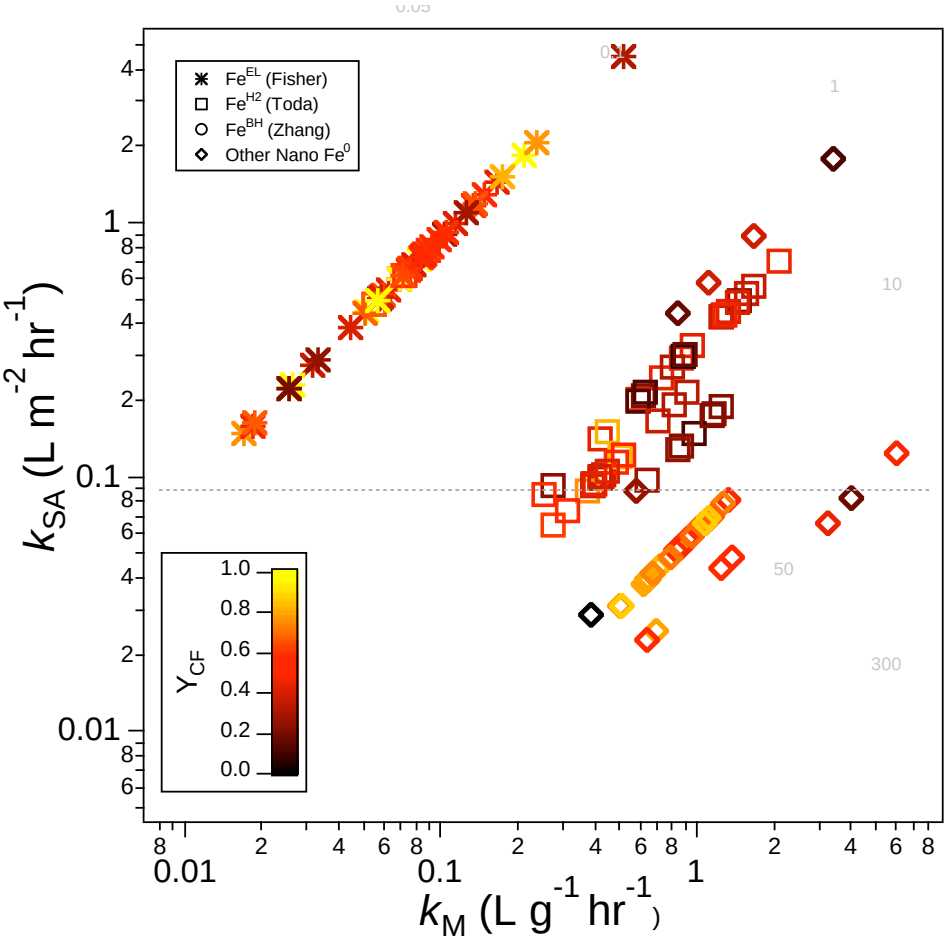

Figure 3.7. k_{SA} versus k_M plots color coded according the yield of chloroform (Y_{CF}). Data is predominantly from experiments done in this study.

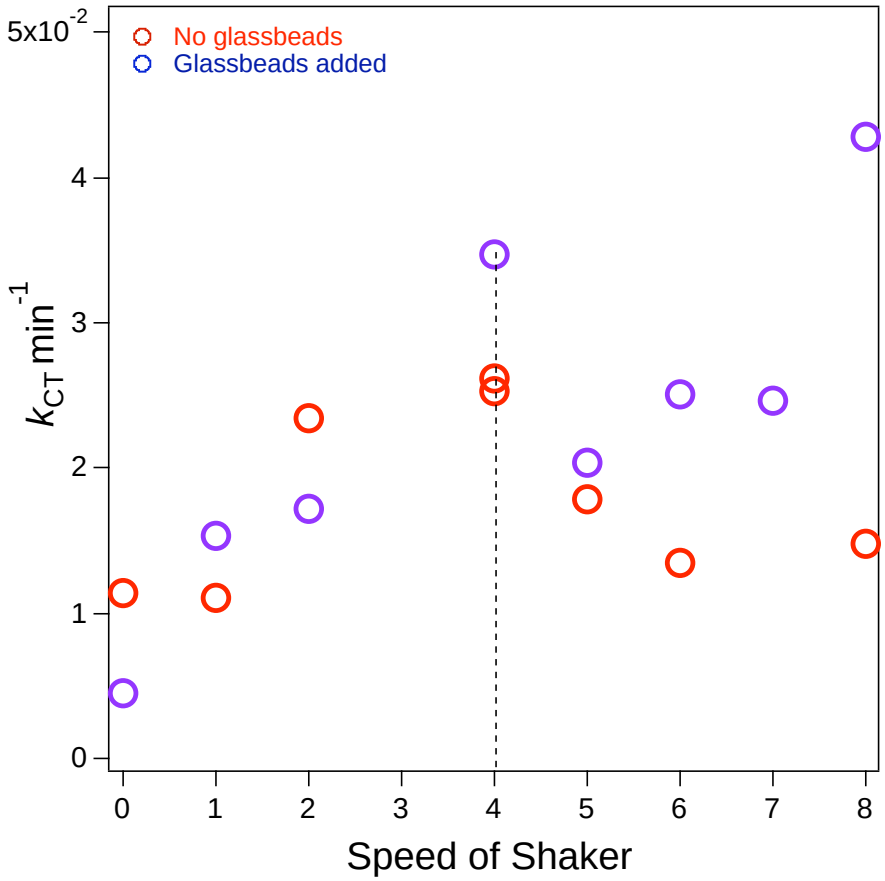

Figure 3.8. Rate constant of CT dechlorination versus speed of mixing. The x-axis is proportional to the actual speed of the shaker in rpm, where '1' ~ 6 rpm. The vertical dashed line represents the speed at which our batch reactions were mixed (~24 rpm).

Chapter 4:

Structure, Composition, and Morphology of Iron Nanoparticles in Solution

pp. 60-83 of thesis appeared as

Vaishnavi Sarathy, Paul G. Tratnyek, James T. Nurmi, Donald R. Baaer, James E. Amonette, Chan Lan Chun, R. Reardon. **2008**. Aging of Iron Nanoparticles in Aqueous Solution: Effects on Structure and Reactivation. *Journal of Physical Chemistry C,* Vol. **112** (7), 2286-2293.

DOI: dx.doi.org/10.1021/jp0777418

5

Remediation of 1,2,3-Trichloropropane: kinetics and feasibility of different pathways

Abstract

1,2,3-trichloropropane (TCP) has been used in a variety of chemical production processes, in agricultural chemicals, and as a solvent (paint and varnish removal, cleaning and degreasing, etc.) resulting in point and non-point source contamination. The chemical properties and available toxicity data suggest that contamination with TCP will pose clean-up challenges that are similar to those associated with other dense chlorinated solvents, but few studies have focused on the fate or remediation of less common chlorinated solvents such as TCP. TCP is different from commonly occurring groundwater contaminants such as carbon tetrachloride, and trichloroethylene, in that it is more recalcitrant towards remediation by oxidation-reduction processes. TCP exhibits little or no reaction with common reductants: construction-grade zero-valent iron, Fe(II) adsorbed to iron oxides, and slurry-aged nano iron. It does, however, react at measurable rates with some unaged dry nano-Fe^0, palladized nano-Fe^0, and fine-grained zinc. TCP can also be significantly degraded via hydrolysis at high pH and temperatures. The results suggest that hydrogenolysis (by electron transfer) is not favorable for TCP and it is comparatively more reactive by elimination or substitution reactions. Oxidation of TCP is much more feasible than reduction, especially when involving strong free-radical intermediates like hydroxyl radical (from activated hydrogen peroxide) and sulfate radical (from activated persulfate). Activated persulfate, in particular, not only oxidizes TCP relatively quickly, but also completely dechlorinates TCP, and might be recommended for field applications.

INTRODUCTION

1,2,3-trichloropropane (TCP) has been recognized as an emerging contaminant by agencies such as SERDP, which targeted TCP for study in 2003. In the past TCP has been used in a variety of chemical production processes and agricultural chemicals, and the primary cause for concern at contaminated sites is spills associated with its use as a solvent (paint and varnish removal, cleaning and degreasing, etc.) [1, 2]. TCP has lately been observed in a number of drinking water wells in California [3]. While the frequency and severity of sites contaminated is not known, the chemical properties [4] and available toxicity data [2] suggest that sites where contamination by TCP is significant will pose some challenges for clean-up that are similar to those associated with other dense chlorinated solvents [5].

However, the electronic structure of TCP will also cause some specific challenges. The three chlorine atoms on TCP are equally distributed among the three carbons causing the carbons to be very weakly electrophilic and consequently very recalcitrant towards reduction. This can be seen in Figure 5.1, which plots one-electron reduction potentials ($E_{1,\,red}$), E_{LUMO} (energy of the lowest occupied molecular orbital), and oxidation states for a number of chlorinated aliphatics including TCP. In general, the lower the "oxidation state"[4] of a carbon atom in the contaminant, the lower its reduction potential, and hence, its rate of reaction (typically) with reductants like iron. However, there are also other effects that influence reduction rate like steric factors, and the molecular mass of contaminant [6], e.g., in Figure 5.1, chloromethane, 1,2-dichloroethane, and TCP, which have the same oxidation state, have different E_{LUMO} and $E_{1,\,red}$ values. Similarly, mass-transfer effects are not reflected in E_{LUMO} and $E_{1,\,red}$ values.

From Figure 5.1, it can be extrapolated that permeable reactive barriers (PRBs) and other Fe^0 based remediation technologies, which typically produce rapid dechlorination of contaminants such as carbon tetrachloride (CT), trichloroethene (TCE), etc. are not likely to be effective for TCP degradation. It is, therefore, of significance to

[4] By assigning an oxidation state of –1 to Cl atoms, and +1 to H atoms, we arrive at average oxidation states for the most electrophilic carbons in contaminants.

understand which abiotic methods—whether reduction, oxidation, substitution, or elimination—will yield more favorable kinetics of TCP dechlorination. While TCP has not been widely studied—partly, due to its very recent classification as an emerging contaminant—there have been a few publications that have offered insights into its potential for reduction, oxidation, hydrolysis and bioremediation [7-10].

Natural attenuation can involve contaminant degradation by substitution and/or elimination. Hydrolysis can involve both substitution and elimination. Acid-catalyzed hydrolysis is not a feasible pathway for saturated organic compounds [11], however, TCP has been seen to react by both neutral and base-catalyzed hydrolysis [8, 9], and one study reported reaction only via base-catalyzed hydrolysis [8]. The various rate constants of neutral and base-catalyzed hydrolysis from different sources are shown in Table 5.1.

The degradation of TCP by iron—in columns—has been studied in [7, 10]. In the experiments using columns filled with micron-sized iron [7], the rate of TCP disappearance was found to increase with increasing percentage of iron used, up to a half-life of 3 hours with 100% iron (corresponding to a surface area to volume ratio of 8 m^2/L) in the column. Sorption onto the iron, or onto impurities such as carbon in the iron was expected to contribute to disappearance, though the extent of this contribution was not determined. In another column study with granular millimeter sized iron [10], it was observed that TCP was much less reactive than TCE, and reacted only in the initial 10% of each column, with a half-life of over 1000 days. There were many differences in the two studies, for example particle size of iron, the presence of a co-contaminant in [10], and un-quantified sorption processes in [7]. However, none of these seem sufficient to explain the large discrepancy between the studies.

A review of the various papers that have studied TCP degradation either by natural attenuation or by reduction processes [7-10] reveals at least 6 different products. Among these are propene, propane, 1,3-dichloropropene, 1-chloropropene, and 2,3-dichloropropene. The formation of non-chlorinated byproducts is at least as relevant, and perhaps more important than maximizing rates of dechlorination [12]. Both column experiments with iron discussed above [7, 10] yielded products, which were primarily composed of propanes and propenes. Base-catalyzed hydrolysis can yield dichloropropenes, which then hydrolyzed to chloropropanol. It is not clear if the

favorable products (i.e., dechlorinated) in column experiments with iron [7, 10] are due to base-catalyzed hydrolysis (of reactants, and byproducts) at large local pH, or reduction by iron.

Reaction byproducts during TCP oxidation, using Fenton's reagent [13] were found to be 1,3-dichloropropanone, chloroacetic acid, and formic acid. TCP had a half-life of ~1.5 days, but the author of this study concluded that this rate is too slow for the successful use of Fenton's reagent in treatment of TCP contaminated groundwater, unless other technologies are not applicable. Among *ex situ* treatments, one study showed that purging of a TCP solution with air follows pseudo first order kinetics with a rate constant = 2.99×10^{-2} min^{-1} [14]. This treatment is quite fast ($t_{1/2}$ = 24 min) compared to all other remediation treatments analyzed above, though the method simply transfers the TCP to the atmosphere, where TCP may be at least partially photo-oxidized to other chlorinated intermediates [15].

Biodegradation is an attractive remediation option for many chlorinated compounds, such as CT, TCE, etc. [16, 17]. However, metabolism requires electron and energy sources to initiate biodegradation, and TCP is not likely to be used as either an electron acceptor or donor, due both to its weak electrophilicity, and the presence of a number of stronger electrophiles, and nucleophiles in the environment. TCP is not known to be biodegraded significantly under aerobic conditions [18]. Naturally occurring bacteria such as *Nitrosomonas europaea*—which are ammonia oxidizing bacteria—have been found to transform TCP via a co-oxidative process, but only up to 9% and 23% in the absence and presence of ammonia, respectively [19]. Other studies [1] found cometabolic conversion of TCP by methanotrophs. Under anaerobic conditions, many studies have tried to engineer bacteria to utitlize TCP as the primary energy source, with little success [18]. However, recently, a recombinant strain was genetically engineered to use TCP as a carbon energy source [20]. While this strain gives high kinetics of TCP degradation, it is unable to degrade the chlorinated byproducts formed. In summary, most methods of biodegradation currently available do not completely degrade TCP, and those that do form recalcitrant chlorinated byproducts that may inhibit further bacterial growth [18].

Clearly, remediation of TCP by biodegradation will be challenging even more so than for most other chlorinated solvents. Among abiotic treatments, there is considerable uncertainty even among studies using the same method of remediation (e.g., iron columns and hydrolysis). To cover this gap, this study aims to be the first rigorous study of pathways suitable for *in situ* remediation of TCP. The primary goal of the work reported in this chapter is to determine the kinetics and pathways of TCP degradation by all of the major types of abiotic reactions that are relevant to natural and engineered strategies for *in situ* remediation—including hydrolysis, elimination, reduction, and oxidation—over the full range of conditions that are relevant to groundwater.

MATERIALS AND METHODS

Reagents. All chemicals were obtained in the highest purity commercially available and used as received. These include 1,2,3-trichloropropane, 1,2-dichloropropane, 1,3-dichloropropane, 1-chloropropane, and 2-chloropropane (Sigma Aldrich, HPLC grade); sodium persulfate, hydrogen peroxide, sodium carbonate, sodium bicarbonate, sodium sulfide, sodium borohydride, ferric chloride and ferrous chloride (Fisher Chemicals); Fe(III)-phthalocyanine from Sigma Aldrich; nitrogen gas (Airgas Inc.). All stocks and reaction solutions were prepared with N_2 degassed deionized water.

Iron types used in this study included Fe^{EL} (micron-sized electrolytic iron from Fisher Scientific), $Fe^{H2(D)}$, and $Fe^{H2(W)}$. $Fe^{H2(D)}$ and $Fe^{H2(W)}$ are both nano-sized iron particles produced by reduction of goethite and hematite by H_2 at high temperatures (200–600 °C), obtained from Toda Kogyo Corporation (Schaumberg, IL), and stand for unaged dry iron , and iron that is stabilized in slurry respectively (see Chapter 4 for more details). Magnetite (nano-powdered, $a_s > 60$ m^2/g) was obtained from Sigma Aldrich, and goethite ($a_s = 17.5$ m^2/g) was obtained from collaborators at PNNL (Bayferrox 910). Four different types of zinc were used— (*i*) zinc dust: 325 mesh; (*ii*) zinc dust <10 micron; (*iii*) granular zinc: 10+50 mesh; (*iv*) “KDF 55” zinc copper alloy; and (*v*) granular zinc: 30 mesh, among which (*iii*), (*iv*), and (*v*) were all used both as-received and acid washed. (*i*), (*ii*), (*iii*), and (*v*) were obtained from Sigma Aldrich, and (*iv*) was obtained from KDF fluid treatment, Inc.

Hydrolysis and Reduction. Batch experiments were conducted to test for (*i*) nucleophilic substitution and/or elimination with 10 mM carbonate buffer (hydrolysis), and 5 mM sulfide, and (*ii*) reduction of TCP with various reductants such as palladized Fe^0 (Fe^0/Pd), goethite, magnetite, micro- and nano-sized iron (Fe^{EL}, $Fe^{H2(W)}$, $Fe^{H2(D)}$) and different preparations of Zn (as mentioned in the reagents section). Goethite (Fe_2O_3) and magnetite (Fe_3O_4) were used in reaction vials with, and without, 1 mM $FeCl_2$. Fe^0/Pd was synthesized by a method under development by collaborator Jae-Hyoun Kim from POSTEC (Korea), by reduction of $FeCl_3$ by sodium borohydride followed by reaction with palladium acetate [21].

All hydrolysis (with buffers, and sulfide) and reduction batch experiments with Fe^0/Pd or Fe-oxides were set up in 40 mL VOA vials capped with *"mini-nert"* septa, and filled with deoxygenated deionized (DO/DI) MilliQ water. Controls had no buffers or reductants added. Carbonate buffered hydrolysis experiments were set up at both pH 9.2 and pH 11. HCl (1M) was added to the carbonate buffer at pH 11, to bring down the pH to 9.2. Replicates were set up for all experiments. 500 μL of saturated TCP solution was injected in each vial to bring the initial concentration of TCP ($[TCP]_0$) to 1.5×10^{-4} M. Other reduction experiments with Fe^{EL}, $Fe^{H2(D)}$, $Fe^{H2(W)}$, and different types of Zn were carried out in a similar fashion, but in 120 mL serum vials, with $[TCP]_0 = 1.0 \times 10^{-4}$ M. Most types of Zn were studied both in their native form, and after acid washing. Reactors typically contained 3 g of Zn and enough DO/DI water to fill the 120 mL serum vial. In most cases, 1 mL of the reaction solution was extracted, and diluted to 10 mL in a 20 mL headspace autosampler vial.

Oxidation. Reactors were set up to test oxidative degradation of TCP with sodium persulfate. Persulfate experiments were carried out in batch reactors, which were 120 mL serum vials with a 10:1 ratio of persulfate to TCP. The initial concentration of TCP was $1.0\text{-}2.0 \times 10^{-4}$ M. Vials were immersed in a water bath at 70 °C for the whole experiment.

Analysis. Gas chromatography with electron capture detection (GC/ECD) was used for detection of TCP. We use HP 5890 Series II GC fitted with an HP 7694 headspace autosampler, an on-column injection port and an electron capture detector, with Peak

Simple software. Autosystem XL GC with a TurboMass Gold mass spectrometer (MS) (mass spectrometry) was also used for end-point detection of products.

RESULTS AND DISCUSSION

Hydrolysis with carbonate buffered water. Neutral and base-catalyzed hydrolysis involve the attack of H_2O and OH^- as nucleophiles respectively. The net rate of reaction is shown in equation 1:

$$k_{obs} = k_N + k_B [OH^-] \quad (1)$$

where, k_N and k_B are first- and second-order rate constants of neutral and base-catalyzed hydrolysis respectively, and k_{obs} is the net pseudo-first order rate constant observed. The general recalcitrance of TCP suggests that it will take a strong nucleophile (OH^-) to initiate hydrolysis. Table 5.1 shows that there are significant differences in the kinetics of neutral and base-catalyzed hydrolysis of TCP as observed by prior studies [8, 9, 11].

In carbonate buffered experiments in DI water at 20 °C, we observed reduction of TCP at very high pH (11.0), but no significant degradation over 30 days at pH 9.2. Unbuffered controls at pH between 7 and 9 showed no decrease in TCP either (Figure 5.2). To compare our data with other studies on hydrolysis of TCP, we plotted data from Pagan et al. [8] as isotherms on a k_{obs} versus pH plot (Figure 5.3). Data from our studies, and from one other publication [9] are also plotted on these isotherms. Our k_B values (1.7×10^{-4} M^{-1} sec^{-1}) are consistent with all other studies (Table 5.1). Consistent with Pagan et al. [8], we also observed that neutral hydrolysis is most likely not significant for TCP, and hydrolysis is predominantly base-catalyzed, i.e., rate of hydrolysis increases with temperature and $[OH^-]$. We saw one product on the GC/ECD, which we did not identify, but we expect it to be 1,2-dichloropropane, based on results in [8]. However, we were not able to confirm this.

Inorganic sulfide. Inorganic sulfide is a significant component of all anoxic groundwater and surface water zones [23]. It is likely that nucleophilic substitution by inorganic sulfide will dominate reduction via natural attenuation for some contaminants [24]. Addition of 5 mM sodium sulfide to hydrolysis experiments (with DI water, and no buffer), caused faster TCP degradation than both carbonate-buffered solutions. However,

the batch reactors with sulfide were observed to have a pH of 11.6, which can contribute to at least half of the observed reactivity by base-catalyzed hydrolysis (Figure 3). Therefore, at ambient groundwater temperatures and pH, it is unclear what the relative contribution of sulfide as opposed to pH is towards degradation of TCP. However at high pH values, it is likely that the major contribution is due to base-catalyzed hydrolysis. Appearance of a product was observed, which was not identified. It is expected to be a dichloropropane, based on previous work [8].

Reduction: micron- and nano-sized Fe^0, and iron oxides. Column experiments with granular iron have shown contradictory results with one source [7] showing reactivity in the order of a few hours, and another publication showing very slow reaction times, over the order of years [10]. We know that pH values are highly elevated in the presence of high concentrations of zero-valent iron [25] (and unpublished data from our group). Therefore, we can safely assume that the local pH values in the column experiments were of the order of at least 10 or higher. Therefore, it is very likely that a significant part of the reaction observed in [7] was due to hydrolysis (Figure 3). Also, theoretical predictions based on extrapolations from QSAR calculations [26] indicate slow but significant kinetics of TCP degradation with Fe^0.

In this work, micron-sized (Fe^{EL}) and "flash-dried"[5] slurry-aged nano-sized zero valent iron ($Fe^{H2(W)}$) gave no degradation of TCP over 30 days. However, batch reactions of TCP with un-aged nano Fe^0 ($Fe^{H2(D)}$, see Chapter 4 for details on iron type and reactivity) gave reaction rates, that were slow, but significant. All rate constants (surface area normalized, i.e., k_{SA}) are compared in Figure 5.4. No products were detected in any of the reactions. pHs at the end of the batch experiments with Fe^0 are all estimated to be ~9-10 based on previous data (not shown). These pHs are not expected to cause competitive rates of hydrolysis.

The slow/negligible rates of dechlorination of TCP by Fe^0 are consistent with the free energies of dechlorination for all the congeners of chlorinated propanes that have been calculated by collaborator, Eric Bylaska, at the Pacific Northwest National

---

[5] $Fe^{H2(W)}$ obtained in slurry form was "flash-dried' by drying the slurry on a filter (nanometer pore size) under vacuum in anoxic conditions [12].

Laboratory. These numbers are shown in Figure 5.5, which has also been annotated with free energies of dechlorination of the chlorinated methanes (i.e., carbon tetrachloride, chloroform, etc.), which were available from previously performed calculations. It is clear from Figure 5.5 that dechlorination of the chlorinated propanes is less favorable for pathways initiated by concerted dissociative electron transfer (which assumed to be the rate limiting step and therefore was the focus of the calculations performed).

We also tested the reaction of Fe(III) and Fe(II)/Fe(III) oxides (goethite and magnetite), both with and without adsorbed Fe(II)—which is known to have a catalytic effect on reduction of contaminants by Fe oxides [27]—with TCP, since these systems have been observed to degrade CT [27-30]. These systems are known to be less reducing than Fe^0, and as expected, none of these systems showed any significant TCP degradation within the time frame of our experiment—30 days (data not shown).

Reduction: Bimetallic Fe^0 and Zn. The question of whether there is some variation on the established zero-valent metal-based reductants that will give relatively fast dechlorination of TCP led to batch experiments with Zn and Fe^0 derivatized with potentially catalytic adjuvants like palladium and phthalocyanine—which is a porphyrin like molecule, with properties of a redox shuttle [31]. Among all reductants studied, Zn reduced TCP the fastest, which is consistent with its thermodynamic reduction potential being higher than that of Fe^0 [32]. Zn is thought to reduce contaminants by β-elimination, which is a dichloro-elimination, as opposed to hydrogenolysis [33].

After 7 days of reaction, no products were observed by GC/MS. A number of types of Zn—of different sources, compositions, sizes, and preparation methods—were studied, results of which are shown in Figure 5.6. The fastest reaction (without surface area-normalization) was observed with <10 um sized Zn particles. Some zinc types were acid washed, but paradoxically showed slower reactivity with TCP. We hypothesize that this is due to rapid passivation of Zn after acid washing, especially when in contact with ambient atmosphere.

Other reductants that yielded viable rates of reduction of TCP were palladized nano Fe^0 (Fe^0/Pd), and $Fe^{H2(D)}$ derivatized with a Fe(III)-phthalocyanine complex, both of which reacted with TCP to yield half-lives of 6.5 and 3 days respectively (data not shown, see Figure 5.4). However, controls with just Fe(III)-phthalocyanine showed

similar reactivity to the complex sorbed on to $Fe^{H2(D)}$, and it therefore seems that it is the complex itself that is responsible for TCP degradation. While Fe(III)-phthalocyanine is known to be catalyze electron transfer [31], it is not clear how it facilitates reduction/oxidation of TCP in the absence of an external redox agent.

Oxidation. TCP was found to degrade at a substantial rate in reactions performed under classical Fenton conditions (Figure 5.7). After the first 20 minutes, the disappearance of TCP appeared to be first-order with a half-life of 4-10 hrs. However, the overall kinetics are not simply pseudo first order and suggest the more complex, bimodal behavior that is often observed with Fenton systems [34]. Although it is easy to rationalize the bimodal kinetics—due to a shift from Fe(II) to Fe(III) catalyzed decomposition of H_2O_2—we have not been successful in modeling this particular data set. A previous study of Fenton degradation of TCP found a half-life of 1.5 days, and products that included 1,3-dichloropropanone, chloroacetic and formic acids [13].

TCP is also rapidly oxidized by persulfate activated by heat (70 °C) as shown in Figure 5.8. Experiments were performed in both oxic and anoxic conditions to see if dissolved oxygen might be activated as a side effect of sulfate radical chemistry, thereby providing additional pathways for TCP degradation and faster degradation rates. Fitting these data gave k_{obs} = 0.15-0.19 hr^{-1} and $t_{1/2}$ = 4 hr for anoxic conditions, and k_{obs} = 0.39 hr^{-1} and $t_{1/2}$ = 1.8 hr for oxic conditions. Clearly, the presence of dissolved oxygen contributes to increased rates of TCP dechlorination, though at this point, we are unclear about the exact mechanism involved.

Concurrent with the experiments shown in Figure 5.8, we also measured chloride and CO_2 concentrations to assess the degree to which TCP degradation resulted from dechlorination and mineralization, respectively. From Table 5.2, we can see that after 6 hrs, and 24 hrs of reaction, we saw ~73% and 85% of the TCP—that had reacted—as chloride (which means 73% and 85% of TCP was compeletely dechlorinated, respectively). These numbers were similar for both oxic, and anoxic reactions. However, at 6 hours, only 36% of TCP showed up as CO_2, but all the 85% degraded after 24 hours showed up as CO_2 indicating complete mineralization. Clearly oxidation by persulfate has very high promise for *in situ* remediation of TCP, both in terms of kinetics and formation of non-chlorinated products.

SUMMARY AND CONCLUSIONS

Generally, in groundwater, TCP is very mobile, persistent, and recalcitrant. Available pathways for biotic/abiotic degradation of TCP include hydrolysis, elimination, reduction, and oxidation. Biodegradation (mostly by oxidation) appears to be slow under most circumstances. Genetically engineered bacteria degrade TCP at a viable rate, but form chlorinated byproducts that are difficult to degrade further. Among abiotic degradation pathways, hydrolysis is slow, except at very high temperatures/pH. Reduction is possible but not very favorable using zero-valent iron, though one preparation of nano-iron ($Fe^{H2(D)}$) showed slow but significant reduction of TCP. At least two systems (Fe^0/Pd and Zn) have been found that reduce TCP at significant rates and have the potential to form favorable products, but more work is needed to determine if these will have any utility in field applications due to cost and toxicity issues, respectively. One electrocatalyst studied—Fe(III)-phthalocyanine—showed high reactivity with TCP, but the mechanism of redox activation is not understood. Abiotic *in situ* oxidation is more promising than the above methods, especially with hydroxyl radicals (e.g., Fenton related reactions) or sulfate radicals (i.e., activated persulfate). Overall, it appears that TCP will prove to be very resistant to natural attenuation and most conventional methods of remediation using Fe^0 or Fe oxides. Only chemical oxidation processes, and reduction using Fe/Pd and Zn appear to have potential for rapid degradation of significant quantities of TCP.

ACKNOWLEDGMENTS

I would like to thank my colleagues at OGI—Jamie Powell, Jae-Hyoun Kim, and Priscilla Lee. Jamie Powell performed the experiments with TCP and Fenton's reagent, Jae-Hyoun Kim prepared the palladized iron, and Priscilla Lee synthesized Fe(III)-phthalocyanine and also performed some experiments with Fe(III)-phthalocyanine and TCP. I would also like to thank Eric Bylaska from the Pacific National Northwest Laboratory for theoretical calculations of free energies of dechlorination of different chlorinated propanes.

REFERENCES

1. Bosma, T.; Janssen, D. B., Conversion of chlorinated propanes by Methylosinus trichosporium OB3b expressing soluble methane monooxygenase. *App. Microbiol. Biotechnol.* **1998,** *50* (1), 105-112.

2. Agency for Toxic Substances and Disease Registry, U.S. Public Health Service Commissioned Corps, *Toxicological profile for 1,2,3-Trichloropropane*; 1992; p 119.

3. California DPH, 1,2,3,-Trichloropropane. In 2007. http://www.cdph.ca.gov/certlic/drinkingwater/Pages/123TCP.aspx

4. Howard, P. H., 1,2,3-Trichloropropane. In *Handbook of Environmental Fate and Exposure Data for Organic Chemicals*, Lewis Publishers: Boca Raton, 1993; Vol. IV, Solvents 2, p 540-545.

5. Pankow, J. F.; Cherry, J. A., *Dense Chlorinated Solvents and Other DNAPLs in Groundwater: History, Behavior, and Remediation*. Waterloo Press: Portland, OR, 1996; p 522.

6. Atkins, P. W., *Physical Chemistry*. W. H. Freeman and Company: New York, 1998; p 999.

7. Focht, M. R. Bench-Scale Treatability Testing to Evaluate the Applicability of Metallic Iron for Above-Ground Remediation of 1,2,3-Trichloropropane Contaminated Groundwater. *M.S. Thesis.* University of Waterloo, 1994.

8. Pagan, M.; Cooper, W. J.; Joens, J. A., Kinetic studies of the homogeneous abiotic reactions of several chlorinated aliphatic compounds in aqueous solution. *App. Geochem.* **1998,** *13* (6), 779-785.

9. Ellington, J. J. *Hydrolysis rate constants for enhancing property-reactivity relationships*; Office of Research and Development,Environmental Research Lab, Athens, GA, USA: 1989; p 59.

10. Klausen, J.; Vikesland, P. J.; Kohn, T.; Burris, D. R.; Ball, W. P.; Roberts, A. L., Longevity of granular iron in groundwater treatment processes: solution composition effects on reduction of organohalides and nitroaromatic compounds. *Environ. Sci. Technol.* **2003,** *37* (6), 1208-1218.

11. Wolfe, N. L.; Jeffers, P. M., Hydrolysis. In *Handbook of Property Estimation Methods for Chemicals: Environmental and Health Sciences*, Lewis: Boca Raton, FL, 2000; p 311-333.

12. Nurmi, J. T.; Tratnyek, P. G.; Sarathy, V.; Baer, D. R.; Amonette, J. E.; Pecher, K.; Wang, C.; Linehan, J. C.; Matson, D. W.; Penn, R. L.; Driessen, M. D., Characterization and properties of metallic iron nanoparticles: Spectroscopy, electrochemistry, and kinetics. *Environ. Sci. Technol.* **2005,** *39* (5), 1221-1230.

13. Hunter, F., Fenton's treatment of 1,2,3-trichloropropane: chemical reaction byproducts, pathways, and kinetics. In *Proceedings of the International Symposium on Chemical Oxidation: Technology for the Nineties*, Technomic: 1997; Vol. 6, pp 50-71.

14. Lin, D. P.; Falkenberg, C.; Payne, D. A.; Thakkar, J.; Tang, C.; Elly, C., Kinetics of purging for the priority volatile organic compounds in water. *Anal. Chem.* **1993,** *65* (8), 999-1002.

15. Voicu, I.; Barnes, I.; Becker, K. H.; Wallington, T. J.; Inoue, Y.; Kawasaki, M., Kinetic and product study of the Cl-initiated oxidation of 1,2,3-trichloropropane (CH2CICHCICH2Cl). *J. Phys. Chem. A* **2001,** *105* (21), 5123-5130.

16. Van Eekert, M. H. A.; Schroder, T. J.; Stams, A. J. M.; Schraa, G.; Field, J. A., Degradation and fate of carbon tetrachloride in unadapted methanogenic granular sludge. *App. Environ. Microbiol.* **1998,** *64*, 2350-2356.

17. Boopathy, R., Anaerobic biotransformation of carbon tetrachloride under various electron acceptor conditions. *Biores. Technol.* **2002,** *84*, 69-73.

18. Konnecker, G.; Schmidt, S., Environmental risk assessment for 1,2,3-trichloropropane - Is there a risk for the aquatic environment? *Fresen. Environ. Bull.* **2003,** *12* (12), 1444-1449.

19. Vannelli, T.; Hooper, A. B., Reductive dehalogenation of the trichloromethyl group of nitrapyrin by the ammonia-oxidizing bacterium Nitrosomonas europaea. *App. Environ. Microbiol.* **1993,** *59* (11), 3597-3601.

20. Bosma, T.; Damborsky, J.; Stucki, G.; Janssen, D. B., Biodegradation of 1,2,3-trichloropropane through directed evolution and heterologous expression of a haloalkane dehalogenase gene. *App. Environ. Microbiol* **2002,** *6 8*(7), 3582-3587.

21. Lien, H.-L. Nanoscale Bimetallic Particles for Dehalogenation of Halogenated Aliphatic Compounds. *Ph.D. Thesis*, Lehigh University, 2000.

22. Environmental Security Technology Certification Program (ESTCP) *Permeable Reactive Wall Remediation of Chlorinated Hydrocarbons in Groundwater*; US Department of Defense (DOD): Arlington, VA, 1999; p 52.

23. Barbash, J. E.; Reinhard, M., Abiotic dehalogenation of 1,2-dichloroethane and 1,2-dibromoethane in aqueous solution containing hydrogen sulfide. *Environ. Sci. Technol.* **1989,** *2 3*(11), 1349-1357.

24. Haag, W. R.; Mill, T., Some reactions of naturally occurring nucleophiles with haloalkanes in water. *Environ. Toxicol. Chem.* **1988,** *7*, 917-924.

25. Matheson, L. J.; Tratnyek, P. G., Reductive dehalogenation of chlorinated methanes by iron metal. *Environ. Sci. Technol.* **1994,** *28* (12), 2045-2053.

26. Scherer, M. M.; Balko, B. A.; Gallagher, D. A.; Tratnyek, P. G., Correlation analysis of rate constants for dechlorination by zero-valent iron. *Environ. Sci. Technol.* **1998,** *32* (19), 3026-3033.

27. Pecher, K.; Haderlein, S. B.; Schwarzenbach, R. P., Reduction of polyhalogenated methanes by surface-bound Fe(II) in aqueous suspensions of iron oxides. *Environ. Sci. Technol.* **2002,** *36* (8), 1734-1741.

28. Amonette, J. E.; Workman, D. J.; Kennedy, D. W.; Fruchter, J. S.; Gorby, Y. A., Dechlorination of carbon tetrachloride by Fe(II) associated with goethite. *Environ. Sci. Technol.* **2000,** *34* (21), 4606-4613.

29. Danielsen, K. M.; Hayes, K. F., pH dependence of carbon tetrachloride reductive dechlorination by magnetite. *Environ. Sci. Technol.* **2004,** *38* (18), 4745 -4752.

30. McCormick, M. L.; Adriaens, P., Carbon tetrachloride transformation on the surface of nanoscale biogenic magnetite particles. *Environ. Sci. Technol.* **2004,** *38* (4), 1045-1053.

31. Vasudevan, P.; Phougat, N.; Shukla, A. K., Metal phthalocyanines as electrocatalysts for redox reactions. *App. Organomet. Chem.* **1996,** *10* (591-604).

32. Lee, J. D., *Concise Inorganic Chemistry*. Fourth Edition ed.; Chapman and Hall, Ltd.: London, 1994.

33. Arnold, W. A.; Ball, W. P.; Roberts, A. L., Polychlorinated ethane reaction with zero-valent zinc: Pathways and rate control. *J. Contam. Hydrol.* **1999,** *40* (2), 183-200.

34. Pignatello, J. J.; Oliveros, E.; MacKay, A., Advanced oxidation processes for organic contaminant destruction based on the Fenton reaction and related chemistry. *Crit. Rev. Environ. Sci. Technol.* **2006,** *36* (1), 1-84.

35. Totten, L. A.; Roberts, A. L., Calculated one- and two-electron reduction potentials and related molecular descriptors for reduction of alkyl and vinyl halides in water. *Crit. Rev. Environ. Sci. Technol.* **2001,** *31* (2), 175-221.

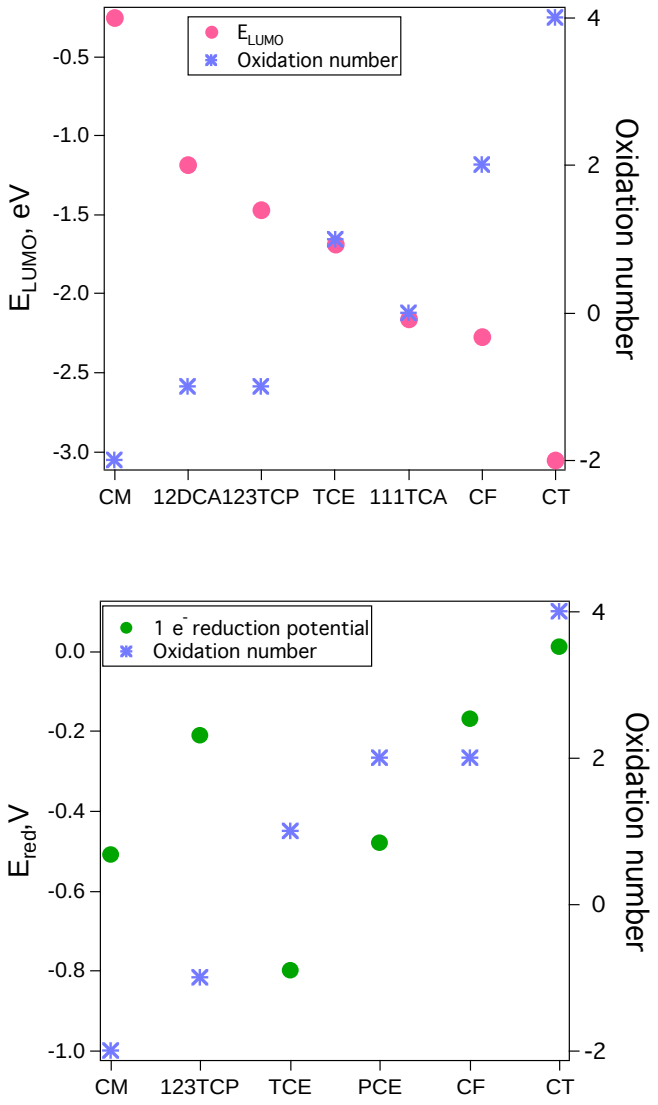

Figure 5.1. E_{LUMO} (top), and $E_{1,red}$ (bottom) plotted for TCP and related contaminants. E_{LUMO} is the energy of the lowest occupied molecular orbital [26], and $E_{1,\,red}$ is the 1 electron reduction potential of the contaminant [35]. Oxidation numbers for the active carbon in organic contaminants are calculated as per footnote number 2.

Table 5.1. Hydrolysis rate constants from different sources

Neutral hydrolysis k_N, sec^{-1}	Base-catalyzed hydrolysis k_B, $M^{-1}sec^{-1}$	Source
8.8×10^{-2}	3.0×10^{-5}	Wolfe and Jeffers, 2000 [11]
N/A	1.6×10^{-4} (20 °C)	Pagan, et al. 1998 [8]
2.8×10^{-7} (25 °C)	5.0×10^{-10} (25 °C)	Ellington et al. 1987 [9]
N/A	1.7×10^{-4} (20 °C)	This study

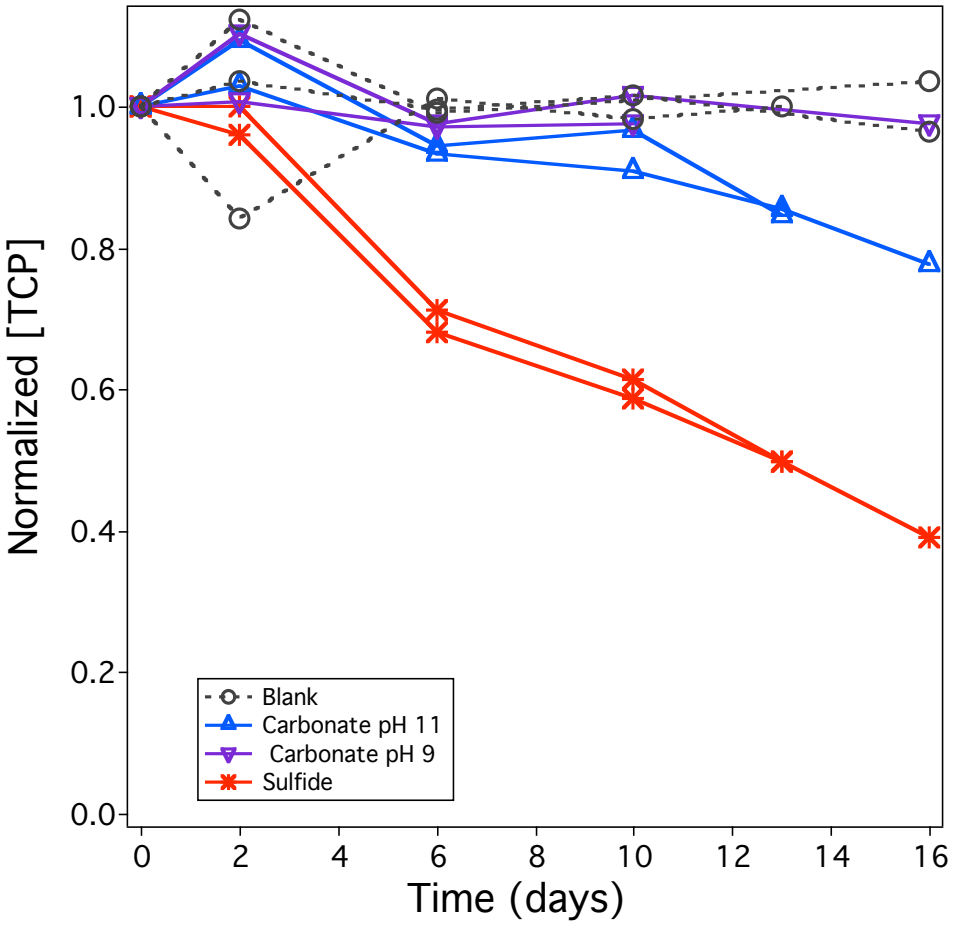

Figure 5.2. Disappearance kinetics of TCP by hydrolysis in 10 mM carbonate buffered water (at pH 9.2 and 11), and by substitution/hydrolysis in 5 mM sulfide solutions. $[TCP]_0 = 1.5 \times 10^{-4}$ M in all experiments. 'Blanks' have TCP, but no sulfide or carbonate. All experiments were carried out in duplicate, except the blanks, which were carried out in triplicate.

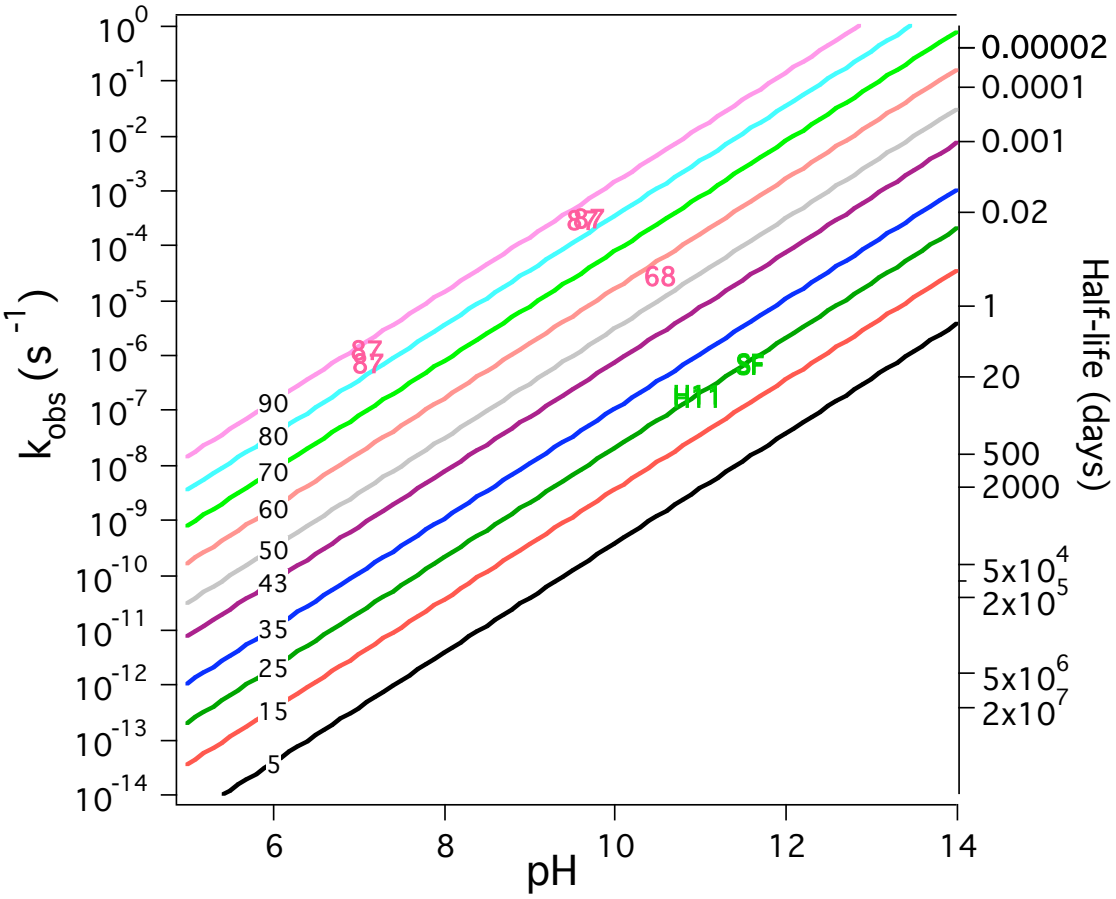

Figure 5.3. Hydrolysis rate constants plotted versus pH and temperature. Rate constants at different pH and temperatures were calculated based on Arrhenius constants in [8], and plotted as isotherms. Our data are marked on top of the isotherms are shown (green markers: 'H11' for pH 11 carbonate buffer and 'SF' for 5 mM Na_2S). Pink markers, labeled according to the temperature of experiments, are data from [9].

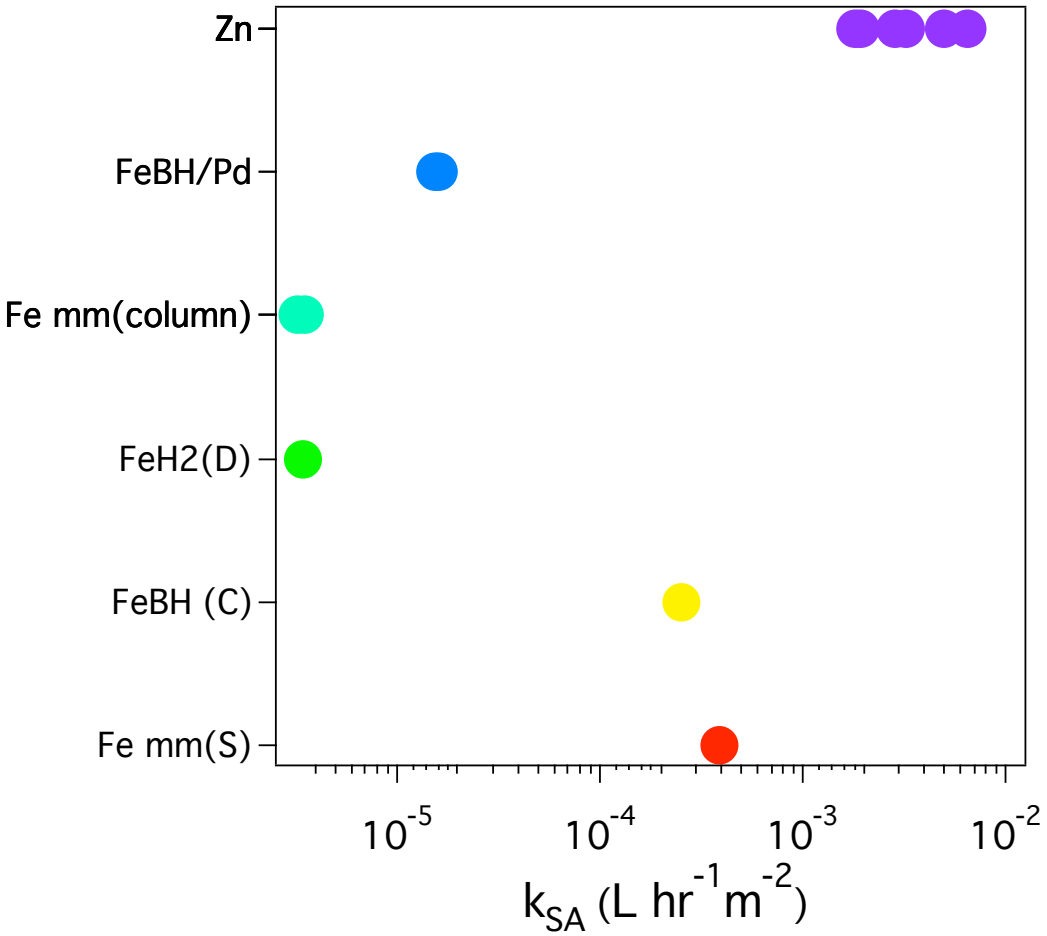

Figure 5.4. Estimated and experimental surface area normalized reaction rate constants of different reductants with TCP. Fe^{BH}(C) refers to estimated values from Song and Carraway (2005) for borohydride reduced nano-iron (which we extrapolated based on their QSAR and E_{LUMO} values from Scherer et al. [26]). Fe^{mm} (S) refers to estimated numbers for granular millimeter sized iron from Scherer et al. [26]. Both papers use QSARs to predict reaction rates from E_{LUMO} energies. Fe^{mm} (column) refers to data from [7], where milli-meter sized iron was used in column experiments. $Fe^{H2(D)}$, Fe/Pd and Zn refer to un-aged dry nano-Fe^0, palladized iron, and zinc, respectively, and are all analyzed in this study.

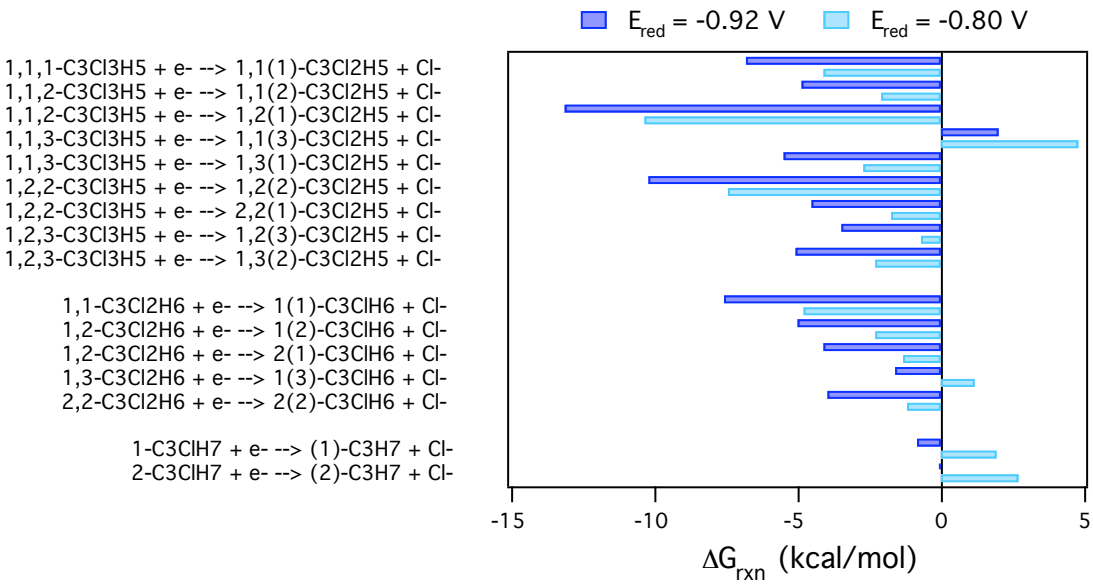

Figure 5.5. Calculated free energies of reaction for dechlorination of all the chlorinated propanes, calculated with respect to two reductants with E_{red} = -0.92 and –0.8 V (Courtesy of Eric Bylaska, PNNL).

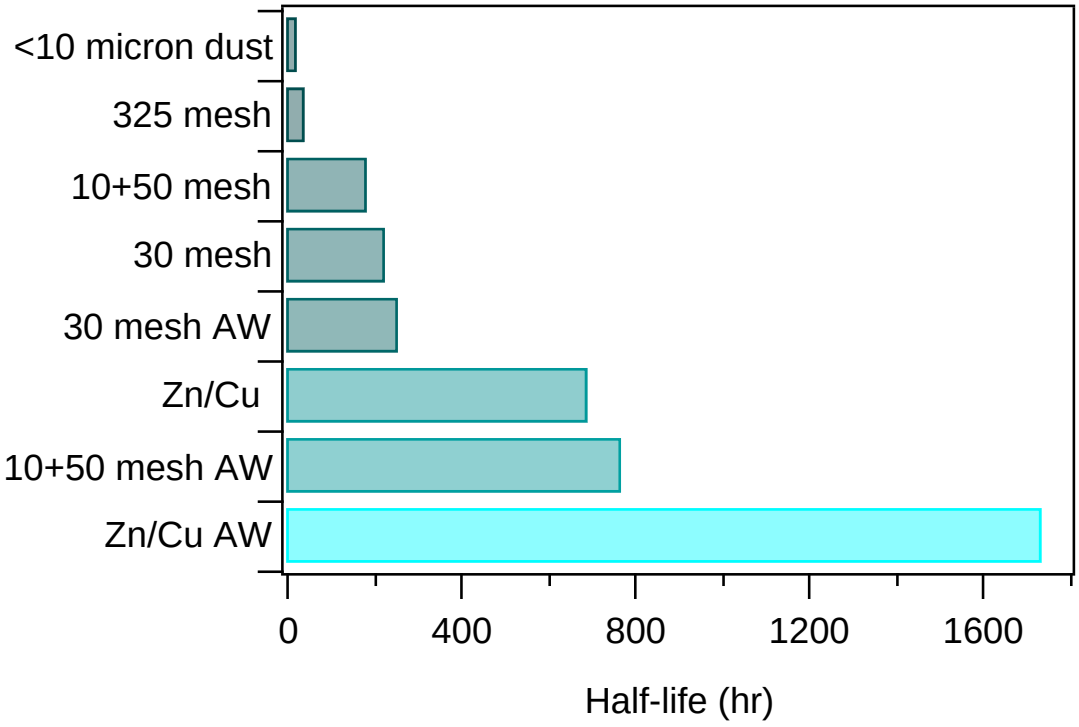

Figure 5.6. Half-lives of TCP degradation with various types of Zn. The labeling on the y-axis reflects the sizes of Zn particles. Some of the zinc was acid-washed—which is represented by "AW".

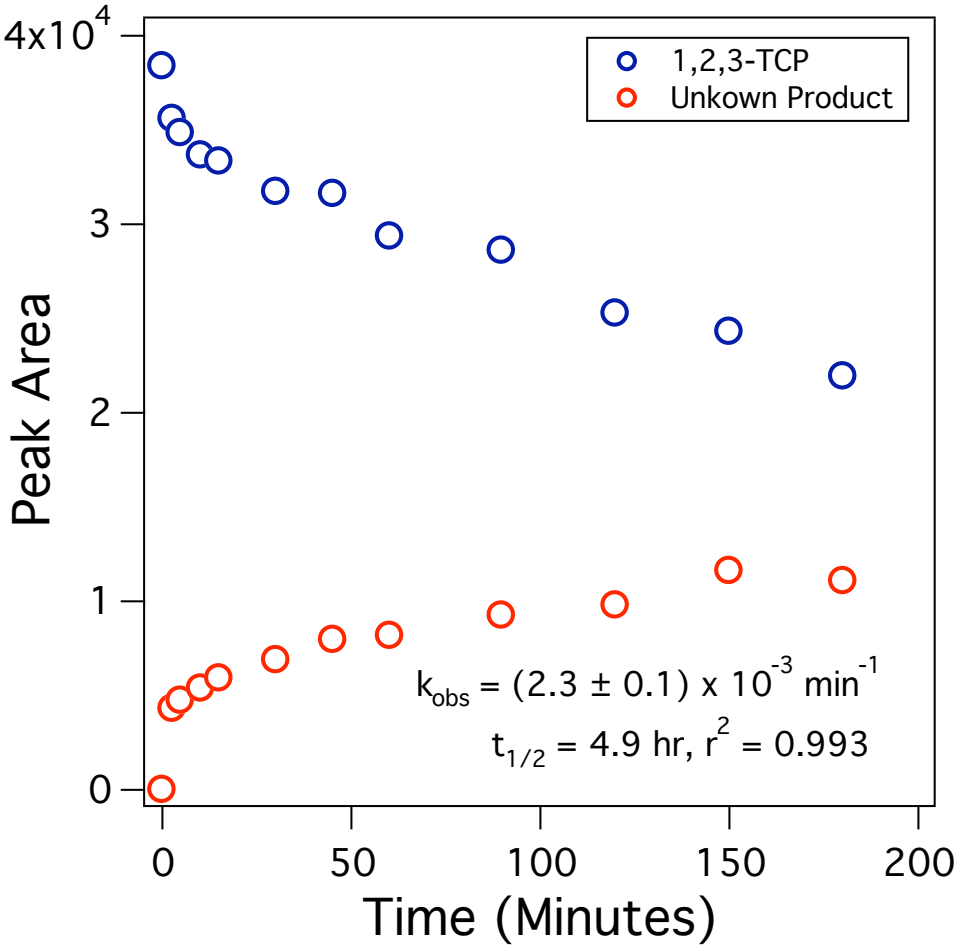

Figure 5.7. Results from batch experiments under classic Fenton conditions. $[TCP]_0$ = 0.05 mM, $[H_2O_2]$ = 300 mM, $[FeCl_2]$ = 25 mM, pH = 2.9, T = 25°C.

Table 5.2. Summary of products from oxidation of 0.1 mM TCP with activated persulfate.

Conditions	Cl^- sampling time	Final $[Cl^-]$ (% of $[TCP]_0$)	CO_2 sampling time	Final $[CO_2]$ (% of $[TCP]_0$)
Oxic	6.1 hr	0.38 mM (74%)	--	--
Oxic	23.4 hr	0.48 mM (84%)	--	--
Anoxic	6.5 hr	0.24 mM (71%)	3 hr	0.076 mM (36%)
Anoxic	23.5 hr	0.40 mM (86%)	26 hr	0.42 mM (88%)

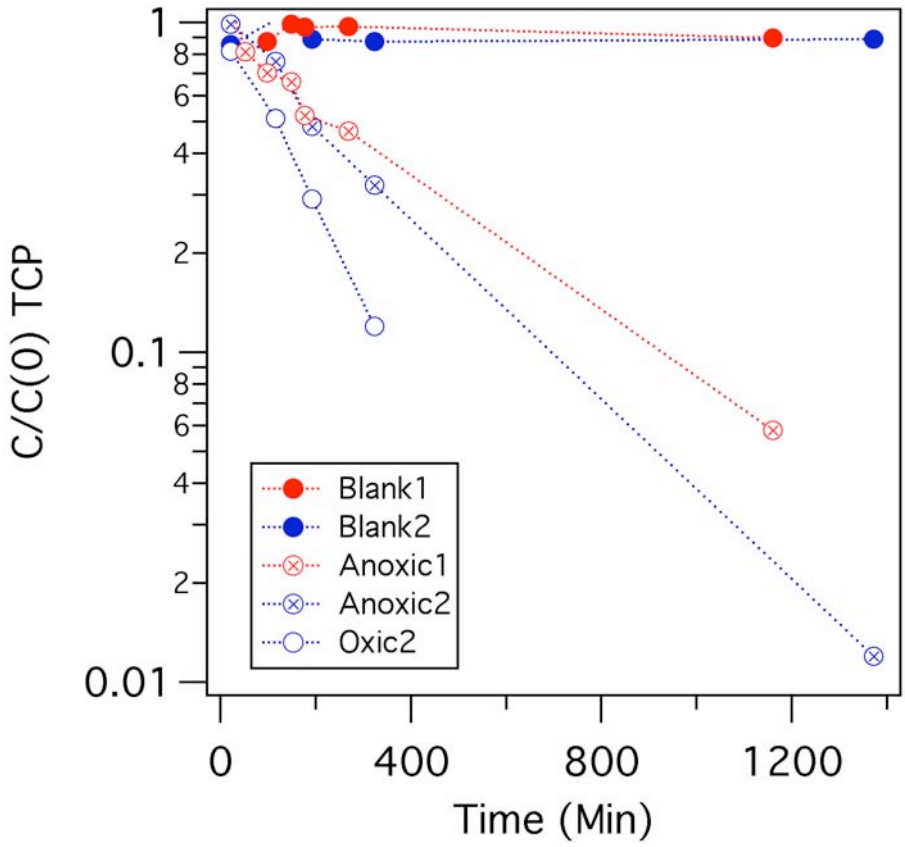

Figure 5.8. **Pseudo first-order disappearance kinetics of TCP in unbuffered, heat activated, persulfate. '1' and '2' refer to replicate experiments. $[TCP]_0 = 10^{-4}$ M, [persulfate] = 10^{-3} M.**

Appendix

This table is a summary of data obtained from all batch experiments conducted with carbon tetrachloride (CT) in the course of this study. The first column lists the type (or objective) of experiment conducted. Most important experimental variables associated with the experiments are listed in the following columns. The column labeled "Other" lists variables that have not been covered by the other columns. All batch reactions were carried out in 120 mL serum vials capped with Hycar rubber septa, in deoxygenated DI water. "Sparge gas" refers to the gas used to deoxygenate the DI water. In the column labeled "Iron Type", Fe^{H2}, Fe^{BH}, Fe^{AR}, Fe^{OM}, Fe^{EL}, and Fe^{PL} refer to nano-iron (from H_2 reduction of oxides), nano-iron (from reduction of oxides by borohydride), ball-milled nano iron, nano-iron in an alumina matrix, electrolytically produced micro-iron, and construction-grade granular iron, respectively. These iron types have also been defined in Chapters 2 and 4. k_{obs}, k_M, and k_{SA} are the pseudo-first order rate constant, the mass-normalized rate constant, and the surface area-normalized rate constant for CT dechlorination, respectively. Y_{CF} is the yield of chloroform produced during CT reduction.

Dataset	Iron Type	Other	Sparge Gas	$\log_{10}$ ($[CT]_0$ in M)	$\log_{10}$ (k_{obs} in hr^{-1})	$\log_{10}$ (k_M in L g^{-1} hr^{-1})	$\log_{10}$ (k_{SA} in L m^{-2} hr^{-1})	Y_{CF}	m^2/L
$[CT]_0$ variation	Fe^{H2}	Unbuffered	Ar	-7.05	-0.37	-0.36	-1.00	0.44	4.19
$[CT]_0$ variation	Fe^{H2}	Unbuffered	Ar	-6.43	-0.38	-0.37	-1.01	0.37	4.19
$[CT]_0$ variation	Fe^{H2}	Unbuffered	Ar	-5.98	-0.38	-0.37	-1.00	0.37	4.19
$[CT]_0$ variation	Fe^{H2}	Unbuffered	Ar	-4.89	-0.30	-0.29	-0.93	0.64	4.19
$[CT]_0$ variation	Fe^{H2}	Unbuffered	Ar	-4.30	-0.41	-0.40	-1.03	0.68	4.19
$[CT]_0$ variation	Fe^{H2}	Unbuffered	Ar	-4.96	-0.32	-0.31	-0.95	0.49	4.19
$[CT]_0$ variation	Fe^{H2}	Unbuffered	Ar	-4.38	-0.41	-0.40	-1.03	0.38	4.19
$[CT]_0$ variation	Fe^{H2}	Unbuffered	Ar	-4.01	-0.57	-0.56	-1.19	0.61	4.19
$[CT]_0$ variation	Fe^{EL}	Unbuffered	Ar	-6.34	0.42	-0.98	-0.04	0.51	2.93
$[CT]_0$ variation	Fe^{H2}	Unbuffered	Ar	-6.19	-0.16	-0.15	-0.78	0.22	4.19
$[CT]_0$ variation	Fe^{H2}	Unbuffered	Ar	-5.72	-0.44	-0.42	-1.06	0.39	4.19
$[CT]_0$ variation	Fe^{EL}	Unbuffered	Ar	-4.73	0.29	-1.11	-0.18	0.39	2.92
$[CT]_0$ variation	Fe^{EL}	Unbuffered	Ar	-4.24	0.18	-1.22	-0.29	0.44	2.92
$[CT]_0$ variation	Fe^{EL}	Unbuffered	Ar	-3.72	0.34	-1.06	-0.13	0.29	2.92
$[CT]_0$ variation	Fe^{EL}	Unbuffered	Ar	-4.84	0.30	-1.10	-0.17	0.27	2.93
$[CT]_0$ variation	Fe^{EL}	Unbuffered	Ar	-4.29	0.17	-1.23	-0.30	0.32	2.93
$[CT]_0$ variation	Fe^{EL}	Unbuffered	Ar	-3.81	0.24	-1.16	-0.22	0.28	2.93
$[CT]_0$ variation	Fe^{H2}	Unbuffered	Ar	-7.05	-0.37	-0.36	-1.00	0.44	4.19
$[CT]_0$ variation	Fe^{H2}	Unbuffered	Ar	-6.43	-0.38	-0.37	-1.01	0.37	4.19
$[CT]_0$ variation	Fe^{H2}	Unbuffered	Ar	-5.98	-0.38	-0.37	-1.00	0.37	4.19
$[CT]_0$ variation	Fe^{H2}	Unbuffered	Ar	-4.89	-0.30	-0.29	-0.93	0.64	4.19
$[CT]_0$ variation	Fe^{H2}	Unbuffered	Ar	-4.30	-0.41	-0.40	-1.03	0.68	4.19
$[CT]_0$ variation	Fe^{H2}	Unbuffered	Ar	-4.96	-0.32	-0.31	-0.95	0.49	4.19
$[CT]_0$ variation	Fe^{H2}	Unbuffered	Ar	-4.38	-0.41	-0.40	-1.03	0.38	4.19

Dataset	Iron Type	Other	Sparge Gas	$\log_{10}$ ($[CT]_0$ in M)	$\log_{10}$ (k_{obs} in hr^{-1})	$\log_{10}$ (k_M in L g^{-1} hr^{-1})	$\log_{10}$ (k_{SA} in L m^{-2} hr^{-1})	Y_{CF}	m^2/L
$[CT]_0$ variation	Fe^{H2}	Unbuffered	Ar	-4.01	-0.57	-0.56	-1.19	0.61	4.19
$[CT]_0$ variation	Fe^{EL}	Unbuffered	Ar	-6.34	0.42	-0.98	-0.04	0.51	2.93
$[CT]_0$ variation	Fe^{H2}	Unbuffered	Ar	-6.19	-0.16	-0.15	-0.78	0.22	4.19
$[CT]_0$ variation	Fe^{H2}	Unbuffered	Ar	-5.72	-0.44	-0.42	-1.06	0.39	4.19
$[CT]_0$ variation	Fe^{EL}	Unbuffered	Ar	-4.73	0.29	-1.11	-0.18	0.39	2.92
$[CT]_0$ variation	Fe^{EL}	Unbuffered	Ar	-4.24	0.18	-1.22	-0.29	0.44	2.92
$[CT]_0$ variation	Fe^{EL}	Unbuffered	Ar	-3.72	0.34	-1.06	-0.13	0.29	2.92
$[CT]_0$ variation	Fe^{EL}	Unbuffered	Ar	-4.84	0.30	-1.10	-0.17	0.27	2.93
$[CT]_0$ variation	Fe^{EL}	Unbuffered	Ar	-4.29	0.17	-1.23	-0.30	0.32	2.93
$[CT]_0$ variation	Fe^{EL}	Unbuffered	Ar	-3.81	0.24	-1.16	-0.22	0.28	2.93
$[CT]_0$ variation	Fe^{H2}	Unbuffered	N_2	-6.54	-0.41	-0.40	-1.04	0.66	4.19
$[CT]_0$ variation	Fe^{H2}	Unbuffered	N_2	-6.13	-0.52	-0.50	-1.14	0.72	4.19
$[CT]_0$ variation	Fe^{EL}	Unbuffered	N_2	-6.64	0.28	-1.12	-0.19	1.00	2.93
$[CT]_0$ variation	Fe^{EL}	Unbuffered	N_2	-5.93	0.24	-1.15	-0.22	0.87	2.93
$[CT]_0$ variation	Fe^{H2}	Unbuffered	N_2	-4.98	-0.38	-0.37	-1.01	0.37	4.19
$[CT]_0$ variation	Fe^{H2}	Unbuffered	N_2	-4.42	-0.41	-0.40	-1.03	0.42	4.19
$[CT]_0$ variation	Fe^{H2}	Unbuffered	N_2	-3.98	-0.42	-0.41	-1.04	0.38	4.19
$[CT]_0$ variation	Fe^{EL}	Unbuffered	N_2	-5.12	0.26	-1.14	-0.21	0.77	2.92
$[CT]_0$ variation	Fe^{EL}	Unbuffered	N_2	-4.60	0.14	-1.25	-0.32	0.96	2.93
$[CT]_0$ variation	Fe^{EL}	Unbuffered	N_2	-4.18	0.14	-1.26	-0.32	1.00	2.92
$[CT]_0$ variation	Fe^{H2}	Unbuffered	N_2	-4.98	-0.30	-0.29	-0.92	0.47	4.19
$[CT]_0$ variation	Fe^{EL}	Unbuffered	N_2	-4.02	0.26	-1.14	-0.21	0.66	2.93
$[CT]_0$ variation	Fe^{H2}	Unbuffered	N_2	-4.40	-0.36	-0.35	-0.98	0.41	4.19
$[CT]_0$ variation	Fe^{H2}	Unbuffered	N_2	-4.00	-0.41	-0.40	-1.03	0.43	4.19
$[CT]_0$ variation	Fe^{EL}	Unbuffered	N_2	-4.41	0.29	-1.11	-0.18	0.62	2.92

Dataset	Iron Type	Other	Sparge Gas	$\log_{10}$ ($[CT]_0$ in M)	$\log_{10}$ (k_{obs} in hr^{-1})	$\log_{10}$ (k_M in L g^{-1} hr^{-1})	$\log_{10}$ (k_{SA} in L m^{-2} hr^{-1})	Y_{CF}	m^2/L
$[CT]_0$ variation	Fe^{EL}	Unbuffered	N_2	-4.96	0.35	-1.04	-0.11	0.54	2.92
$[CT]_0$ variation	Fe^{H2}	Unbuffered	N_2	-6.71	-0.05	-0.04	-0.67	0.68	4.19
$[CT]_0$ variation	Fe^{H2}	Unbuffered	N_2	-6.32	-0.10	-0.09	-0.72	0.65	4.19
$[CT]_0$ variation	Fe^{EL}	Unbuffered	N_2	-6.63	0.32	-1.08	-0.14	0.88	2.92
$[CT]_0$ variation	Fe^{EL}	Unbuffered	N_2	-6.22	0.39	-1.00	-0.07	0.89	2.92
$[CT]_0$ variation	Fe^{BH}	Unbuffered	Ar	-6.94	-0.21	0.12	-1.09	0.44	7.56
$[CT]_0$ variation	Fe^{BH}	Unbuffered	N_2	-7.12	-0.23	0.11	-1.11	0.94	7.56
$[CT]_0$ variation	Fe^{BH}	Unbuffered	Ar	-6.01	-0.29	0.05	-1.17	0.89	7.56
$[CT]_0$ variation	Fe^{BH}	Unbuffered	N_2	-6.01	-0.28	0.05	-1.16	0.66	7.56
$[CT]_0$ variation	Fe^{BH}	Unbuffered	Ar	-5.01	-0.52	-0.18	-1.40	0.83	7.56
$[CT]_0$ variation	Fe^{BH}	Unbuffered	N_2	-4.96	-0.41	-0.07	-1.29	0.55	7.56
$[CT]_0$ variation	Fe^{BH}	Unbuffered	Ar	-4.05	-0.63	-0.30	-1.51	0.85	7.56
$[CT]_0$ variation	Fe^{BH}	Unbuffered	Ar	-6.35	-0.42	-0.08	-1.29	0.45	7.56
$[CT]_0$ variation	Fe^{BH}	Unbuffered	N_2	-6.41	-0.32	0.02	-1.19	0.75	7.56
$[CT]_0$ variation	Fe^{BH}	Unbuffered	Ar	-5.47	-0.33	0.01	-1.21	0.83	7.56
$[CT]_0$ variation	Fe^{BH}	Unbuffered	N_2	-5.39	-0.31	0.03	-1.18	0.50	7.56
$[CT]_0$ variation	Fe^{BH}	Unbuffered	Ar	-4.37	-0.53	-0.19	-1.41	0.70	7.56
$[CT]_0$ variation	Fe^{BH}	Unbuffered	N_2	-4.37	-0.48	-0.14	-1.36	0.72	7.56
$[CT]_0$ variation	Fe^{BH}	Unbuffered	Ar	-6.97	-0.31	0.03	-1.19	0.50	7.56
$[CT]_0$ variation	Fe^{BH}	Unbuffered	N_2	-7.15	-0.28	0.06	-1.15	0.95	7.56
$[CT]_0$ variation	Fe^{BH}	Unbuffered	Ar	-6.07	-0.29	0.05	-1.16	1.00	7.56
$[CT]_0$ variation	Fe^{BH}	Unbuffered	N_2	-6.07	-0.37	-0.03	-1.25	0.65	7.56
$[CT]_0$ variation	Fe^{BH}	Unbuffered	Ar	-5.04	-0.51	-0.17	-1.39	0.83	7.56
$[CT]_0$ variation	Fe^{BH}	Unbuffered	N_2	-4.99	-0.40	-0.07	-1.28	0.70	7.56
$[CT]_0$ variation	Fe^{BH}	Unbuffered	N_2	-6.43	-0.36	-0.02	-1.23	0.74	7.56

Dataset	Iron Type	Other	Sparge Gas	$\log_{10}$ ($[CT]_0$ in M)	$\log_{10}$ (k_{obs} in hr^{-1})	$\log_{10}$ (k_M in L g^{-1} hr^{-1})	$\log_{10}$ (k_{SA} in L m^{-2} hr^{-1})	Y_{CF}	m^2/L
$[CT]_0$ variation	Fe^{BH}	Unbuffered	Ar	-6.33	-0.40	-0.06	-1.27	0.43	7.56
$[CT]_0$ variation	Fe^{BH}	Unbuffered	Ar	-5.47	-0.30	0.03	-1.18	1.00	7.56
$[CT]_0$ variation	Fe^{BH}	Unbuffered	N_2	-5.38	-0.49	-0.15	-1.37	0.80	7.56
$[CT]_0$ variation	Fe^{BH}	Unbuffered	Ar	-4.38	-0.63	-0.29	-1.51	0.82	7.56
$[CT]_0$ variation	Fe^{BH}	Unbuffered	N_2	-4.32	-0.55	-0.21	-1.43	0.66	7.56
$[CT]_0$ variation	Fe^{EL}	Unbuffered	N_2	-7.02	0.16	-1.24	-0.31	1.00	2.92
$[CT]_0$ variation	Fe^{BH}	Unbuffered	N_2	-3.95	-0.53	-0.19	-1.41	0.71	7.56
$[CT]_0$ variation	Fe^{BH}	Unbuffered	N_2	-3.93	-0.51	-0.17	-1.39	0.62	7.56
$[CT]_0$ variation	Fe^{BH}	Unbuffered	Ar	-3.88	-0.44	-0.10	-1.32	0.54	7.56
Fe load variation	Fe^{H2}	Unbuffered	N_2	-7.00	-3.28	-3.63	-4.35	0.18	11.70
Fe load variation	Fe^{H2}	Unbuffered	N_2	-7.00	-2.92	-3.58	-4.30	0.20	23.83
Fe load variation	Fe^{H2}	Unbuffered	N_2	-7.00	-2.33	-3.38	-4.10	0.25	58.93
Fe load variation	Fe^{H2}	Unbuffered	N_2	-7.00	-2.30	-3.66	-4.37	0.24	118.30
Fe load variation	Fe^{H2}	Unbuffered	N_2	-2.93	-5.37	-4.77	-5.49	0.33	1.30
Fe load variation	Fe^{H2}	Unbuffered	N_2	-3.00	-5.27	-5.10	-5.81	0.19	3.47
Fe load variation	Fe^{H2}	Unbuffered	N_2	-3.45	-4.02	-4.28	-5.00	0.28	9.53
Fe load variation	Fe^{H2}	Unbuffered	N_2	-3.29	-3.50	-4.06	-4.78	0.38	19.07
Fisher buffered	Fe^{EL}	pH 7.3,EPPS	Ar	-5.39	0.64	-0.76	0.17	0.80	2.93
Fisher buffered	Fe^{EL}	pH 7.3, EPPS	Ar	-5.39	0.78	-0.62	0.31	0.76	2.92
Fisher buffered	Fe^{EL}	pH 7.3, Borate	Ar	-5.39	0.53	-0.87	0.06	0.60	2.93
Fisher buffered	Fe^{EL}	pH 7.3, Borate	Ar	-5.39	0.53	-0.86	0.07	0.65	2.92
Fisher buffered	Fe^{EL}	pH 7.3, EPPS	Ar	-5.39	1.12	-0.28	0.65	0.32	2.92
Fisher buffered	Fe^{EL}	pH 8.4, Borate	Ar	-5.39	-0.54	-1.76	-0.83	0.75	1.95
Fisher buffered	Fe^{EL}	pH 8.4, Borate	Ar	-5.39	-0.13	-1.35	-0.42	0.41	1.95

Dataset	Iron Type	Other	Sparge Gas	$\log_{10}$ ($[CT]_0$ in M)	$\log_{10}$ (k_{obs} in hr^{-1})	$\log_{10}$ (k_M in L g^{-1} hr^{-1})	$\log_{10}$ (k_{SA} in L m^{-2} hr^{-1})	Y_{CF}	m^2/L
Fisher buffered	Fe^{EL}	pH 8.4, Borate	Ar	-5.39	-0.34	-1.73	-0.80	0.47	2.92
Fisher buffered	Fe^{EL}	pH 8.4, Borate	Ar	-5.39	-0.10	-1.50	-0.56	0.37	2.92
Fisher buffered	Fe^{EL}	pH 8.4, EPPS	Ar	-5.39	-0.35	-1.57	-0.64	0.99	1.95
Fisher buffered	Fe^{EL}	pH 8.4, EPPS	Ar	-5.39	-0.19	-1.59	-0.65	0.50	2.92
Fisher buffered	Fe^{EL}	pH 8.4, EPPS	Ar	-5.39	-0.08	-1.48	-0.54	0.25	2.92
Fisher buffered	Fe^{EL}	pH 8.4, EPPS	Ar	-5.39	-0.50	-1.72	-0.79	0.66	1.95
Fisher unbuffered	Fe^{EL}	pH ~ 9	Ar	-5.39	0.38	-1.08	-0.15	1.00	3.41
Fisher unbuffered	Fe^{EL}	pH ~ 9	Ar	-5.39	0.34	-1.12	-0.19	1.00	3.41
Fisher unbuffered	Fe^{EL}	pH ~ 9	Ar	-5.39	0.18	-1.28	-0.35	1.00	3.41
Fisher unbuffered	Fe^{EL}	pH ~ 9	Ar	-5.39	0.17	-1.30	-0.36	0.67	3.41
Fisher unbuffered	Fe^{EL}	pH ~ 9	Ar	-5.39	0.55	-0.67	0.26	1.00	1.95
Fisher unbuffered	Fe^{EL}	pH ~ 9	Ar	-5.39	0.15	-0.77	0.16	0.43	0.98
Fisher unbuffered	Fe^{EL}	pH ~ 9	Ar	-5.39	0.10	-0.82	0.11	0.53	0.98
Iron type variation	Fe^{EL}	Unbuffered	Ar	-5.39	0.46	-0.94	-0.01	0.41	2.93
Iron type variation	Fe^{H2}	Unbuffered	Ar	-5.39	0.06	0.07	-0.75	0.24	6.51
Iron type variation	Fe^{H2}	Unbuffered	Ar	-5.39	-0.02	-0.01	-0.83	0.11	6.51
Iron type variation	Fe^{PL}	Unbuffered	Ar	-5.39	-0.19	-1.59	-1.77	0.34	38.50
Iron type variation	Fe^{PL}	Unbuffered	Ar	-5.39	-0.14	-1.53	-1.72	0.24	38.50
Iron type variation	Fe^{AR}	Unbuffered	Ar	-5.39	0.35	0.23	-0.06	0.38	2.57
Iron type variation	Fe^{AR}	Unbuffered	Ar	-5.39	0.17	0.05	-0.24	0.37	2.57
Iron type variation	Fe^{EL}	Unbuffered	Ar	-5.39	0.33	-1.06	-0.13	0.39	2.93
Iron type variation	Aged Fe^{BH}	Unbuffered	Ar	-5.39	0.50	0.51	-1.19	0.44	48.72
Iron type variation	Aged Fe^{BH}	Unbuffered	Ar	-5.39	0.60	0.61	-1.09	0.17	48.72

Dataset	Iron Type	Other	Sparge Gas	$\log_{10}$ ($[CT]_0$ in M)	$\log_{10}$ (k_{obs} in hr^{-1})	$\log_{10}$ (k_M in L g^{-1} hr^{-1})	$\log_{10}$ (k_{SA} in L m^{-2} hr^{-1})	Y_{CF}	m^2/L
Iron type variation	Fresh Fe^{BH}	Unbuffered	Ar	-5.39	-0.16	-0.15	-1.61	0.79	27.89
Iron type variation	Fresh Fe^{BH}	Unbuffered	Ar	-5.39	-0.16	-0.15	-1.61	0.79	27.89
Iron type variation	Fresh Fe^{BH}	Unbuffered	Ar	-5.39	-0.20	-0.19	-1.65	0.57	27.89
Iron type variation	Fe^{H2}	Unbuffered	N_2	-5.39	-0.20	-0.19	-1.02	0.28	6.51
Iron type variation	Aged Fe^{BH}	Unbuffered	N_2	-5.39	0.77	0.79	-0.91	0.47	48.72
Iron type variation	Fe^{H2}	Unbuffered	N_2	-5.39	0.09	0.10	-0.72	0.22	6.51
Iron type variation	Fresh Fe^{BH}	Unbuffered	N_2	-5.39	0.09	0.10	-1.36	0.57	27.89
Iron type variation	Fe^{EL}	Unbuffered	N_2	-5.39	0.19	-1.20	-0.27	0.44	2.93
Iron type variation	Fe^{AR}	Unbuffered	N_2	-5.39	0.05	-0.07	-0.36	0.16	2.59
Iron type variation	Fe^{AR}	Unbuffered	N_2	-5.39	0.66	0.54	0.25	0.11	2.59
Iron type variation	Fe^{OM}	Unbuffered	N_2	-5.39	-0.42	-0.41	-1.55	0.01	13.39
Iron type variation	Fe^{PL}	Unbuffered	N_2	-5.39	-0.19	-1.59	-1.77	0.42	38.50
Iron type variation	Fe^{PL}	Unbuffered	N_2	-5.39	-0.08	-1.48	-1.67	0.39	38.50
Iron type variation	Fe^{EL}	Unbuffered	He	-5.39	0.50	-0.90	0.03	0.28	2.93
Iron type variation	Fe^{EL}	Unbuffered	He	-5.39	0.42	-0.98	-0.05	0.29	2.93
Iron type variation	Fe^{H2}	Unbuffered	He	-5.39	-0.07	-0.06	-0.88	0.22	6.51
Iron type variation	Fe^{H2}	Unbuffered	He	-5.39	-0.24	-0.23	-1.06	0.25	6.51
Iron type variation	Fe^{EL}	Unbuffered	Fe scrubbed	-5.39	-0.19	-1.59	-0.66	0.19	2.93
Iron type variation	Fe^{EL}	Unbuffered	Fe scrubbed	-5.39	0.16	-1.24	-0.31	0.33	2.93
Iron type variation	Fe^{H2}	Unbuffered	Fe scrubbed	-5.39	0.05	0.06	-0.77	0.21	6.51

Dataset	Iron Type	Other	Sparge Gas	$\log_{10}$ ($[CT]_0$ in M)	$\log_{10}$ (k_{obs} in hr^{-1})	$\log_{10}$ (k_M in L g^{-1} hr^{-1})	$\log_{10}$ (k_{SA} in L m^{-2} hr^{-1})	Y_{CF}	m^2/L
Iron type variation	Fe^{H2}	Unbuffered	Fe scrubbed	-5.39	-0.08	-0.07	-0.90	0.25	6.51
Iron type variation	Fe^{H2}	Unbuffered	Fe scrubbed	-5.39	-0.08	-0.07	-0.90	0.25	6.51
Iron type variation	Fe^{BH}	Unbuffered	N_2	-5.39	0.13	0.14	-1.32	0.53	27.89
Iron type variation	Fe^{EL}	Unbuffered	N_2	-5.39	0.37	-1.03	-0.10	0.53	2.93
Mixing speed variation	Fe^{H2}	48 rpm	N_2	-5.40	-0.05	-0.14	-0.61	0.44	3.65
Mixing speed variation	Fe^{H2}	24 rpm	N_2	-5.40	0.20	0.20	-0.28	0.36	3.00
Mixing speed variation	Fe^{H2}	12 rpm	N_2	-5.40	0.15	0.17	-0.31	0.23	2.85
Mixing speed variation	Fe^{H2}	48 rpm	N_2	-5.40	0.41	0.22	-0.26	0.36	4.64
Mixing speed variation	Fe^{H2}	24 rpm	N_2	-5.40	0.32	0.32	-0.16	0.45	2.98
Mixing speed variation	Fe^{H2}	12 rpm	N_2	-5.40	0.01	-0.01	-0.49	0.42	3.18
Mixing speed variation	Fe^{H2}	36 rpm	N_2	-5.40	-0.09	-0.09	-0.57	0.31	3.00
Mixing speed variation	Fe^{H2}	36 rpm	N_2	-5.40	0.18	0.10	-0.38	0.38	3.60
Mixing speed variation	Fe^{H2}	6 rpm	N_2	-5.40	-0.18	-0.22	-0.70	0.43	3.35
Mixing speed variation	Fe^{H2}	6 rpm	N_2	-5.40	-0.04	-0.06	-0.54	0.42	3.15
Mixing speed variation	Fe^{H2}	0 rpm	N_2	-5.40	-0.16	-0.21	-0.68	0.22	3.30

Dataset	Iron Type	Other	Sparge Gas	$\log_{10}$ ($[CT]_0$ in M)	$\log_{10}$ (k_{obs} in hr^{-1})	$\log_{10}$ (k_M in L g^{-1} hr^{-1})	$\log_{10}$ (k_{SA} in L m^{-2} hr^{-1})	Y_{CF}	m^2/L
Mixing speed variation	Fe^{H2}	0 rpm	N_2	-5.40	-0.57	-0.56	-1.04	0.23	2.95
Mixing speed variation	Fe^{H2}	42 rpm	N_2	-5.40	0.17	0.16	-0.32	0.40	3.08
Mixing speed variation	Fe^{H2}	30 rpm	N_2	-5.40	0.09	0.11	-0.37	0.44	2.85
Mixing speed variation	Fe^{H2}	30 rpm	N_2	-5.40	0.03	-0.05	-0.53	0.04	3.63
Mixing speed variation	Fe^{H2}	24 rpm	N_2	-5.40	0.18	0.10	-0.38	0.38	3.63
pH variation	Fe^{H2}	pH 7.3 HCl/NaOH	N_2	-5.40	-3.23	-3.33	-4.05	0.32	6.50
pH variation	Fe^{H2}	pH 9.8 HCl/NaOH	N_2	-5.40	-3.20	-3.30	-4.01	0.25	6.50
pH variation	Fe^{H2}	pH 11.1 HCl/NaOH	N_2	-5.40	-3.40	-3.50	-4.22	0.47	6.50
pH variation	Fe^{H2}	pH 6.59 HCl/NaOH	N_2	-5.40	-3.83	-3.92	-4.64	0.24	6.50
pH variation	Fe^{H2}	pH 7.4 HCl/NaOH	N_2	-5.40	-3.35	-3.45	-4.17	0.33	6.50
pH variation	Fe^{H2}	pH 7.9 HCl/NaOH	N_2	-5.40	-3.31	-3.40	-4.12	0.21	6.50
pH variation	Fe^{H2}	pH 7.7 HCl/NaOH	N_2	-5.40	-3.61	-3.71	-4.43	0.38	6.50
pH variation	Fe^{H2}	pH 6.6 HCl/NaOH	N_2	-5.40	-3.47	-3.57	-4.28	0.18	6.50
pH variation	Fe^{H2}	pH 6.45 HCl/NaOH	N_2	-5.40	-3.78	-3.88	-4.60	0.28	6.50
pH variation	Fe^{H2}	pH 6.38 HCl/NaOH	N_2	-5.40	-3.93	-4.03	-4.75	0.30	6.50

Dataset	Iron Type	Other	Sparge Gas	$\log_{10}$ ($[CT]_0$ in M)	$\log_{10}$ (k_{obs} in hr^{-1})	$\log_{10}$ (k_M in L g^{-1} hr^{-1})	$\log_{10}$ (k_{SA} in L m^{-2} hr^{-1})	Y_{CF}	m^2/L
pH variation	Fe^{H2}	pH 10.9 HCl/NaOH	N_2	-5.40	-3.20	-3.30	-4.02	0.26	6.50
Pre-exposure (dry Fe^{H2})	Fe^{H2}	5.00 days	N_2	-5.40	-3.21	-3.13	-4.54	0.44	21.33
Pre-exposure (dry Fe^{H2})	Fe^{H2}	5.00 days	N_2	-5.40	-3.30	-3.22	-4.62	0.51	21.33
Pre-exposure (dry Fe^{H2})	Fe^{H2}	10.06 days	N_2	-5.40	-3.12	-3.04	-4.45	0.30	21.33
Pre-exposure (dry Fe^{H2})	Fe^{H2}	10.06 days	N_2	-5.40	-3.17	-3.09	-4.50	0.29	21.33
Pre-exposure (dry Fe^{H2})	Fe^{H2}	3.03 days	N_2	-5.40	-3.11	-3.03	-4.44	0.44	21.33
Pre-exposure (dry Fe^{H2})	Fe^{H2}	3.03 days	N_2	-5.40	-3.36	-3.28	-4.69	0.44	21.33
Pre-exposure (dry Fe^{H2})	Fe^{H2}	13.90 days	N_2	-5.40	-3.62	-3.54	-4.95	0.42	21.33
Pre-exposure (dry Fe^{H2})	Fe^{H2}	13.90 days	N_2	-5.40	-3.52	-3.44	-4.85	0.41	21.33
Pre-exposure (dry Fe^{H2})	Fe^{H2}	20.03 days	N_2	-5.40	-3.42	-3.34	-4.75	0.31	21.33
Pre-exposure (dry Fe^{H2})	Fe^{H2}	20.03 days	N_2	-5.40	-3.51	-3.43	-4.84	0.37	21.33
Pre-exposure (dry Fe^{H2})	Fe^{H2}	1.02 days	N_2	-5.40	-2.94	-2.86	-4.27	0.43	21.33
Pre-exposure (dry Fe^{H2})	Fe^{H2}	1.02 days	N_2	-5.40	-2.92	-2.84	-4.25	0.36	21.33
Pre-exposure (dry Fe^{H2})	Fe^{H2}	0.00 days	N_2	-5.40	-4.13	-4.06	-5.46	0.22	21.33
Pre-exposure (dry Fe^{H2})	Fe^{H2}	0.00 days	N_2	-5.40	-4.10	-4.02	-5.43	0.31	21.33

Dataset	Iron Type	Other	Sparge Gas	$\log_{10}$ ($[CT]_0$ in M)	$\log_{10}$ (k_{obs} in hr^{-1})	$\log_{10}$ (k_M in L g^{-1} hr^{-1})	$\log_{10}$ (k_{SA} in L m^{-2} hr^{-1})	Y_{CF}	m^2/L
Pre-exposure (dry Fe^{H2})	Fe^{H2}	30.17 days	N_2	-5.40	-3.48	-3.40	-4.81	0.45	21.33
Pre-exposure (dry Fe^{H2})	Fe^{H2}	30.17 days	N_2	-5.40	-3.43	-3.35	-4.76	0.44	21.33
Pre-exposure (dry Fe^{H2})	Fe^{H2}	0.24 days	N_2	-5.40	-4.04	-3.96	-5.37	0.29	21.33
Pre-exposure (dry Fe^{H2})	Fe^{H2}	0.24 days	N_2	-5.40	-4.00	-3.92	-5.33	0.32	21.33
Pre-exposure (dry Fe^{H2})	Fe^{H2}	2.00 days	N_2	-5.40	-2.96	-2.88	-4.29	0.61	21.33
Pre-exposure (dry Fe^{H2})	Fe^{H2}	2.00 days	N_2	-5.40	-2.85	-2.77	-4.18	0.52	21.33
Pre-exposure (dry Fe^{H2})	Fe^{H2}	0.25 days	N_2	-5.40	-4.06	-3.98	-5.39	0.25	21.33
Pre-exposure (dry Fe^{H2})	Fe^{H2}	0.25 days	N_2	-5.40	-4.02	-3.94	-5.35	0.26	21.33
Pre-exposure (dry Fe^{H2})	Fe^{H2}	0.50 days	N_2	-5.40	-3.76	-3.68	-5.09	0.44	21.33
Pre-exposure (dry Fe^{H2})	Fe^{H2}	0.50 days	N_2	-5.40	-3.59	-3.51	-4.92	0.52	21.33
Pre-exposure (dry Fe^{H2})	Fe^{H2}	0.65 days	N_2	-5.40	-3.69	-3.61	-5.02	0.49	21.33
Pre-exposure (dry Fe^{H2})	Fe^{H2}	0.65 days	N_2	-5.40	-3.76	-3.68	-5.09	0.57	21.33
Pre-exposure (dry Fe^{H2})	Fe^{H2}	0.90 days	N_2	-5.40	-3.75	-3.67	-5.07	0.61	21.33
Pre-exposure (dry Fe^{H2})	Fe^{H2}	0.90 days	N_2	-5.40	-3.53	-3.45	-4.86	0.62	21.33
Pre-exposure (slurry Fe^{H2})	Fe^{H2}	1.00 days	N_2	-5.41	-1.58	-1.59	-2.46	0.24	7.60

Dataset	Iron Type	Other	Sparge Gas	$\log_{10}$ ($[CT]_0$ in M)	$\log_{10}$ (k_{obs} in hr^{-1})	$\log_{10}$ (k_M in L g^{-1} hr^{-1})	$\log_{10}$ (k_{SA} in L m^{-2} hr^{-1})	Y_{CF}	m^2/L
Pre-exposure (slurry Fe^{H2})	Fe^{H2}	1.00 days	N_2	-5.41	-1.72	-1.74	-2.60	0.25	7.60
Pre-exposure (slurry Fe^{H2})	Fe^{H2}	2.00 days	N_2	-5.41	-1.71	-1.73	-2.60	0.23	7.60
Pre-exposure (slurry Fe^{H2})	Fe^{H2}	2.00 days	N_2	-5.41	-1.78	-1.80	-2.66	0.23	7.60
Pre-exposure (slurry Fe^{H2})	Fe^{H2}	5.00 days	N_2	-5.41	-1.75	-1.77	-2.64	0.29	7.60
Pre-exposure (slurry Fe^{H2})	Fe^{H2}	5.00 days	N_2	-5.41	-1.83	-1.85	-2.71	0.30	7.60
Pre-exposure (slurry Fe^{H2})	Fe^{H2}	16.00 days	N_2	-5.41	-2.02	-2.04	-2.90	0.26	7.60
Pre-exposure (slurry Fe^{H2})	Fe^{H2}	16.00 days	N_2	-5.41	-1.95	-1.97	-2.83	0.24	7.60
Pre-exposure (slurry Fe^{H2})	Fe^{H2}	16.00 days	N_2	-5.41	-2.15	-2.17	-3.04	0.43	7.60
Pre-exposure (slurry Fe^{H2})	Fe^{H2}	16.00 days	N_2	-5.41	-2.04	-2.06	-2.92	0.30	7.60
Pre-exposure (slurry Fe^{H2})	Fe^{H2}	21.00 days	N_2	-5.41	-2.07	-2.08	-2.95	0.29	7.60
Pre-exposure (slurry Fe^{H2})	Fe^{H2}	0.50 days	N_2	-5.41	-1.61	-1.63	-2.49	0.24	7.60
Pre-exposure (slurry Fe^{H2})	Fe^{H2}	0.50 days	N_2	-5.41	-1.59	-1.60	-2.47	0.26	7.60
Pre-exposure (slurry Fe^{H2})	Fe^{H2}	12.00 days	N_2	-5.41	-1.94	-1.96	-2.82	0.21	7.60
Pre-exposure (slurry Fe^{H2})	Fe^{H2}	12.00 days	N_2	-5.41	-2.04	-2.05	-2.92	0.23	7.60
Pre-exposure (slurry Fe^{H2})	Fe^{H2}	0.00 days	N_2	-5.41	-1.76	-1.78	-2.64	0.27	7.60

Dataset	Iron Type	Other	Sparge Gas	$\log_{10}$ ($[CT]_0$ in M)	$\log_{10}$ (k_{obs} in hr^{-1})	$\log_{10}$ (k_M in L g^{-1} hr^{-1})	$\log_{10}$ (k_{SA} in L m^{-2} hr^{-1})	Y_{CF}	m^2/L
Pre-exposure (slurry Fe^{H2})	Fe^{H2}	0.00 days	N_2	-5.41	-1.72	-1.74	-2.60	0.25	7.60
Pre-exposure (slurry Fe^{H2})	Fe^{H2}	0.21 days	N_2	-5.41	-1.78	-1.80	-2.66	0.33	7.60
Pre-exposure (slurry Fe^{H2})	Fe^{H2}	0.21 days	N_2	-5.41	-1.79	-1.81	-2.67	0.30	7.60
Pre-exposure (slurry Fe^{H2})	Fe^{H2}	0.00 days	N_2	-5.41	-1.83	-1.85	-2.71	0.33	7.60
Pre-exposure (slurry Fe^{H2})	Fe^{H2}	0.00 days	N_2	-5.41	-1.82	-1.84	-2.70	0.27	7.60
Pre-exposure (slurry Fe^{H2})	Fe^{H2}	0.00 days	N_2	-5.41	-1.70	-1.76	-2.62	0.32	8.33
Pre-exposure (slurry Fe^{H2})	Fe^{H2}	0.00 days	N_2	-5.41	-1.77	-1.80	-2.66	0.24	7.73
Fe^{H2} general	Fe^{H2}	pH 9	N_2	-5.40	-0.37	-0.59	-1.07	0.57	5.00
Fe^{H2} general	Fe^{H2}	pH 9	N_2	-5.40	0.35	0.12	-0.35	0.42	5.00
Fe^{H2} general	Fe^{H2}	pH 9	N_2	-5.40	0.33	0.11	-0.36	0.45	5.00
Fe^{H2} general	Fe^{H2}	pH 9	Ar	-5.40	0.18	-0.04	-0.52	0.17	5.00
Fe^{H2} general	Fe^{H2}	pH 9	N_2	-5.40	0.03	-0.20	-0.67	0.12	5.00
Fe^{H2} general	Fe^{H2}	pH 9	N_2	-5.40	0.00	-0.23	-0.70	0.12	5.00
Fe^{H2} general	Fe^{H2}	pH 9	N_2	-5.40	-0.15	-0.38	-0.85	0.42	5.00
Fe^{H2} general	Fe^{H2}	pH 9	Ar	-5.40	-0.12	-0.35	-0.82	0.81	5.00

Biographical Sketch

The author, Vaishnavi Sarathy (also called Vaish), was born in Madras (now Chennai), India in August 1977. Schooling was split among 8 schools due to her father's transferable job in the Indian Air Force. After high school, she joined a five-year integrated masters program in chemistry in the Indian Institute of Technology, Bombay (now Mumbai). 5 years of rigorous training in all aspects of chemistry coupled with a semester at the chemistry department in the University of Florida helped Vaishnavi realize that her interests lay in applying chemistry to environmental science. She went on to pursue another masters in environmental engineering from the University of Delaware with Dr. Herbert E. Allen, during which time she studied copper bioavailablity in surface- and waste-waters. At the end of her masters, she married Rahul Ghosh, who was employed with Radisys Corp. in Portland, Oregon. The move to Portland brought a shift to a Ph.D. in environmental chemistry at the Oregon Graduate Institute (now OHSU) with Dr. Paul G. Tratnyek, studying the pathways and kinetics of dechlorination of organic groundwater contaminants. Siddhartha Ghosh was born to Vaishnavi and Rahul a few months before the defense. Some of Vaishnavi's awards and publications include:

- Graduate Student Award, American Chemical Society (ACS) Jan '07
- Paul Clayton Student Achievement Award (OHSU) May '06
- Sarathy, V., Tratnyek, P.G., Nurmi, J.T., Baer, D.R., Amonette, J.E., Chun, C.L., Penn, R.L, Reardon, E.J. (2008) *Aging of Iron Nanoparticles in Aqueous Solution: Effects on Structure and Reactivity.* J. Phys. Chem. C., *112* (7), 2286-2293.
- Sarathy, V. and Allen, H.E. (2005) Copper Complexation to Dissolved Organic Matter from Surface Water and Wastewater Effluent. Ecotoxicology and Environmental Safety. 61: 337-344.
- Nurmi, J.T., Tratnyek, P.G., Sarathy, V., Baer, D.R., Amonette, J.E., Pecher, K.,Wang, C., Linehan, J.C., Matson, D., Penn, R.L., Driesens, M.D. (2005) *Characterization and Properties of Metallic Iron and Iron-Oxide Nanoparticles: Spectroscopy, Electrochemistry, and Kinetics.* Environmental Science and Technology. 39: 1221-1230.